2015-05-01

Burnout, NO, and Flame Characterization from an Oxygen-Enriched Biomass Flame

Steven Andrew Owen
Brigham Young University - Provo

Burnout, NO, and Flame Characterization from an Oxygen-Enriched Biomass Flame

Steven Andrew Owen

A thesis submitted to the faculty of
Brigham Young University
in partial fulfillment of the requirements for the degree of

Master of Science

Dale R. Tree, Chair
Julie Crockett
David O. Lignell

Department of Mechanical Engineering

Brigham Young University

May 2015

ABSTRACT

Burnout, NO, and Flame Characterization from an
Oxygen-Enriched Biomass Flame

Steven Andrew Owen
Department of Mechanical Engineering, BYU
Master of Science

Concern for the environment and a need for more efficient energy generation have sparked a growing interest throughout the world in renewable fuels. In order to reduce emissions that negatively contribute to global warming, especially CO_2, enormous efforts are being invested in technologies to reduce our impact on the environment. Biomass is an option that is considered CO_2 friendly due to the consumption of CO_2 upon growth. Co-firing biomass with coal offers economic advantages because of reduced capital costs as well as other positive impacts, such as NO_x and SO_x emission reductions. However, due to the large average particle size of biomass, issues arise such as poor flame stability and poor carbon burnout. Larger particles can also result in longer flames and different heat transfer characteristics. Oxygen enrichment is being investigated as a possible solution to mitigate these issues and enable co-firing in existing facilities.

An Air Liquide designed burner was used in this work to explore the impact of oxygen enrichment on biomass flame characteristics, emissions, and burnout. Multiple biomass fuels were used (medium hardwood, fine hardwood, and straw) in conjunction with multiple burner configurations and operating conditions. Exhaust ash samples and exhaust NO were collected for various operating conditions and burner configurations. All operating parameters including O_2 addition, swirl, and O_2 location could be used to reduce LOI but whenever LOI was reduced, NO increased producing an NO-LOI trade-off.

Starting with high LOI, various parameters such as O_2 addition and increased swirl could be used to reduce LOI with only small increases of NO. As O_2 or swirl increased further, small decreases in LOI were obtained only with large increases in NO. This behavior was captured through NO-LOI trade-off curves where a given configuration or operating condition was deemed better when the curve was shifted toward the origin. Global enrichment or O_2 addition to the secondary stream and O_2 addition to the primary stream produced better trade-off results than center O_2 injection. Straw produced NO-LOI trade-off curves just as the wood particles but the curve was shifted further from the origin, likely due to the higher nitrogen content of the straw. Flame characterization results showed that small amounts of O_2 in the center improved flame attachment and stability while increasing flame temperature and pyrolysis rates.

Keywords: biomass combustion, hardwood biomass, wheat straw biomass, oxygen injection, oxygen enrichment, oxygen combustion, NO emission, carbon burnout

ACKNOWLEDGEMENTS

I am grateful for the opportunity I have had to attend Brigham Young University. My academic experience has been a tremendous growing opportunity and I am grateful to be a part of this great and well respected university.

I would like to thank Dr. Dale Tree for his support and encouragement throughout this entire process. He has been an irreplaceable and enormous influence and mentor through his knowledge and experience. I would like to thank my family for their love and support, especially my wife, Chantelle, for her patience and understanding. I am grateful to my coworkers, Daniel Tovar, Joshua Thornock, Daniel Ellis, and David Ashworth, who have assisted in the operation of the Burner Flow Reactor and the collection of data. Their support and experience have been particularly helpful. Yuan Xue, Kenneth Kaiser, Hwanho Kim, Remi Tsiavi and Louis, all from Air Liquide, have each been more than helpful in supporting this project. Also, Air Liquide has been an amazing sponsor for the financial support of this work, which is greatly appreciated.

TABLE OF CONTENTS

LIST OF TABLES

LIST OF FIGURES

NOMENCLATURE

ASTM	American Society for Testing and Materials
BFR	Burner Flow Reactor
BYU	Brigham Young University
C	Carbon
CCS	Carbon Capture Sequestration
CO	Carbon Monoxide
CO_2	Carbon Dioxide
°C	Degrees Celsius
EAC	Enriched Air Combustion
F	Fahrenheit
FTIR	Fourier Transform Infrared Spectrometer
H	Hydrogen
HHV	Higher Heating Value
IFRF	International Flame Research Foundation
kg/hr	Kilograms Per Hour
kW_{th}	Kilowatts of Thermal Power
K	Kelvin
LOI	Loss on Ignition
m	Meters
mm	Millimeters
N	Nitrogen
ND-IR	Non-Dispersive Infrared
NO	Nitric Oxide
NO_x	Nitrogen Oxides
O	Oxygen
OFC	Oxy-Fuel Combustion
OIC	Oxygen Injection Combustion
ppm	Parts Per Million
S	Sulfur
SO_x	Sulfur Oxides
SR	Stoichiometric Ratio
μm	Microns or Micrometers
wt %	Weight Percent
W_{mfa}	Weight of Ash with Moisture Removed
W_{cfa}	Weight of Carbon Free Ash
Y_{ash}	Mass Fraction of Ash

1 INTRODUCTION

Concern for the environment and the need for efficient energy generation have sparked a growing interest throughout the world in renewable fuels and options geared to secure the future of clean energy. In recent years, there has been an increasing effort to reduce emissions that are known to negatively contribute to global climate change. One of the main contributors to global climate change is carbon dioxide (CO_2) emissions. In 2012, CO_2 accounted for 82% of all U.S. greenhouse gas emissions from human activities with combustion of fossil fuels for energy and transportation noted as the main source for CO_2 emissions [1]. Power plants and other combustion facilities often have large CO_2 emissions because CO_2 is the end product for fuels containing carbon. While regulations on the emission of greenhouse gases continue to rise, enormous efforts have been invested into technologies that reduce CO_2. Viable options include various fuels that are more CO_2 neutral. One way CO_2 emissions from power generation can be reduced, both effectively and inexpensively, is to substitute coal with biomass or by burning the two simultaneously in a process known as co-firing [2].

Biomass is often considered relatively CO_2 neutral due to the biological nature of biomass consuming CO_2 during photosynthesis [3]. Co-firing biomass with coal reduces CO_2 emissions and often simultaneously produces other positive impacts, such as emission reductions of nitrogen oxides (NO_x) and sulfur oxides (SO_x) [4]. A review of over 100 successful field demonstrations in 16 countries with various combinations of coal and biomass using every major type of boiler have identified several challenges including fuel preparation, storage, and delivery,

potential increases in corrosion, ash deposition issues, carbon burnout, ash utilization and overall cost [2, 5, 6]. When roller mills used for coal are instead used for biomass, it is difficult to produce the same small particle size. The cost of grinding biomass to the same size as coal is prohibitive. Due to its properties, such as shape and density, biomass exhibits rapid oxidation and combustion rates. However, these rates are not rapid enough to make up for the increased particle size resulting in unburned carbon and fouling as problematic areas for boilers converted to or co-firing biomass. Excessive moisture along with excessive particle size can pose a challenge for fuel conversion efficiency [3, 4].

Although biomass can reduce NO_x and SO_x emissions these pollutants are still a matter of concern and need to be controlled in biomass combustion. NO_x and SO_x are harmful to both health and the environment. NO_x emissions can result in negative respiratory effects from various amounts of exposure and concentration levels. It negatively affects the environment by contributing to acid deposition and forming particulate matter. It is important to maintain low levels of NO in order to protect the environment and ensure safe and healthy living conditions [7]. SO_x emissions also have negative respiratory effects as they react and form particulate matter with other compounds. Fossil fuel combustion (73%) and other industrial facilities (20%) account for 93% of SO_2 emissions [8]. NO_x emission is typically more prevalent than SO_x in biomass combustion and will be one of the main focus points of this work.

Studies have shown that an oxygen enriched environment during biomass combustion can improve mass loss rates and particle burnout [9, 10]. While oxygen enrichment may increase particle burnout, NO formation can be negatively affected. Bool et al. [11, 12] made several observations where oxygen was injected into coal flames and concluded certain methods of oxygen injection can be successfully implemented for NO reduction. Oxygen enrichment is

being investigated as a possible solution to mitigate emission and particle burnout issues and thus enable co-firing in many existing facilities. This work explores the possibility of using oxygen to improve carbon burnout without significantly increasing NO emissions.

1.1 Objectives

The objective of this work is to explore the design space of oxygen injection in a swirl stabilized burner for the reduction of unburned carbon and improvement of flame stability without increasing NO_x emissions. Data will be collected on a 150 kW_{th} laboratory scale reactor and will include the measurement of carbon burnout and exhaust emissions of NO, CO, CO_2, and O_2 as well as visual flame characterization of flame length and flame lift-off. Three fuels, medium hardwood, fine hardwood, and wheat straw, will be used as representative biomass particles. The data will be used to explore an empirical characterization of the flame and determine the optimal conditions for which oxygen enrichment will simultaneously improve burnout and reduce NO emissions.

1.2 Scope

This work will focus on the impact of various design parameters on exhaust products, primarily NO_x and particle loss on ignition. Flame characterization will be done by visual observation. Detailed mapping of flame species, burnout, and temperature will not be completed for this work. The work will also be limited to three fuels; medium hardwood, fine hardwood, and straw. Computational work will include the application of existing scaling laws to the current work and the development of those scaling laws but will not include comprehensive combustion modeling.

2 BACKGROUND

Information needed for understanding the methods used as well as the results and their significance is presented in this chapter, including a discussion of NO formation, the process of carbon burnout, and the definition of swirl.

2.1 Formation of Nitric Oxides

NO_x is the term used for the combined pollutants of NO and NO_2. In coal combustion the primary component of NO_x is NO. The formation of NO for biomass combustion follows three main chemical pathways often referred to as thermal, prompt, and fuel NO. An understanding of these pathways provides the background necessary for the interpretation of the results to be presented and an understanding of how to produce minimum NO_x emissions.

Thermal NO_x is strongly dependent on temperature, being unimportant below temperatures of 1800 K. The extended Zeldovich mechanism, shown in Equations 2.1 through 2.3, provides the reactions and species involved [13]. It has been noted, however, that timescales of the thermal mechanism are much slower than that of fuel oxidation processes, and has therefore been demonstrated that NO is formed in post flame gas regions. In addition, previous work from the reactor used in this work has shown that temperatures are above 1800 K solely in the region of the flame, and therefore this path for NO formation is assumed negligible in these experiments [14].

$$O + N_2 \Leftrightarrow NO + N \quad (2.1)$$

$$N + O_2 \Leftrightarrow NO + O \quad (2.2)$$

$$N + OH \Leftrightarrow NO + H \quad (2.3)$$

Prompt NO is rapidly formed during the combustion of hydrocarbons by the Fenimore mechanism, shown in Equations 2.4 and 2.5 [13]. For prompt NO, hydrocarbon radicals react with nitrogen and result in cyanides. These cyanide compounds convert to intermediate compounds and can ultimately result in NO. This pathway of NO formation can occur more rapidly than the time needed for thermal NO_x, thus earning its name.

$$CH + N_2 \Leftrightarrow HCN + N \quad (2.4)$$

$$C + N_2 \Leftrightarrow CN + N \quad (2.5)$$

Fuel NO is the third main path and the major contributor of NO in pulverized biomass and coal combustion [15]. Biomass and coal contain nitrogen in their molecular structure which is released as volatiles, or light gases, when the fuel particles are heated. The process of volatiles being released is called devolatilization. Nitrogen in biomass volatiles is typically released as ammonia (NH_3), whereas with coal a mixture of hydrogen cyanide (HCN) and NH_3 is more common. These volatiles can then oxidize and form NO, as shown in the sequence of Equations 2.6 through 2.9 [13].

$$HCN + O \Leftrightarrow NCO + H \quad (2.6)$$

$$NCO + H \Leftrightarrow NH + CO \quad (2.7)$$

$$NH + H \Leftrightarrow N + H_2 \quad (2.8)$$

$$N + OH \Leftrightarrow NO + H \quad (2.9)$$

The sequence shown is not the only method for fuel nitrogen conversion to NO but represents one of the primary pathways. Significant nitrogen products include NO, NO_2, and N_2. Figure 2.1 is a diagram depicting how nitrogen in the fuel can be converted to either NO or N_2 depending on the local stoichiometry. Intermediates such as NH_3 and HCN can either react with oxidizing species to produce NO or they can react with NO to produce N_2 under reducing environments. It should be noted, however, that NO cannot be eliminated entirely in this way. A fuel rich region, essential for NO reduction, must be maintained at an optimal oxidizer to fuel ratio to enable NO reduction to be a maximum.

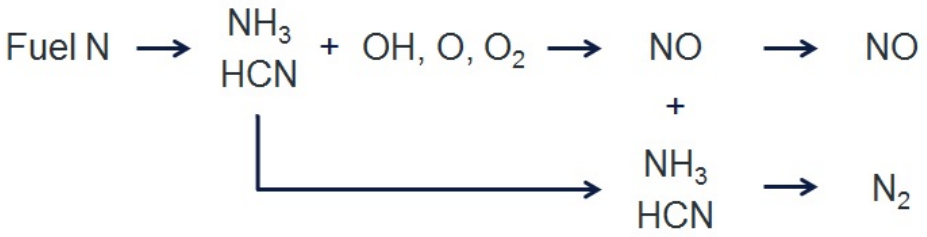

Figure 2.1: Reaction mechanism converting fuel nitrogen to NO and N_2

Reburning is a term introduced by Wendt [16, 17] which refers to the addition of fuel to produce a fuel rich zone wherein NO is reduced to N_2. The stoichiometric ratio (SR) for reburning appears to have an optimum in the range of 0.65 to 0.85 depending on the fuel and temperature [18]. These same reburning reactions are present in the fuel rich recirculation zone of a swirled burner and therefore there should also be an optimal SR within this fuel rich zone for NO reduction.

2.2 Particle Burnout and Loss on Ignition (LOI)

Solid fuel particles have two main types of reaction, volatile combustion and char oxidation. Volatile combustion was discussed briefly with NO formation where light gases react with oxygen. Char oxidation, or particle burnout, is a process that occurs after the volatiles have been released and when carbon remaining in the particle reacts with surrounding oxygen. At the particle surface, carbon can react with an oxidizer via the global reactions shown in Equations 2.10 through 2.13 [19].

$$C + O_2 \Leftrightarrow CO_2 \tag{2.10}$$

$$2C + O_2 \Leftrightarrow 2CO \tag{2.11}$$

$$C + CO_2 \Leftrightarrow 2CO \tag{2.12}$$

$$C + H_2O \Leftrightarrow CO + H_2 \tag{2.13}$$

The primary product at the surface of the particle is CO. The CO will diffuse away from the particle and can react further with O_2, shown in Equation 2.14 [19]. These equations indicate that if particles have not been completely consumed, or oxidized, it may result in a high level of CO in the exhaust gas.

$$CO + \frac{1}{2}O_2 \Leftrightarrow CO_2 \tag{2.14}$$

The final product of the carbon in char is CO_2. Some of the factors that control the rate of char oxidation, or the rate of the consumption of the carbon, are temperature, pressure, and particle size. When the temperature and pressure are high and the particle size is large the diffusion of oxygen to the particle limits the rate of the chemical reaction. This means the chemical reaction happens as fast as oxygen is able to get to the particle and is referred to as a

diffusion controlled reaction. When the temperature and pressure are low and the particle size is small the rate at which the carbon is consumed is limited by the chemical reaction, referred to as a kinetically controlled reaction. Kinetically controlled reactions do not have a dependence on the oxygen concentration. For diffusion controlled reactions an increase of oxygen would increase the rate at which the char particle is consumed, whereas kinetically controlled reactions would be not be as greatly impacted by the increase. It is common for both diffusion and kinetics to play a role in the rate of char oxidation depending on the location of the particle and the time-temperature history.

Loss on ignition (LOI) is an important indicator of combustion efficiency. It is a measure of the amount of mass removed from a particle when completely oxidized. The majority of the mass remaining in coal and biomass ash is carbon although other trace elements may also contribute to mass loss.

To obtain an LOI measurement, ash is placed in a crucible, weighed, heated to remove moisture, and then weighed again. Once the moisture free weight is established, the ash is then subjected to a higher temperature that consumes the remaining carbon, and the mass of the remaining ash is then compared to the mass of the moisture free ash. If there is only a small amount of carbon remaining, the ash will lose only a small amount of mass and will be low in LOI. A larger amount of carbon in the ash will lose more mass through this process and the LOI value will be higher. Section 4.5 contains a detailed process used to measure LOI for this work. The carbon content in the ash can be used as a measure of how much energy is not released upon ignition and reaction. It would be desirable that all the carbon in ash is consumed during the combustion process and that a small amount of carbon remain in the ash.

In addition to revealing combustion efficiency, ash waste from coal is beneficial as an ingredient in concrete and can even contribute to a significant percentage of concrete in roads, but this is only the case if the carbon content of the ash is low. If there is too much carbon in the ash, more than 6% LOI, then the ash must be disposed in a landfill rather than being reused in another form [20].

2.3 Swirl Stabilized Solid Fuel Flames

Swirl is an important parameter used to maintain a stable flame that is reduced in size with increased intensity. Swirl is defined as the ratio of axial flux of tangential momentum to axial flux of axial momentum times the nozzle radius [21]. Equations for the calculation of swirl are shown in Appendix A.1. According to the International Flame Research Foundation, IFRF, there are four classifications of flame types [22]. Each of these is seen in Figure 2.2. Type 0 corresponds to external recirculation. In this flame type there may be some outer rotation, but little swirl is present. Flame type 1 is internal recirculation with fuel jet penetration. This flame is stronger than type 0 and has a closed recirculation zone. Flame type 1 is typical of a characteristic flame as seen in this work. Flame type 2 is where the fuel jet stagnates and spreads in the internal recirculation zone. This recirculation remains closed with no jet penetration and is typically a very short intense flame. Lastly, flame type 3 is the same as flame type 1, but with a second downstream internal recirculation zone. Flame type 3 has high confinement of the flame. As swirl increases the flame type moves from type 0 to type 3.

Swirl not only decreases the length of the flame, but also can reduce flame lift off and improve flame stability. Swirl can be used to improve NO and/or LOI emissions. Swirl is created by adding tangential flow to an axial flow component. When the air exits the tube, the momentum caused by the swirling flow causes air to move outward and produces a low pressure

region in the center. This low pressure in the reactor draws combustion products towards the burner enabling devolatilization of the solid fuel, facilitating ignition of volatiles and the creating of a fuel rich region through which the fuel and recirculated products must pass.

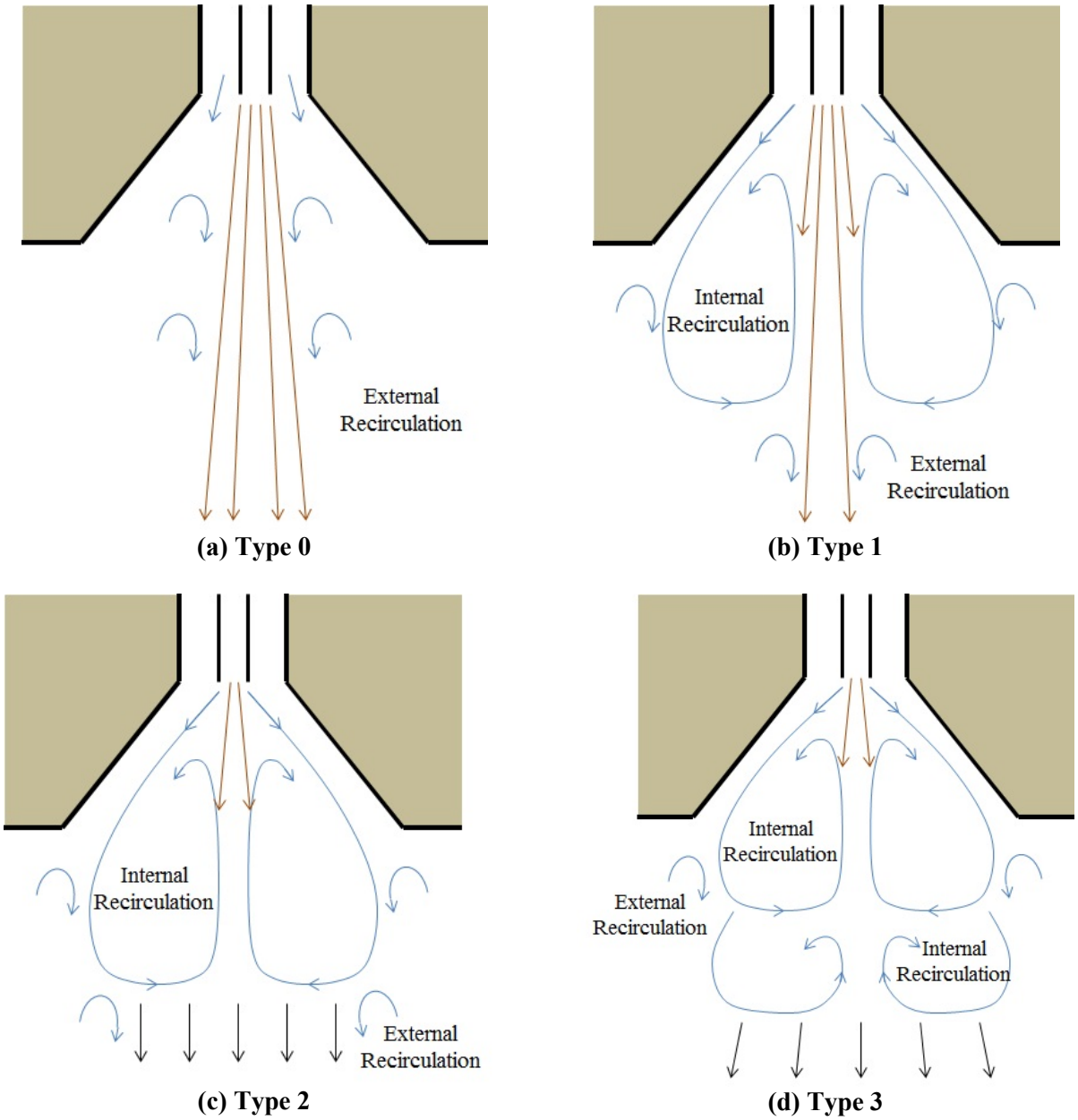

Figure 2.2: Four different types of swirled flames as designated by the IFRF: (a) Type 0, (b) Type 1, (c) Type 2, and (d) Type 3

Figure 2.3 shows a cross-sectional diagram depicting a fuel rich region that is surrounded by a swirled secondary flow. The recirculation zone is important to maintain the fuel rich zone in the center where NO can then be reduced through contact with fuel volatiles. As discussed in Section 2.1, the SR within this fuel rich region controls NO reduction and is expected to be optimal when the SR is in the range of 0.65 – 0.85. Beginning with zero swirl, the addition of swirl will initially decrease NO emissions by creating a fuel rich region and drawing NO in the products through this region. NO emission will reach a minimum as swirl is increased after which additional swirl can cause an increase in NO by leaning out, reducing the fuel richness of, the recirculation zone.

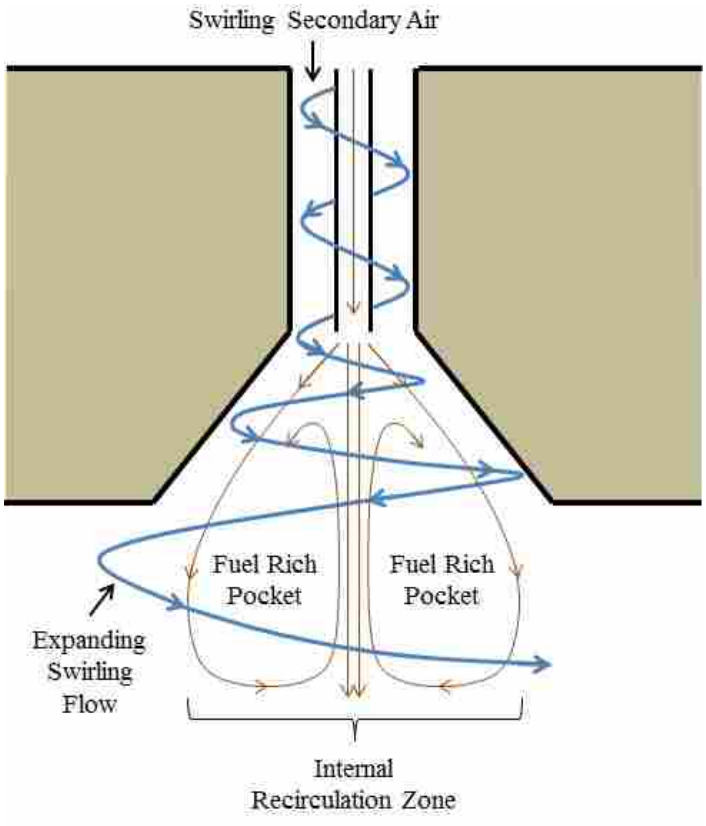

Figure 2.3: Swirled burner cross-sectional diagram depicting a fuel rich region that is surrounded by a recirculating secondary flow

Swirl also has an impact on carbon burnout. The shortened flame produced by increased swirl provides an increased residence time for particles in the post volatile flame region. Having a large amount of swirl can also entrain solid fuel particles effectively into regions of lower axial velocity increasing their residence time. Decreasing swirl typically elongates the flame allowing particles to travel toward the exhaust exit within a fuel rich region without access to burnout oxygen.

It is therefore important to have an appropriate swirl value that is both beneficial to NO_x emission and carbon burnout. In this research effort, oxygen is added in various locations and amounts to flames of varying swirl to determine if the oxygen can be beneficial to burnout without negatively impacting NO emission. One scenario where this might be possible would be the use of oxygen to increase flame temperature and devolatilization rates so that the optimal SR in the fuel rich region can be reached in shorter distances and allow increased burnout.

3 LITERATURE REVIEW

This chapter provides a review of previous research efforts in the area of oxygen injection combustion in biomass flames. This review first provides an explanation and examples of several ways that biomass can be burned and ways in which oxygen can be used in conjunction with biomass for combustion, but the specific topic of the review is limited to oxygen being injected into biomass flames to improve combustion.

3.1 Biomass Swirl Assisted Flames

Although there are several methods used to burn fuels in boilers, one of the most prominent is pulverized coal transported in primary air injected into swirled air (secondary air). The swirl creates the recirculation of hot product gases that ignite and stabilize the flame. Studies have shown that swirl is effective in producing short, intense flames that increase the residence times of solid fuel particles [22]. Swirl was initially introduced to burners for flame stability and to decrease boiler size. Later, swirl and secondary flow was decreased to produce a near burner fuel rich zone followed by tertiary air injection. This staged air is effective at NO_x reduction and is referred to as a low NO_x burner. Low NO_x burners can reduce NO_x up to 50-60% but have flames one and a half times longer than previous burners [23]. Mixing rates for swirled flows also dramatically increase. Chen and Driscoll [24] found that the fuel-air mixing rate of a swirl-stabilized flame is five times greater than a simple diffusion flame, as evidenced by the five times shortening of a methane flame.

While studying a coal flame, Draper et al. [25] concluded that moderate swirl was effective in improving both burnout and NO emissions, but that high swirl resulted in poor burnout. This was believed to be the result of coal particles in a swirled primary flow being transported by radial momentum outside of the secondary oxidizer flow. It is therefore imperative to use the appropriate swirl to minimize NO_x and maintain good carbon burnout.

3.2 Burner Co-Firing

Co-firing is the burning of coal and biomass at the same time. The term, however, can be confusing because boilers typically have several burners and therefore if biomass is burned exclusively in one burner while coal is burned in the other burners, then the boiler is co-firing. It is more economical and more easily implemented to burn a single fuel in each burner and therefore the majority of full-scale co-firing is done by burning different fuels in separate burners. The term burner co-firing will be used to describe two fuels within a burner, and boiler co-firing to describe two fuels in separate burners.

Biomass removes carbon from the atmosphere when grown. It also contains less sulfur and in some cases may also contain less nitrogen. Therefore, co-firing is an option that can reduce the impact of coal emissions on the environment. Baxter [4] concludes that biomass residues represent possibly the cheapest and lowest risk renewable energy option for many power producers. He states that co-firing biomass with coal yields both low-risk and low-cost sustainable renewable energy that promises reduction in net CO_2 emissions and often NO_x emissions.

Experimental results obtained by Kruczek et al. [26] show that in general, biomass burner co-firing, using willow sawdust and mallow, leads to a decrease in NO_x and SO_2 emissions for nearly all coals tested. The particle size of biomass used in the experiment was comparable to

coal where 99% of biomass was smaller than 200 μm. For this particle size, biomass led to a beneficial effect in the burnout of the fuel mixture. The decrease of NO_x emission increased with increasing amounts of biomass.

Testing by Boylan [27] has shown that with biomass burner co-firing, mill power increased and NOx emission were about the same or slightly less than coal firing. With co-firing there is, however, an enhanced slagging and fouling propensity due to the lower fusion temperature of biomass [28].

Munir et al. [29] performed burner co-firing experiments using a Russian coal with a range of biomasses (shea meal, cotton stalk, sugarcane bagasse, and wood chips) to evaluate their potential as an agent for NO_x control. There was a trade-off between NO reduction and carbon burnout in determining optimum conditions. Under the optimum conditions, determined in the study, the air-staging technique using a 10% biomass blending ratio was noted to have a synergistic effect on biomass-coal co-firing for NO_x reductions and carbon burnout. With co-firing under optimum air-staged conditions NO reductions ranged from 49-72% for the biomass fuels.

A comparative study of burner co-firing under oxy-fuel and air conditions was done in a laboratory scale reactor by Pawlak-Kruczek et al. [30]. When combined with carbon capture sequestration (CCS) technology, biomass oxy-co-firing can be a carbon negative technology. NO_x reductions for oxy-co-firing were dependent on the primary stream oxygen concentration. Emissions, specifically NO_x and SO_2, can be minimized from oxy co-firing biomass with coal by controlling the oxygen injection method to the burner. Also, the increase of biomass per amount of coal lowers the SO_2 emission.

Yin et al. [31] modeled coal and wheat straw flames of similar operating conditions and compared their results to data taken previously in the BYU Burner Flow Reactor (BFR). The model suggested coal particles were entrained into the secondary air jet effectively increasing their residence time and oxygen availability. The straw particles were less affected by the swirling air and passed through the recirculation zone into an oxygen-lean core, resulting in low carbon burnout and a large flame volume. The difference between the coal and the straw were attributed to an increased fuel/air jet momentum, lower energy density, and the large particle size of the straw. Larger particles are not as affected by the recirculation zone as small particles and are more likely to penetrate through the stagnation point in a flame.

3.3 Oxygen Usage in Biomass Flames

Oxygen is used in various combustion applications with expected benefits of flame stability, improved burnout, and increased temperature [32]. Three main types of oxygen addition are used and have been explored in numerous studies. They are oxy-fuel or oxy-combustion (OFC), oxygen injection combustion (OIC), and enriched air combustion (EAC). Oxy-fuel combustion and oxygen injection combustion typically require the cryogenic separation of oxygen and nitrogen in air whereas enriched air combustion does not.

3.3.1 Oxy-Fuel Combustion (OFC)

Oxy-fuel combustion does not use conventional air combustion, but relies on the separation of oxygen and nitrogen. This method is typically an expensive retrofit technology as it requires the use of neat oxygen. While OFC will not be a focus in this work, it can offer various opportunities for combustion improvement and provide some insights into OIC and EAC. OFC uses recycled flue gas to help control the temperature of the flame within the reactor and

provides an opportunity for capturing CO_2 from combustion facilities. A reduction in pollutant emissions and improved burnout are among the other potential benefits in OFC. Some of the issues that arise with OFC are heat transfer differences, flame ignition, and flame stability. Toftegaard et al. [33], Buhre et al. [34], and Wall et al. [35] have each given reviews of this technology in great detail.

3.3.2 Enriched Air Combustion (EAC)

Enriched Air Combustion is a method where the oxygen concentration in the secondary air is increased. It is less expensive to implement and operate than OFC. A 0.5 MW Doosan-Babcock burner was used by Smart and Riley [36] to explore oxygen enriched air combustion. The results show that oxygen enriched air combustion is a viable technique for carbon capture and storage providing CO_2 enriched flue gas. Oxygen enrichment can improve CO_2 scrubbing and capture due to the reduced volume of flue gas with higher concentrations, similar to OFC.

Experimental evidence from Daood et al. [37] suggests that for enriched air combustion with coal NO emissions can be reduced along with improvement of carbon burnout. EAC also significantly increases thermal efficiency and improves flame stability. In another study on EAC, NO_x emission has been shown to increase with increasing oxygen concentrations [38].

Nimmo et al. [39] reported for burner co-firing with shea meal and Pakistani cotton stalk in a 20 kW_{th} combustor that oxygen enrichment improved carbon burnout with a positive impact on NO_x emissions. NO_x emissions can either increase or decrease depending on a variety of variables including, but not limited to, stoichiometry of the near-burner zone, flame dynamics, and intensity of combustion related to gas velocity and swirl, i.e. flame attachment, length, etc. To maintain NO_x emission levels within an acceptable range, it may be necessary to adjust the swirl intensity.

Bai et al. [40] investigated the NO and N_2O formation characteristics for five biomass fuels (rice straw, wheat straw, corn stalk, sugarcane leaf, and eucalyptus bark) and one bituminous coal in a horizontal fixed-bed reactor. They determined that NO and N_2O were formed primarily in the devolatilization stage for the biomass fuels and that optimizing air and fuel during biomass combustion would allow achievement of ultralow nitrogen oxide emissions. While there was no correlation found between NO and N_2O yields and fuel nitrogen, the fuel nitrogen conversion to NO and N_2O increased with the increase of inlet oxygen concentration and became more pronounced at higher temperatures.

Other results from using small biomass and coal particle sizes have shown improvements to both burnout and NO particularly with oxygen enriched or oxy-fuel combustion [41].

3.3.3 Oxygen Injection Combustion (OIC)

Oxygen injection combustion is a technique where oxygen is added to a specific location via a lance. Oxygen can be injected in varying quantities and various locations within the burner or throughout the combustion chamber. This method is targeted to improve flame stabilization, lowering emissions, and improving ignition.

In a study by Marin et al. [42] OIC was used with Illinois coal focusing on NO_x and carbon burnout. They noted a deterioration of combustion, or increase of unburnt carbon, that accompanied a reduction in NO_x emissions upon air staging. Upon injecting oxygen, the LOI decreased to about 60% of the base operation while NO_x emissions were relatively unchanged compared to operation that was seen using tertiary air without oxygen. Their experimental work suggested the means, or location, where oxygen is introduced plays an important role in optimizing performance.

Bool et al. [11, 12] has investigated oxygen injection with pulverized coal for various size burners, from pilot- and full-scale single burners to commercial operation. Their work includes various oxygen lance designs. Included in their results are comparisons between the various lance designs and the effect of NO_x reductions with varying oxygen replacement rates. NO_x emissions increased with the increase of swirl. They also found that direct oxygen injection with a lance provided a dramatic improvement on flame stability and length, particularly when air staging with commercial operation. NO_x emissions were reported to have been reduced by as much as 60%, 45% for commercial systems, from a staged baseline. It was noted that a slower mixing strategy allows a wider range of oxygen replacement, while achieving good flame stability, improving carbon burnout, and reducing NO_x. Adding oxygen to the combustion can accelerate ignition and enhance the yield of volatiles, which will yield higher flame temperatures. They advise that care must be taken so that oxygen doesn't 'punch through' the fuel rich portion of the flame, which in some cases can lead to an increase in NO_x.

Other experiments use oxygen as an aid to reduce emissions and determine relationships of emissions and oxygen injection. Draper et al. [25] found that by injecting O_2 into the center of the swirled flow, NO emission increased and initially improved burnout, but decreased burnout at flow rates above 8.54 kg/hr. Moderate swirl improved aspects of the burner, such as improved burnout and reduced NO_x. Generally, burnout was limited by the transport of oxygen to the particle surface. NO_x formation and control in oxy-coal flames was similar to air-fired coal flames. While NO was seen to decrease with increasing swirl, it was attributed to a reduction in oxygen entrainment prior to volatiles combustion. An increase in center O_2 flow rate generally increased NO, and conversely burnout was generally reduced when center O_2 injection increased. Either too much swirl or too much O_2 injection produced undesirable effects. The addition of

CO_2 also increased flame lift-off and entrainment into the fuel rich recirculation zone which increased NO and improved burnout.

Previous research by Thornock [14] with the same reactor used in this work showed that OIC improved LOI for medium wood particles, but had little impact on LOI for small wood particles. The addition of oxygen was more beneficial in aiding the combustion of the medium particles. The amount of increased NO emissions for the small particles was significantly higher than for medium particles under similar oxygen flow rates. This work will continue exploring OIC for wheat straw and hardwood and its effects on NO_x and LOI as well as provide additional insight into EAC. A main focus will compare EAC and OIC along with various injecting techniques. Oxygen injected via a lance in the center corresponds to OIC and oxygen added to the secondary line, or global enrichment, corresponds to EAC.

3.4 Summary and Objective

Biomass combustion with particle size similar to that of coal has been found to be beneficial for almost all aspects of combustion emissions. Biomass particles in practical applications, however, are larger and can produce problems with flame stability, burnout, and heat generation in addition to deposition. Oxygen addition has been found to improve both NO_x and carbon burnout in coal flames although data on the simultaneous reductions are limited. An extensive data set establishing conditions under which NO_x and LOI reductions can be achieved for biomass flames utilizing OIC or EAC are lacking. The objective of this work is to explore the benefits of oxygen injection combustion and enhanced air combustion on swirl stabilized biomass flames.

4 EXPERIMENTAL SETUP AND METHOD

This chapter details the facilities and supporting equipment used to perform the experiments in this work. Other information in this chapter includes fuel analyses and experimental method.

4.1 BYU Combustion Facility

The experiments were completed at the BYU oxy-combustion research facility shown schematically in Figure 4.1. The fuel was burned in a 150 kW_{th} down-fired Burner Flow Reactor (BFR). The BFR is a cylindrical chamber with an inside diameter of 750 mm and length of 2.4 m, consisting of six vertical, 400 mm sections. Each of the sections has four access ports 90 degrees apart. The access ports are rectangular in shape with a height of 280 mm and width of 90 mm. The burner was mounted at the top and the fuel was down-fired. The reactor has a movable-block, variable-swirl burner designed by Air Liquide.

The BFR is refractory lined on the inside and surrounded by water cooled walls. At the base of the reactor there is a water barrel to catch deposits and to maintain positive pressure within the reactor. Primary, secondary, and tertiary air lines are supplied by an Ingersol Rand Compressor. A 265 liter liquid dewar supplies neat oxygen to the BFR in various locations using the equipment as described and documented by Zeltner [43]. The fuel is fed to the reactor via a bulk bag unloader and a gravimetric, computer-controlled, dual auger feeder.

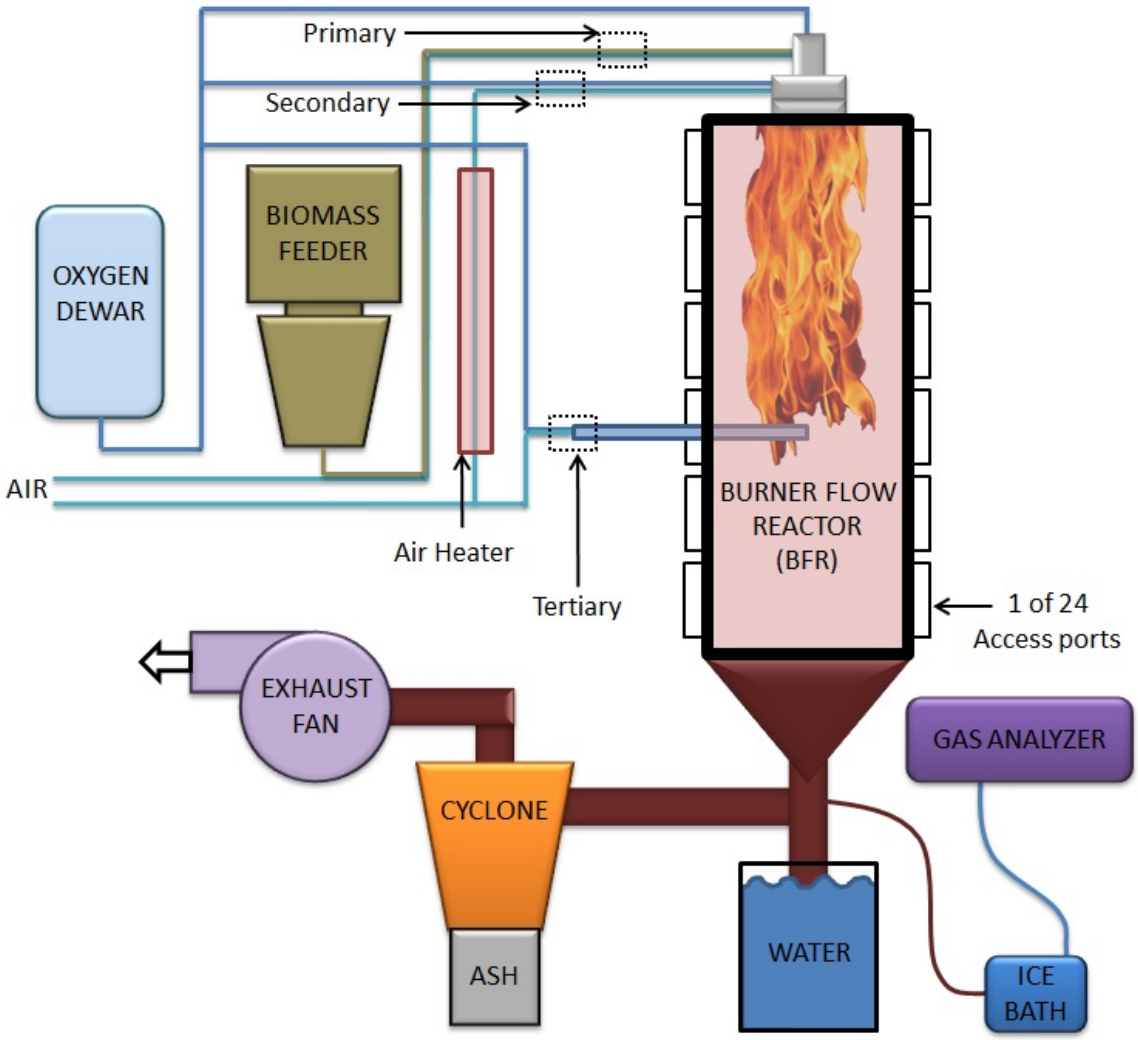

Figure 4.1: Schematic diagram of the Burner Flow Reactor (BFR) and supporting equipment

The main types of data collected include exhaust gas measurements, exhaust ash samples, and visual flame characteristics in the reactor. Exhaust gas measurements were analyzed using a PG-250 Horiba gas analyzer after an ice bath condensed and captured water in the products. Gases measured using the analyzer included O_2 (galvanic cell), CO_2 (ND-IR), CO (ND-IR), and NO_x (chemiluminescence). The ash samples were collected in a barrel below a post-combustion cyclone. The cyclone has been shown to collect particles above 2 μm. ASTM procedure D7348 was used to determine loss on ignition (LOI) of the ash samples. Flame length, attachment, and

O_2 flame characteristics were recorded from visual observation through glass windows on the access ports of the reactor.

4.2 Fuel Analyses

Three types of biomass fuels, wheat straw, medium hardwood, and fine hardwood, were used in this work. The proximate and ultimate analyses of the three types of fuel are displayed in Table 4.1. The fuels have similar proximate and ultimate analyses with some difference in the amount of ash and nitrogen. The straw has twice as much nitrogen content as the medium hardwood (0.54% versus 0.26%) but neither has particularly high nitrogen content.

The ash content is much higher in the straw, 4.5%, compared to the wood, 0.3% and 0.54%. In addition to the larger ash fraction, ash from straw typically contains alkali which lowers the melting temperature. This combined with the larger ash fraction causes a much larger deposition rate for ash but the ash does not significantly impact combustion properties such as flame length and flame stability. The fine wood is very similar to the medium wood, despite being derived from different biomass stock.

The three fuels also differ in particle size distribution as shown in Figure 4.2. Both the straw and the medium wood have a similar mean particle size but the wood particles have a much narrower size distribution meaning that the straw has both a greater number of larger and a greater number of smaller particles. The straw may therefore be easier to ignite because of the larger number of small particles but also more difficult to burn out because of the large particles. Damstedt et al. [44] showed that straw contains particles called knees that are difficult to grind and burn. The knees originate from the material between the hollow tube-like portions of the straw. These knees are more dense and less volatile than the remainder of the straw particles.

Table 4.1: Proximate and ultimate analysis (as received), heating value, and mean particle size of the three biomass fuels used

Proximate (as received, wt.%)	Straw Particles	Med. Wood Particles	Fine Wood Particles
Moisture	7.15	5.28	5.83
Ash	4.56	0.30	0.54
Volatiles	73.81	79.06	76.42
Fixed Carbon	14.48	15.36	17.21
Ultimate (as received, wt.%)			
H	5.68	5.40	5.36
C	47.3	49.85	49.87
N	0.54	0.26	0.32
S	<0.01	0.09	0.10
O	41.6	38.82	38.82
HHV (kJ/kg)	17,069	17,463	17,638
Mean Size (μm)	451	500	224

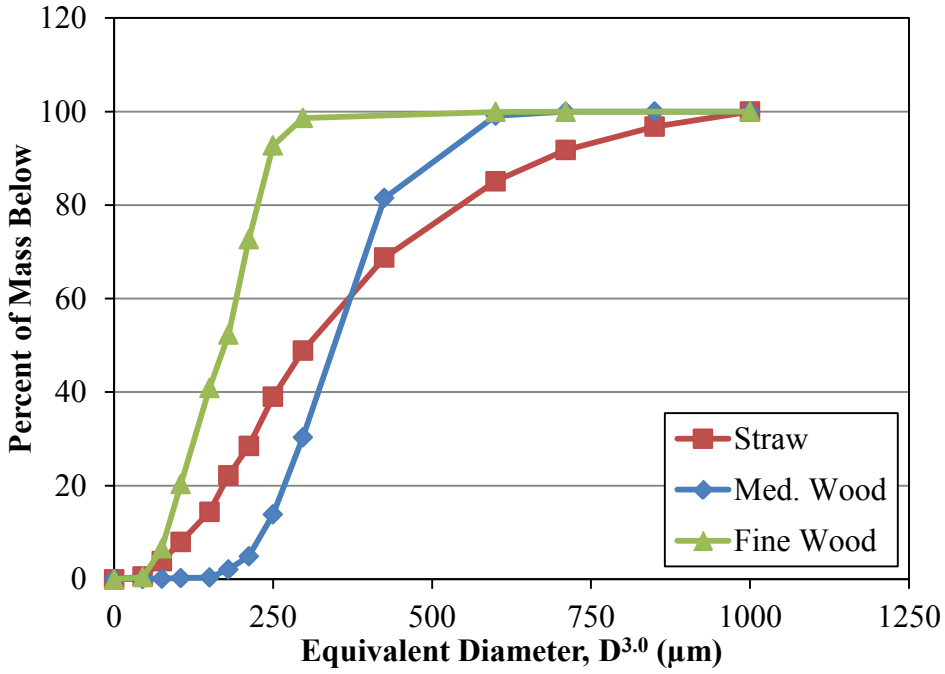

Figure 4.2: Size distributions for the solid fuel particles

4.3 Burner Configurations and Operating Conditions

Below the variable block swirl chamber, the burner, designed by Air Liquide, utilized three concentric tubes creating three flow channels. Multiple configurations were possible by using tubes of various diameters. The tubes are numbered consecutively from the center outward 1-3, see Figure 4.3. For tube 1, three sizes are available: small, medium, and large. For tube 2, two tubes: small and large. And for tube 3, two tubes: small and large. Abbreviations are used to specify the burner configurations: for example 1S2L3L indicates the inner tube is small, the second tube is large and the outer tube is large. The relative diameters of each tube in comparison to the smallest diameter for tube 1 (19.05 mm) are shown in Table 4.2.

Figure 4.3 shows the cross section of the pipe in pipe burner showing locations of the three concentric flows. Flow channel 1 represents the center tube of the burner through where neat oxygen was typically injected. Flow channel 2 represents the annulus through which fuel was entrained with the primary air. The flow rate of fuel was held constant at 29 kg/hr biomass. This was selected to produce a nominal heating rate of 150 kW_{th} which is sufficient to maintain wall temperatures that will ignite and continuously burn fuel in the reactor. The primary air was held constant at 14 kg/hr for both hardwood fuels and 20 kg/hr for straw unless otherwise specified. In flow channel 3, secondary air was preheated to about 260 ℃ and held at a baseline flow rate of 170 kg/hr for medium hardwood, 180 kg/hr for fine hardwood, and 158 kg/hr for straw. The flow rate for primary air was selected by determining the lowest flow rate that would consistently convey fuel from the feeder to the burner without plugging. The secondary air flow was swirled using a variable swirl block prior to the burner exit. A ceramic quarl sits outside of flow channel 3 that is shown in Figure 4.3 extends a relative length of 4.167 from the burner exit and has dimensions as contained in Table 4.2.

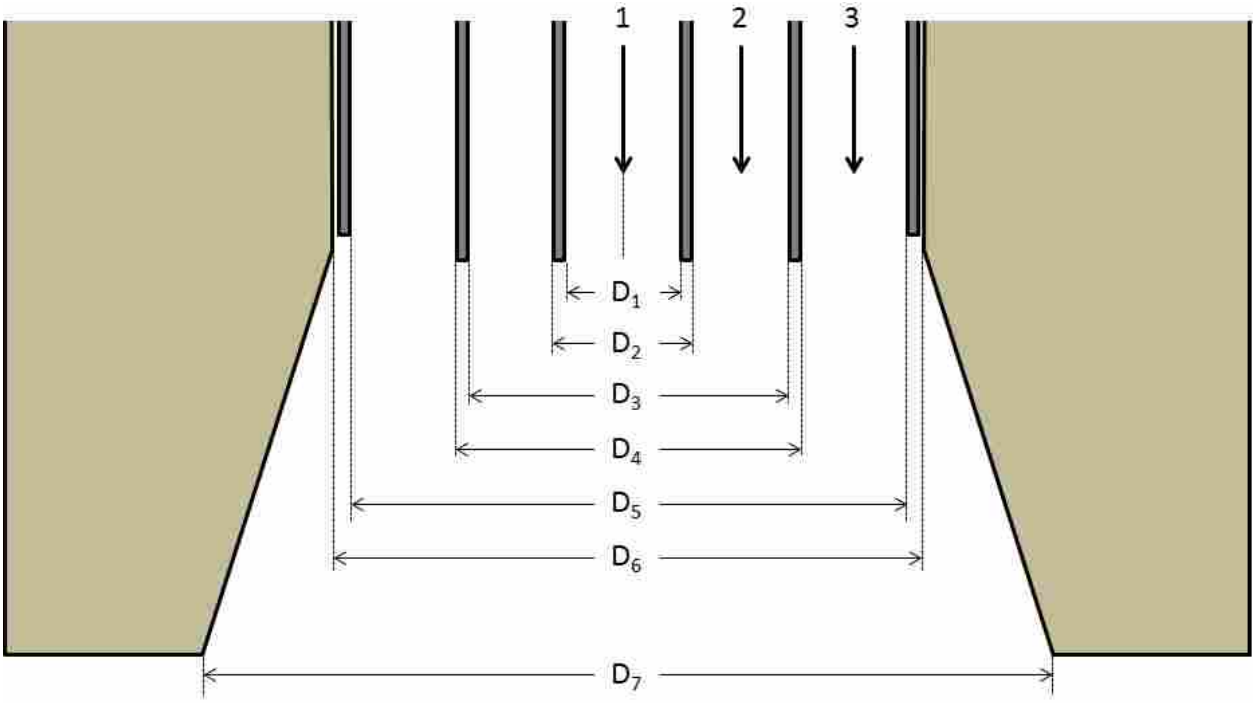

Figure 4.3: Design of Air Liquide pipe in pipe burner showing locations of three concentric flows

Table 4.2: Relative diameters of each of the tubes in the Air Liquide Burner

	S	M	L
D_1	1.000	1.500	1.840
D_2	1.400	1.753	2.213
D_3	2.243	N/A	2.876
D_4	2.533	N/A	3.167
D_5	5.667	N/A	7.000
D_6	6.167	N/A	7.500
D_7	8.833	N/A	10.500

Multiple burner configurations were used in the work presented here. The physical position of the swirl blocks was typically fixed at three primary locations corresponding to maximum swirl and two other locations identified by the number of turns on the screw that moves the swirl block (0, 6 and 9 turns). This led to the ideal secondary swirl numbers shown in

Table 4.3 for the case where no oxygen was added. As oxygen was added to the center tube, the swirl decreased slightly as there was no tangential component in the center flow, but increased axial flow. Oxygen added to the secondary air negligibly increased the swirl.

Various operating conditions were completed for the selected number of configurations used. For most of the conditions, oxygen varied from 0 – 8 kg/hr, in increments of 2 kg/hr. This sweep of oxygen flow rates was completed for combinations of six burner configurations, three oxygen locations, and the three fuels. The matrix of operating conditions for these configurations is presented in Table 4.3.

Table 4.3: Test matrix of burner geometry configurations, flow rates, and condition nomenclature

Condition	Fuel Type	Burner Configuration	O_2 Flow Rates (kg/hr)	Swirl (0, 6, 9 Turns)
1	M. Wood	1S2S3S	0, 2, 4, 6, 8	1.16 (0 Turns)
2	M. Wood	1S2L3S	0, 2, 4, 6, 8	1.02, 0.78, 0.59
3	Straw	1S2L3S	0, 2, 4, 6, 8	1.00, 0.77, 0.58
4	F. Wood	1S2L3L	0, 2, 4, 6, 8	1.44, 1.11, 0.84
5	M. Wood	1S2L3L	0, 2, 4, 6, 8	1.44, 1.11, 0.84
6	Straw	1S2L3L	0, 2, 4, 6, 8	1.40 (0 Turns)
7	Straw	1M2L3S	0, 2, 4	0.77 (6 Turns)
8	M. Wood	1M2L3L	0, 2, 4, 6, 8,12,16	1.43, 1.10, 0.84
9	M. Wood	1L2L3L	0, 2, 4, 6, 8	1.41, 1.09, 0.82

In addition to the multiple configurations and conditions, a variety of modified oxygen lance tubes were used to explore the impact of how the oxygen was injected into the reactor. In Figure 4.4, the five different oxygen lances used in data collection are shown schematically. The modifications bluff-body, four-hole, and eight-hole were done to one center tube, size medium, and the modification six-hole was done to one center tube, size small. The large size center tube remained unchanged. Data with the open lance was taken with two center tubes, sizes small and

large. Adding oxygen into lances four-hole, six-hole, and eight-hole are termed premixed, as they premix the oxygen with the fuel before the burner exit.

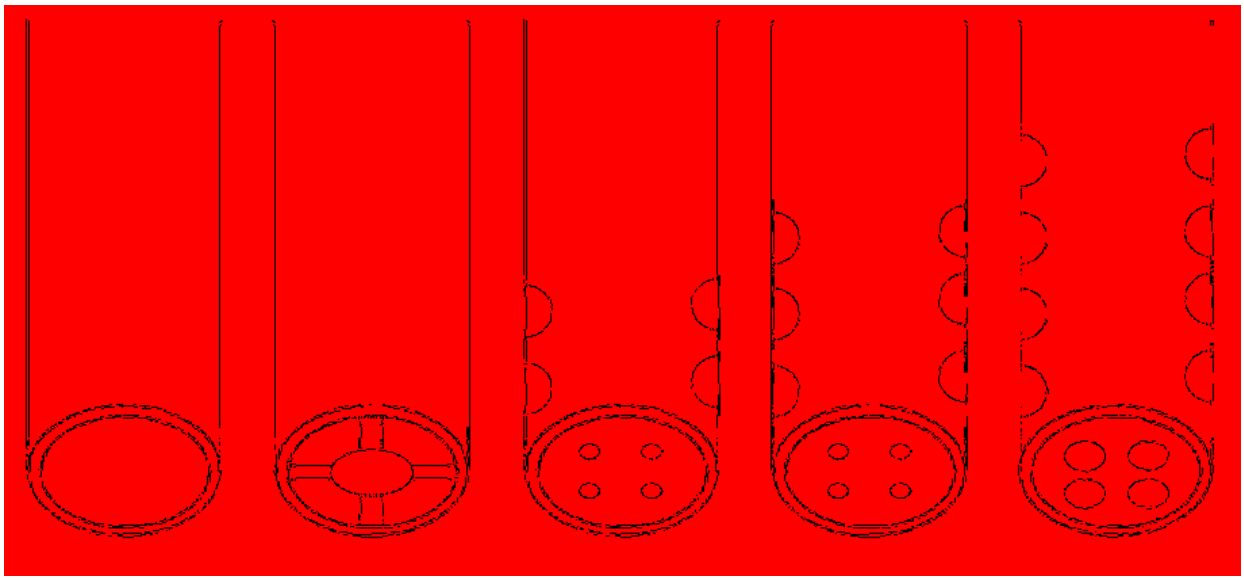

Figure 4.4: Schematic of various oxygen lances used in data collection; tubes are named from left to right: open, bluff-body, four-hole, six-hole, and eight-hole

Another test strategy explored was the injection of air in a tertiary line, depicted in Figure 4.1. This allowed for a fuel rich region near the burner and an air rich region near the reactor exit. This was completed for one configuration, 1S2L3L, and various oxygen flow rates. Staged air, as it is termed, utilized center injection oxygen, but began under the base operating condition of a fuel rich region in the top section followed by a burnout section aided by the tertiary over-fire air. An oxygen flow rate of 6 kg/hr would be sufficient to allow for complete combustion without the addition of the tertiary air, and the maximum amount of oxygen injected into the center used was 8 kg/hr.

Simply increasing the secondary air, termed air addition, was yet another oxygen addition method that was used. This is comparable to global enrichment, or adding oxygen to the secondary air, except nitrogen is also being increased. For air addition, secondary air increased

incrementally in amounts comparable to 2, 4, and 6 kg/hr of oxygen (roughly 9, 17, and 26 kg/hr of air). Additional air was not added further due to the pressure of the supply line.

Lastly, the burner is capable of varying the exit location of the center tube relative to the other tubes in the burner. The tube could be mounted flush, recessed, or extended beyond the exit plane of the other two tubes. Multiple experiments were completed at various amounts of recess and extension as well as a flush position with the burner exit.

4.4 NO Measurements

A continuous flow of the exhaust gas was sampled near the reactor exit as seen in Figure 4.1. The sample line first went through an ice bath to condense the water out of the exhaust line and then continued to the gas analyzer. Upon entering the analyzer the gas passes through a desiccant to produce a dry measurement. A PG-250 Horiba gas analyzer measured O_2 (galvanic cell), CO_2 (ND-IR), CO (ND-IR), and NO_x (chemiluminescence). Each of these gas species were recorded three times at each operating condition during ash collection. The majority of this work focuses on NO emission data collected and is reported herein. A calibration was completed in the morning each day that data were collected. Changes in calibration from day to day were typically less than 10%.

Two Rosemount Analytical ND-IR analyzers, for CO_2 and CO, and a Beckman chemiluminescence analyzer, for NO_x, were used intermittently to verify the accuracy of the gas measurements. A continuous zirconia based O_2 sensor, like those used in automobile exhaust lines was located near the gas sampling location. This sensor was used to monitor reactor operation and provided a wet O_2 concentration for comparison with the Horiba galvanic cell measurement. After correcting for wet vs dry O_2, the two sensors were normally in very good

agreement. Any differences between the two measurements were used to identify and correct problems with the Horiba sample line.

4.5 Ash Collection and Loss on Ignition

Ash samples were collected in a barrel below the cyclone at the base of the reactor as shown in Figure 4.1. Approximately 5 minutes after changing an operating condition, gases measured became steady. At this point, an ash sample was initiated. To begin ash sampling, a thin metal plate was cleaned and placed in the bottom of the cyclone barrel. The barrel was also cleaned with a jet of air before each sample. Once sufficient time passed for the ash to collect in the barrel, roughly 5 to 10 minutes, the metal plate was removed and the ash was placed in a small vial. Finally, the ash samples were placed in crucibles for loss on ignition (LOI) measurement.

LOI is a measure of the mass fraction removed from a dried sample when heated to a temperature high enough to oxidize the non-inert material. Typically, the mass removed is almost entirely carbon and therefore LOI can be used to approximate carbon burnout. ASTM procedure D7348 was normally used to determine LOI for the ash samples. This procedure involves first heating the particles to 105℃ for 4 hours to remove the moisture. The weight of the moisture free ash, W_{mfa}, is then measured. The ash is then heated to 950℃ for 6-8 hours and weighed to produce the weight of the carbon free ash, W_{cfa}. The two weights are then used to calculate the LOI and carbon burnout as shown in Equations 4.1 and 4.2. Y_{ash} is the ash content as determined from the proximate analysis of the fuel. This procedure was repeated three times for each sample and the average of those three measurements is reported as the LOI value for that sample.

$$LOI = \frac{W_{mfa} - W_{cfa}}{W_{mfa}} \tag{4.1}$$

$$Carbon\ Burnout\ \% = \frac{1 - Y_{ash} - LOI}{(1 - LOI) * (1 - Y_{ash})} \tag{4.2}$$

This procedure was found to be problematic for the straw ash. The straw ash melted and sintered together at 950℃ making complete oxidation of the carbon difficult as it became trapped beneath molten slag. The oxidation temperature was lowered from 950℃ to 750℃ for the straw ash to allow the carbon particles to be consumed without sintering. Tests were then completed to verify the effectiveness of the adjusted method. Samples were removed and weighed after various time periods at 750℃ until the weight reached a minimum and was no longer changing. It was determined that a longer period of time, 10-12 hours, at the lower temperature is needed to ensure complete burnout. Results at the lower temperature on wood ash were also compared to results at the higher temperature to ensure all of the carbon was being oxidized. At a temperature of 750℃ the wood ash resulted in nominally the same LOI as was found at 950℃, see Table 4.4. The table reveals that the higher temperature for the straw was ineffective at producing the total LOI as the mass sintered before the carbon was entirely consumed. Data confirmed that the lower temperature of 750℃ was high enough to complete carbon oxidation.

Table 4.4: LOI measurements from two different fuels and temperatures

Sample	LOI at 950°C	LOI at 750°C	Difference
M. Wood 1	38.21 %	38.61 %	-1.05 %
M. Wood 2	29.28 %	29.10 %	0.59 %
M. Wood 3	23.04 %	22.93 %	0.47 %
M. Wood 4	18.45 %	18.59 %	-0.78 %
Straw 1	25.55 %	20.61 %	19.36 %
Straw 2	18.05 %	14.50 %	19.68 %
Straw 3	16.27 %	11.09 %	31.85 %
Straw 4	9.97 %	6.51 %	34.69 %

5 NO AND LOI RESULTS AND DISCUSSION

Experimental results presented in this chapter include measurements of NO exhaust gas and LOI. Relationships between various operating conditions are presented. Following the presentation of the data, the results will be summarized and discussed.

5.1 Nitric Oxide Emission (NO)

The following data present the impact of swirl, oxygen flow rate, oxygen injection location, and burner configuration on NO in the exhaust. All of the results shown in this section are for medium hardwood biomass. The reported NO measurements are an average of three recorded values at each operating condition during simultaneous ash collection.

5.1.1 NO vs. Swirl

The effect of swirl and oxygen flow rate on exhaust NO, for a burner configuration of 1S2L3L, can been seen in Figure 5.1. Solid lines connect points of equal oxygen flow rate and variable swirl. Figure 5.1a shows data where the oxygen is added to the secondary line (global enrichment) and Figure 5.1b shows data with oxygen being injected through the center via a lance that is in a recessed position of 76 mm from the burner exit plane. For all cases the secondary air flow rate was held constant.

The exhaust NO concentration is seen to increase with an increase in swirl and with an increase in O_2 flow rate. While the increase in NO is relatively linear with increasing swirl, the increase in NO is non-linear with increasing O_2 center injection.

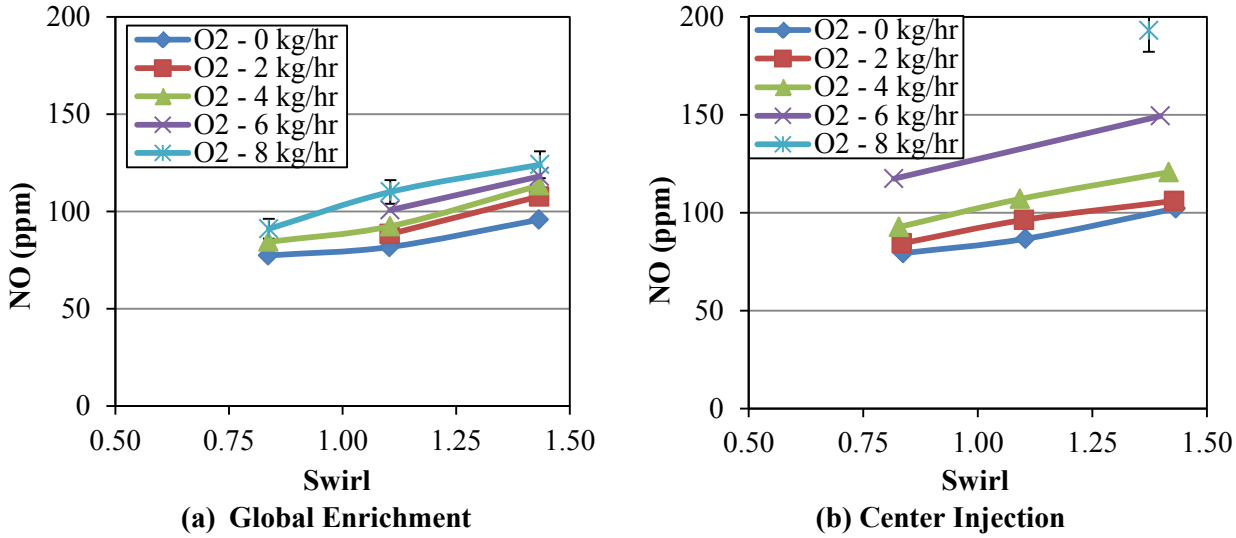

Figure 5.1: NO (ppm) vs. Swirl at varying oxygen flow rates, configuration 1S2L3L, medium hardwood, constant secondary air for (a) Global Enrichment and (b) Center Injection

Error bars located on this plot were determined by an uncertainty analysis provided in Appendix B.1. Precision error for NO was determined to be negligible compared to instrument bias and measurement repeatability. To reduce bias error, the exhaust analyzer was calibrated prior to each day of measurement collection. The most significant source of error was found to be process repeatability. The repeatability was determined by comparing results from 12 data sets where the same operating conditions were repeated at least once. The standard deviation for each of these twelve data sets was calculated and multiplied by two. The standard deviation was then divided by the average to obtain the uncertainty for each of the twelve repeated data sets and this uncertainty was averaged to obtain the results in Table 5.1; ± 5.58% for NO and ±

14.83% for LOI. These are conservative uncertainties that apply to all of the NO and LOI data presented. Error bars have not been added to most of the graphs to maintain readability.

Table 5.1: Summary of uncertainty in the measurements taken

Measurement	Total Relative Error
NO	± 5.58%
LOI	± 14.83%

Figure 5.2 shows NO versus swirl for three burner configurations, all with medium hardwood, constant secondary air, and no oxygen addition. These data show that NO is dependent on both swirl and burner configuration. Swirl alone is insufficient to correlate NO from different burners.

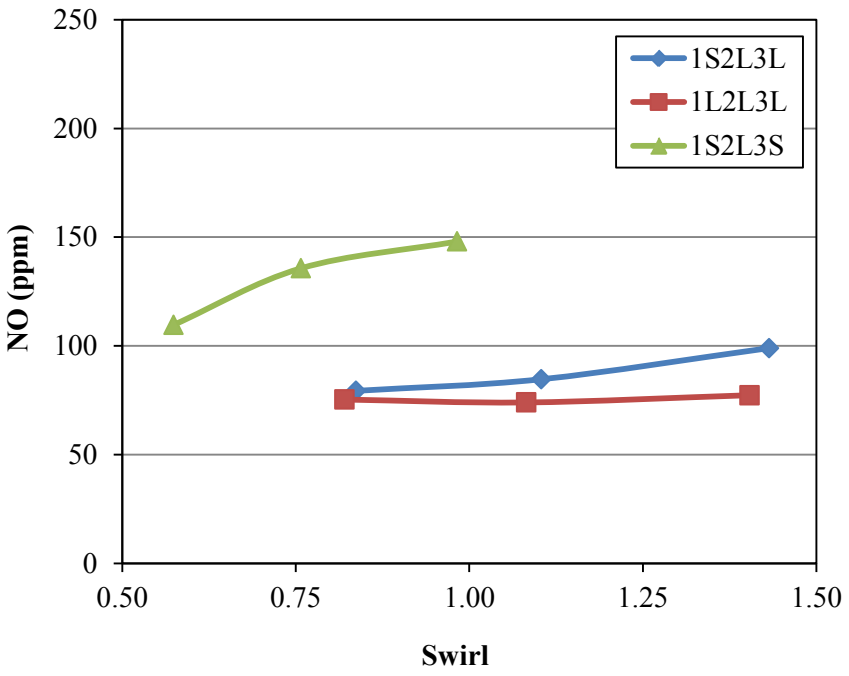

Figure 5.2: NO (ppm) vs. Swirl for various burner configurations, no oxygen, medium hardwood, and constant secondary air

5.1.2 NO vs. O_2

Figure 5.3 shows NO versus oxygen flow rate in the center tube for four different burner configurations. Generally NO increases with increasing O_2 flow rate. Adding small amounts of O_2 (2-4 kg/hr) generally has less impact on NO than larger amounts. As shown previously, NO does not correlate with swirl alone and changes significantly because of burner configuration (geometry).

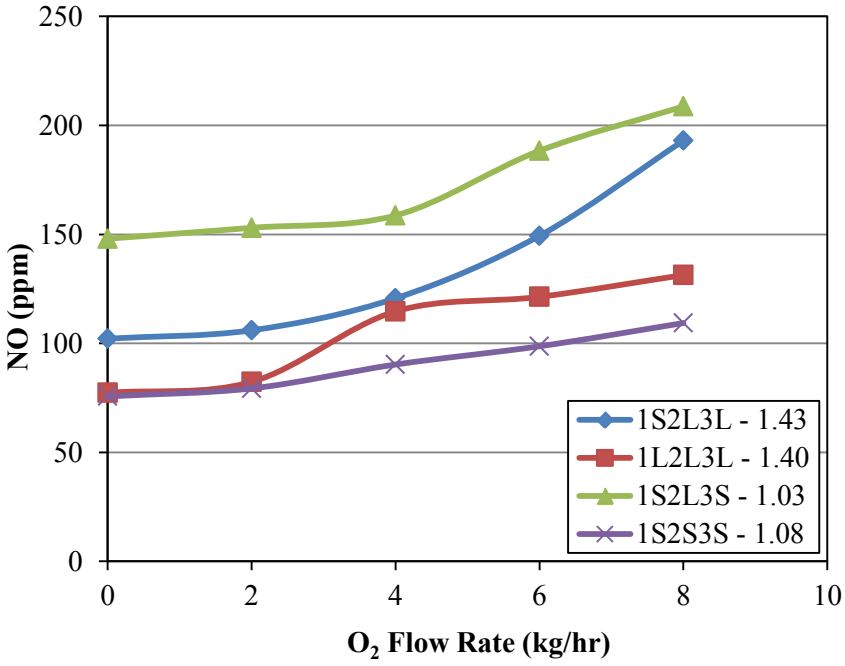

Figure 5.3: NO (ppm) vs. Oxygen Flow Rate (kg/hr) for four configurations at maximum swirl, medium hardwood, center injection, and constant secondary air

Figure 5.4 shows additional data where O_2 sweeps were performed at three swirl values, center oxygen injection, hardwood biomass, configuration 1S2L3L. In this case, the center tube was extended 70 mm from the end of the burner but otherwise conditions were the same as Figure 5.1b where the center tube was recessed 76 mm. The trends with this configuration are the same as those with the oxygen tube extended. Small amounts of O_2 addition (2 kg/hr or less)

produced only small increases of NO. With higher flow rates of oxygen in the center tube, NO emissions increased more significantly.

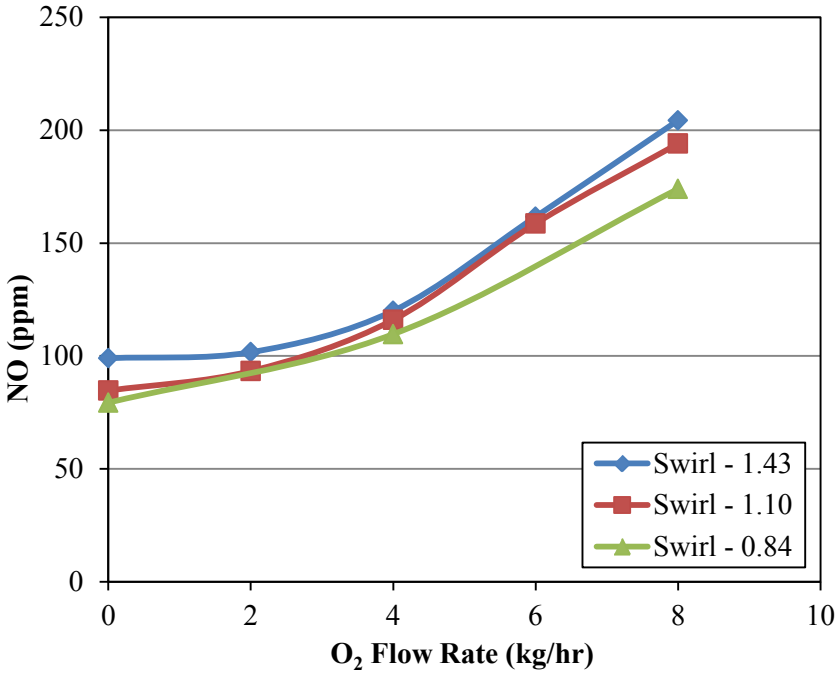

Figure 5.4: NO (ppm) vs. Oxygen Flow Rate (kg/hr) and varying swirl for the medium hardwood, configuration 1S2L3L, center injection, tube 1 extended 70 mm

5.1.3 NO vs. Primary Air

Figure 5.5 shows NO as a function of primary air flow rate for configuration 1S2L3L. In one case, the center tube is recessed 76 mm and in the other case, the center tube is flush with the end of the burner and utilizes the six-hole lance as shown in Figure 4.4. In both of the data sets shown, there is no oxygen introduced into the reactor. The data show that an increase in primary flow decreases NO and that the center tube recessed produces more NO than a flush center tube.

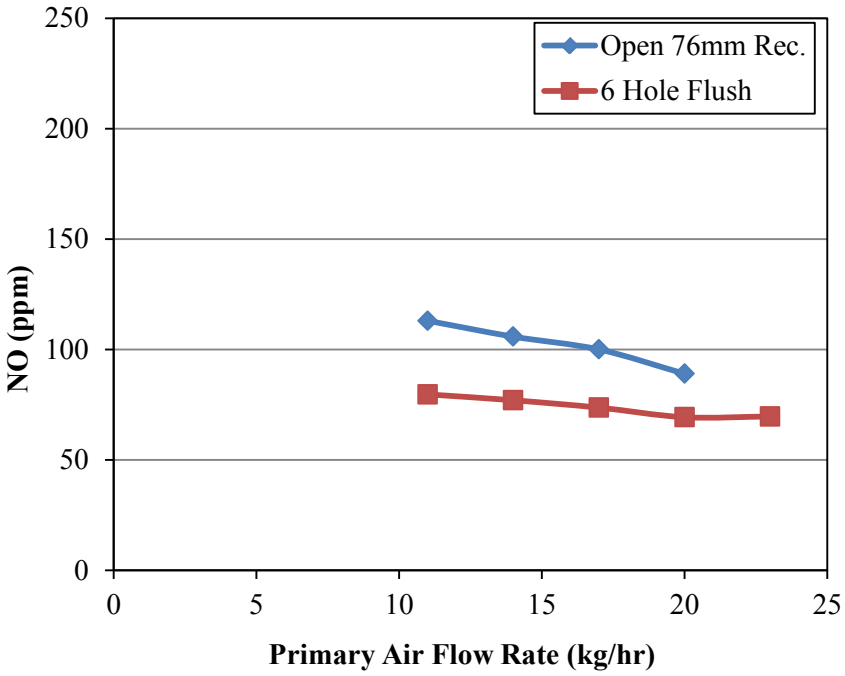

Figure 5.5: NO (ppm) vs. Primary Air Flow Rate (kg/hr) for the medium hardwood, configuration 1S2L3L

5.1.4 NO Summary

In summary, the addition of swirl and oxygen both tend to increase NO emissions in the exhaust. Small amounts of O_2 addition (2-4 kg/hr) produced only a small increase in NO but with center injection, NO increased nonlinearly and more rapidly as O_2 flow increased. When O_2 was added to the secondary air or global injection, the NO increase was slower and more linear at all flow rates. The exhaust concentration of NO at a given swirl was dependent on burner configuration, both the relative diameters of the tubes and the location of the center tube.

5.2 Loss on Ignition (LOI)

This section shows the impact of swirl, oxygen flow rate, oxygen injection location, and burner configuration on LOI. The LOI values reported are an average of three measurements from a single ash sample.

5.2.1 LOI vs. Swirl

The effect of swirl and oxygen flow rate on LOI, for a burner configuration of 1S2L3L, can be seen in Figure 5.6. Figure 5.6a shows data where the oxygen is added to the secondary line (global enrichment), and Figure 5.6b is for center injection. The trends for LOI are opposite in comparison to NO. As swirl increases, LOI decreases. In these figures, the secondary flow rate is held constant effectively increasing the oxygen concentration in the exhaust. As the oxygen flow rate increases the LOI decreases. The LOI values for both global enrichment and center injection are comparable for most oxygen flow rates and swirl values.

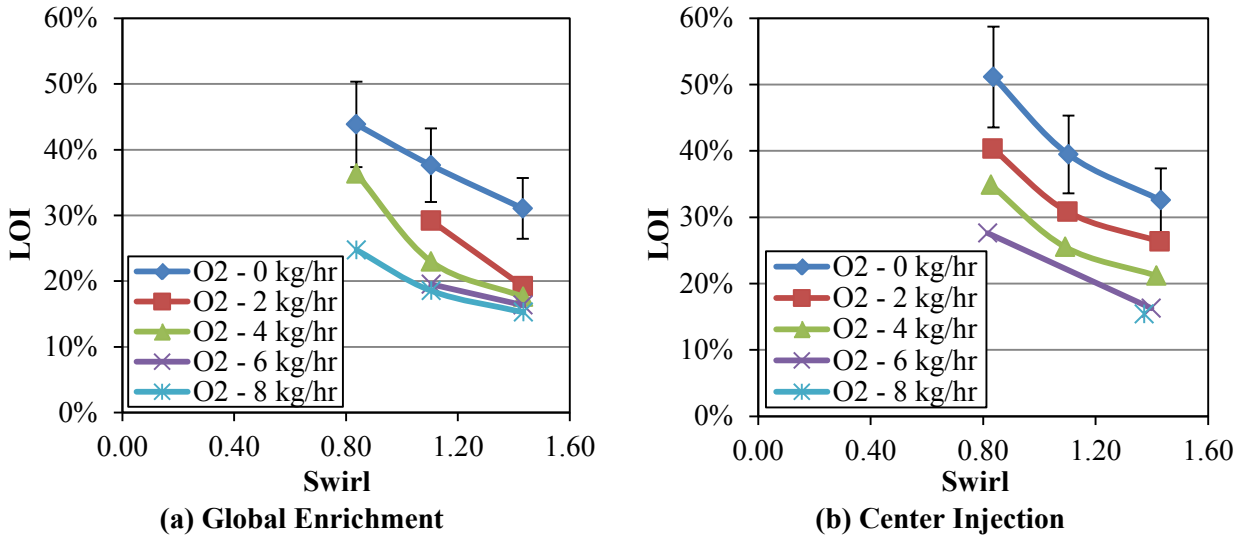

Figure 5.6: LOI vs. Swirl at five flow rates of oxygen in the center, configuration 1S2L3L, medium hardwood, and constant secondary air for (a) Global Enrichment and (b) Center Injection

Error bars on this plot were determined by an uncertainty analysis and explained in the Appendix B.1. See Table 5.1 for a summary of the uncertainty values. These errors bars are estimated to be the error associated with all collected LOI data herein. Most of the remaining plots are shown without error bars.

Figure 5.7 shows LOI versus swirl for three burner configurations, same as those shown in Figure 5.2. These data show that LOI has a dependence on both swirl and burner configuration. Swirl alone cannot be used to correlate LOI from various burners.

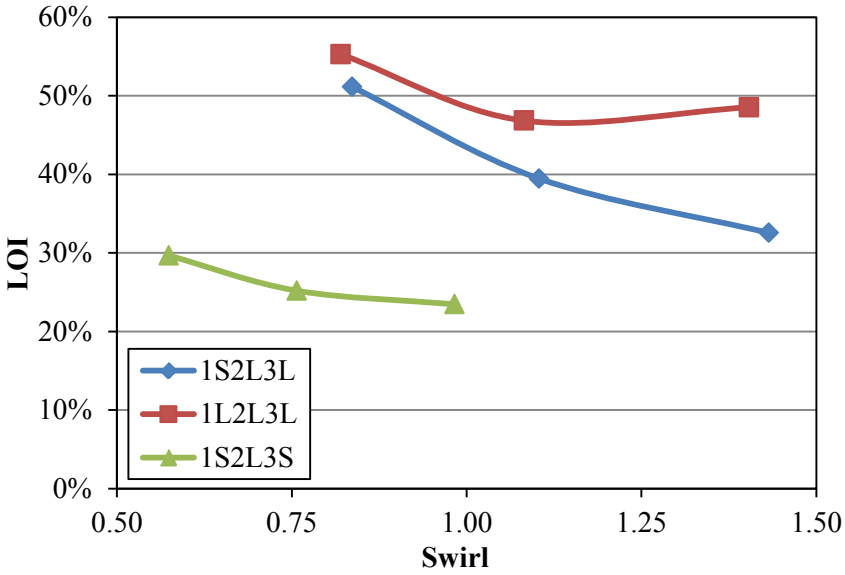

Figure 5.7: LOI vs. Swirl for various burner configurations, no oxygen, medium hardwood, and constant secondary air

5.2.2 LOI vs. O_2

Figure 5.8 shows LOI versus oxygen flow rate in the center tube for four different configurations. LOI decreases with increasing amounts of oxygen. Initially the rate at which LOI decreases can be rapid with small amounts of oxygen (0-4 kg/hr), but then slows at the higher flow rates (6-8 hg/hr).

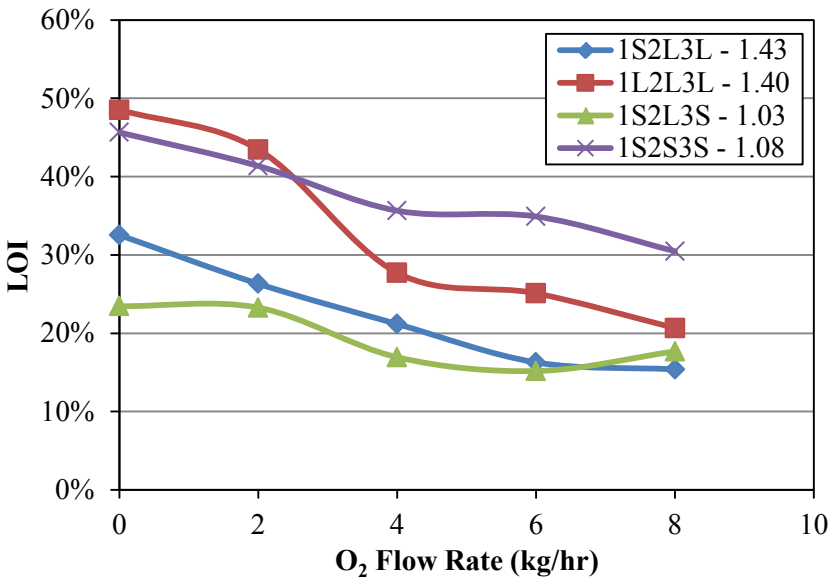

Figure 5.8: LOI vs. Oxygen Flow Rate (kg/hr) for four configurations at maximum swirl, medium hardwood, center injection, and constant secondary air

5.2.3 LOI vs. Primary Air

Figure 5.9 shows LOI as a function of primary air flow rate for configuration 1S2L3L. In both sets of data, no oxygen is introduced into the reactor. The data show a general trend of increasing LOI with an increase in primary flow. The recessed location has lower LOI than the flush location using the six-hole center tube. There appears to be a maximum for the open, recessed tube before the highest primary air flow rate is obtained. Error bars are shown for reference with a 95% relative confidence level.

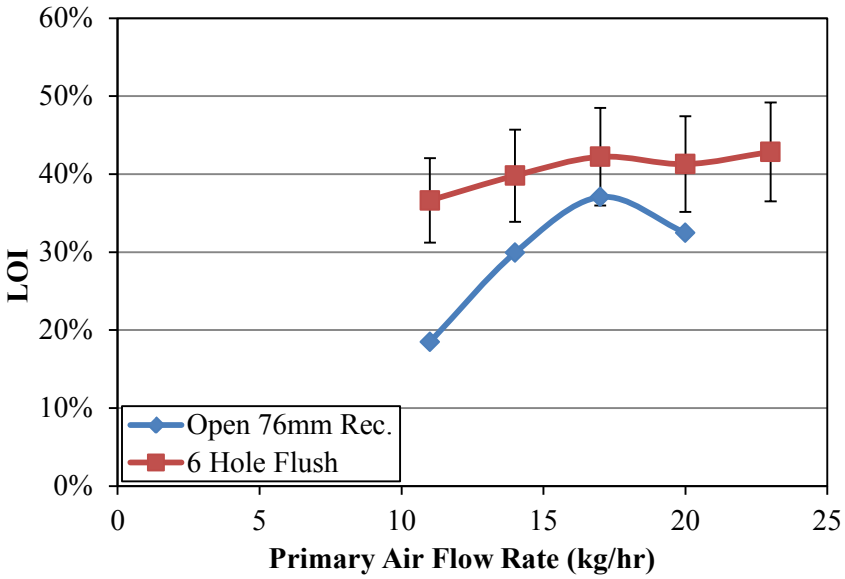

Figure 5.9: LOI vs. Primary Air Flow Rate (kg/hr) for the medium hardwood, configuration 1S2L3L

5.2.4 LOI Summary

LOI was found to decrease with increasing swirl and oxygen concentration. The amount of LOI reduction for a given increase in O_2 was often lower at high O_2 flow rates showing a reduced benefit to O_2 addition. LOI did not correlate with swirl for all burner configurations. Recessing the primary tube or reducing the primary air flow rate had a tendency to decrease LOI.

5.3 NO vs. LOI Trade-off

Given the observation that changes in operating conditions or burner configurations typically produce opposite trends for NO and LOI, decreasing one while increasing the other it is advantageous to analyze the impacts of variable on both exhaust products at the same time. As a result, NO and LOI have been plotted on the same graph producing NO – LOI trade-off curves. This section presents these curves and utilizes them to discuss the results.

5.3.1 Swirl

Trade-off curves are presented for the medium hardwood biomass where oxygen is injected globally, Figure 5.10a, and into the center, Figure 5.10b, for configuration 1S2L3L. The lower right data point at each swirl represents air only or zero O_2 addition. Moving from right to left, O_2 is added in increments of 2 kg/hr. This figure suggests that swirl and oxygen addition produce similar benefits related to the trade-off between LOI reduction and increasing NO. Biomass with large particles tends to produce long, type-1 flames, with poor burnout and high LOI. Adding swirl can reduce the LOI, but oxygen can extend the range over which the LOI can be reduced. Global enrichment is seen to have a better overall trade off curve than center injection, because the increase in NO at higher values of O_2 produces decreased LOI with a lower increase in NO.

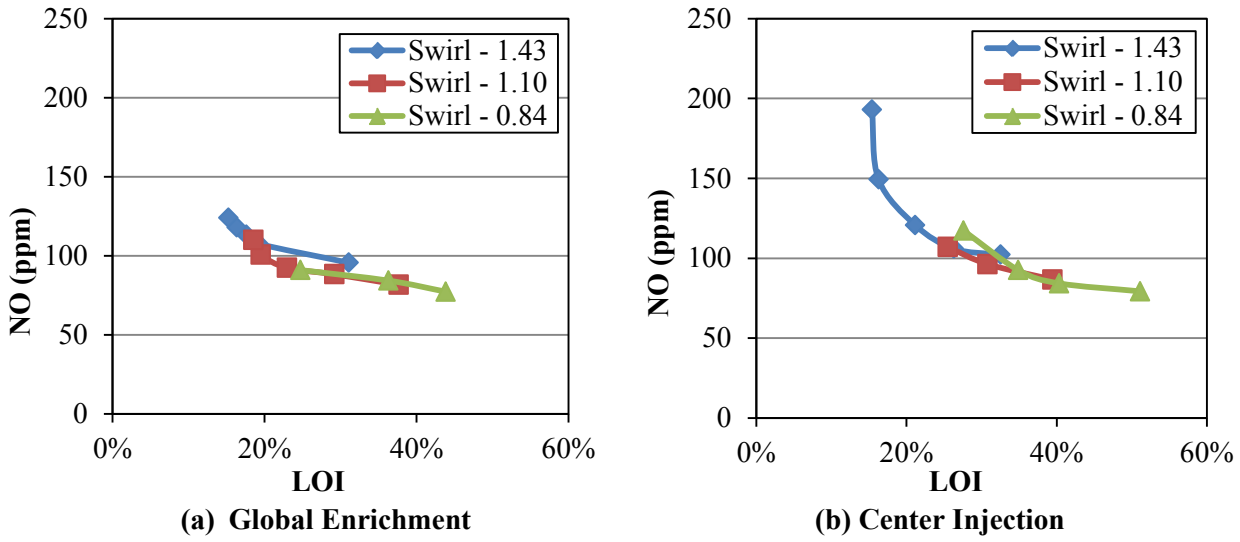

Figure 5.10: NO (ppm) vs. LOI for three swirl values at five oxygen flow rates (0, 2, 4, 6, 8 kg/hr), configuration 1S2L3L, medium hardwood, constant secondary air for (a) Global Enrichment and (b) Center Injection

This figure reveals the tradeoff between increasing NO and decreasing LOI for an increase in swirl. This trend is apparent in both global enrichment and center injection. It is clear from this figure that global enrichment has a better overall trade off curve than center injection, because it has improved NO values for comparable LOI values.

Figure 5.11 shows trade-off curves comparing the location of the fuel and oxygen injection for burner configuration 1L2L3L. Fuel was injected into the center, and oxygen in the annulus Figure 5.11b, and fuel into the annulus with oxygen in the center, Figure 5.11a (standard operation). With O_2 in the center, the trade-off is similar to Figure 5.10, adding oxygen and swirl decreases LOI and increases NO. When fuel is introduced through the center tube, O_2 addition and swirl have little impact on the flame. This flame appears to be type-0 with little mixing or interaction between the center fuel jet and the surrounding air or oxygen. This flame was long, lazy looking and detached.

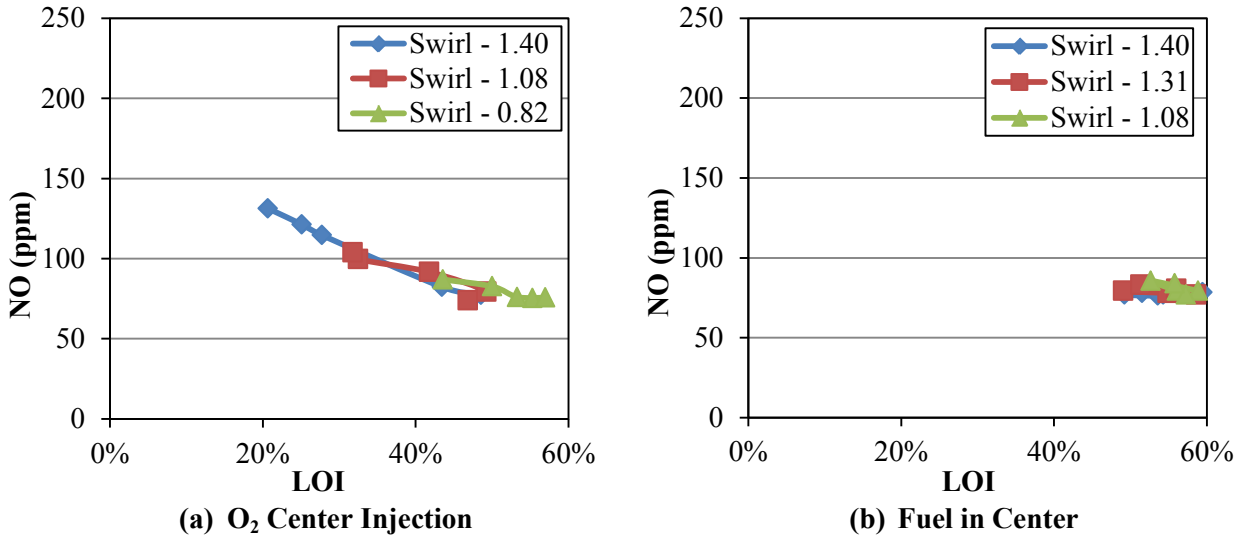

Figure 5.11: NO (ppm) vs. LOI for three swirl values at five oxygen flow rates (0, 2, 4, 6, 8 kg/hr), configuration 1L2L3L, medium hardwood, constant secondary air for (a) Center Injection and (b) Fuel in Center

Results for configuration 1S2L3S are shown in Figure 5.12 for three different swirls and varying O_2 flow rates. For this configuration, the secondary air has a higher axial velocity due to the smaller area of the secondary annulus. The flame was detached initially and could only be attached by increasing the primary air to a flow rate of 24 kg/hr instead of the usual 14 kg/hr. In these data, the high O_2 flow rates are the points on the far left, low LOI, of each swirl condition. The maximum swirl case begins at low NO and produces a trade-off similar to other O_2 sweeps but at lower swirl, the data show trends where both NO and LOI are increasing (lowest swirl) and where NO is decreasing without an increase in LOI (0.76 swirl). It is interesting to note that for this configuration the flame attachment and stability was very poor at low swirl and somewhat unpredictable. There was in indication of changing bulk fluid motion with changes in operating conditions that was not apparent in other configurations.

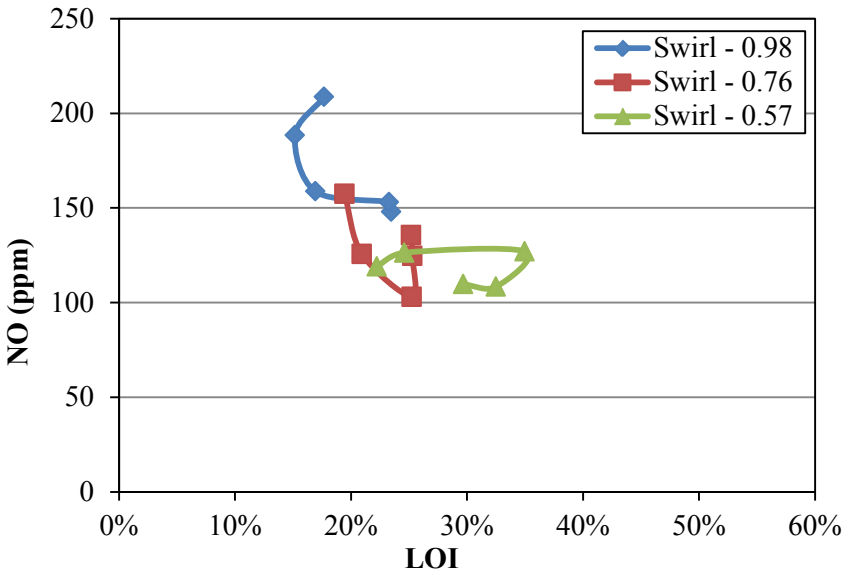

Figure 5.12: NO (ppm) vs. LOI for three swirl values at five oxygen flow rates (0, 2, 4, 6, 8 kg/hr), center injection, 25 mm recess, configuration 1S2L3S, medium hardwood, constant primary air (24 kg/hr), and constant secondary air

Oxygen premixed into the primary fuel tube was investigated for four different center tube geometries using the 1M2L3L burner in Figure 5.13. The four and eight-hole center tubes produced similar trade-off curves. In the case where the tube was extended from the burner (bluff body, 93 mm extension) NO increased considerably without improvement in LOI.

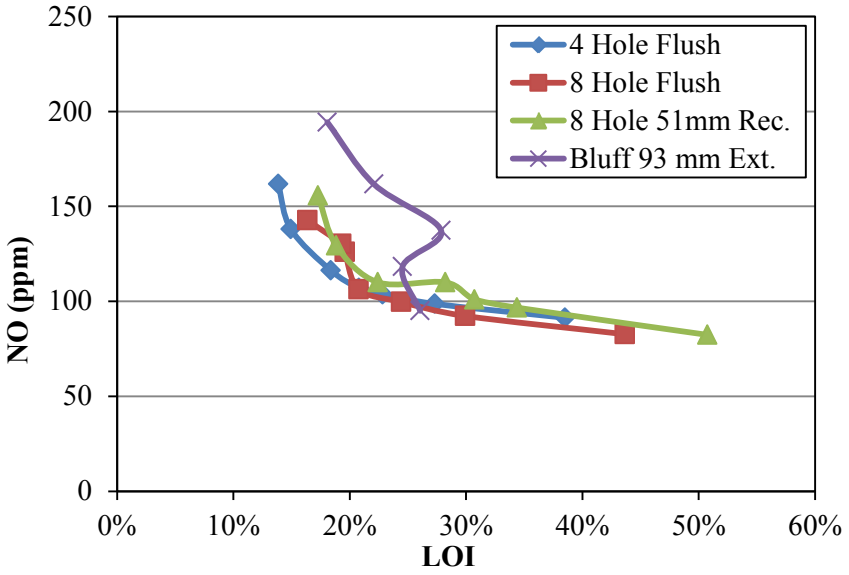

Figure 5.13: NO (ppm) vs. LOI for four type of oxygen injection techniques, configuration 1M2L3L, medium hardwood, flush location unless otherwise specified, and constant secondary air

Trade-off curves for configuration 1S2L3L with three different center tube injection locations are shown in Figure 5.14. For all levels of extension, the NO values lie within the confidence level of the data, but the LOI values vary more than the confidence level at certain oxygen flow rates. The configuration where the lance was extended axially the furthest into the flow (70 mm) produced the poorest trade-off curve. Note that in these cases, the oxygen was injected axially while in the previous data, the oxygen was injected radially through holes in the lance or through holes designed to produce a bluff body and recirculation.

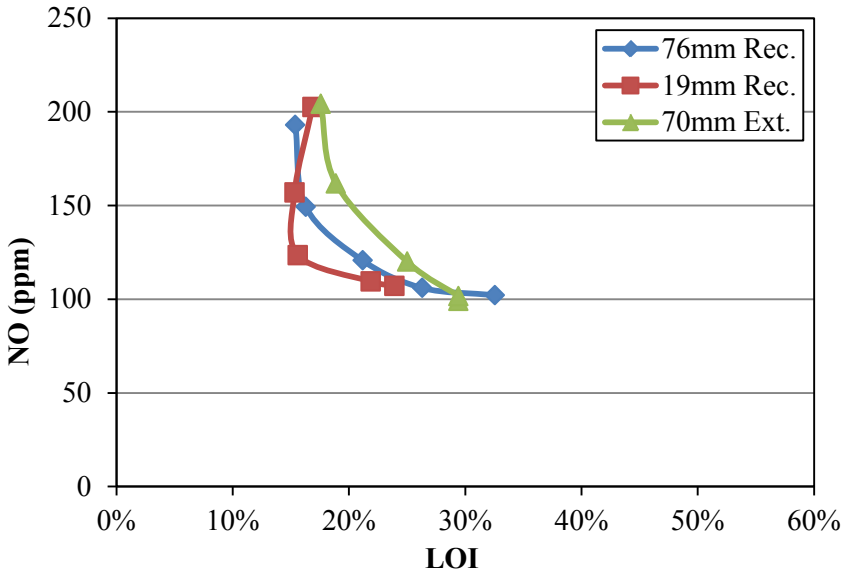

Figure 5.14: NO (ppm) vs. LOI for three levels of extension of the oxygen lance, center injection, configuration 1S2L3L, medium hardwood, and constant secondary air

One other example of the center tube location effect is shown in Figure 5.15. This data shows five heights of extension for the medium hardwood and center injection at a moderate flow rate of oxygen (4 kg/hr). In Figure 5.15a, configuration 1S2S3S was used to analyze what height might be most appropriate to inject oxygen into the center. The data of this first configuration all lie within the 95% confidence interval of uncertainty and therefore suggests no measurable difference in the configurations. For configuration 1M2L3L, Figure 5.15b, the data are more separated. Given the uncertainty it is not clear, but points of greatest extension (76 and 93 mm) are above and to the right of the data from the configurations of lesser extension.

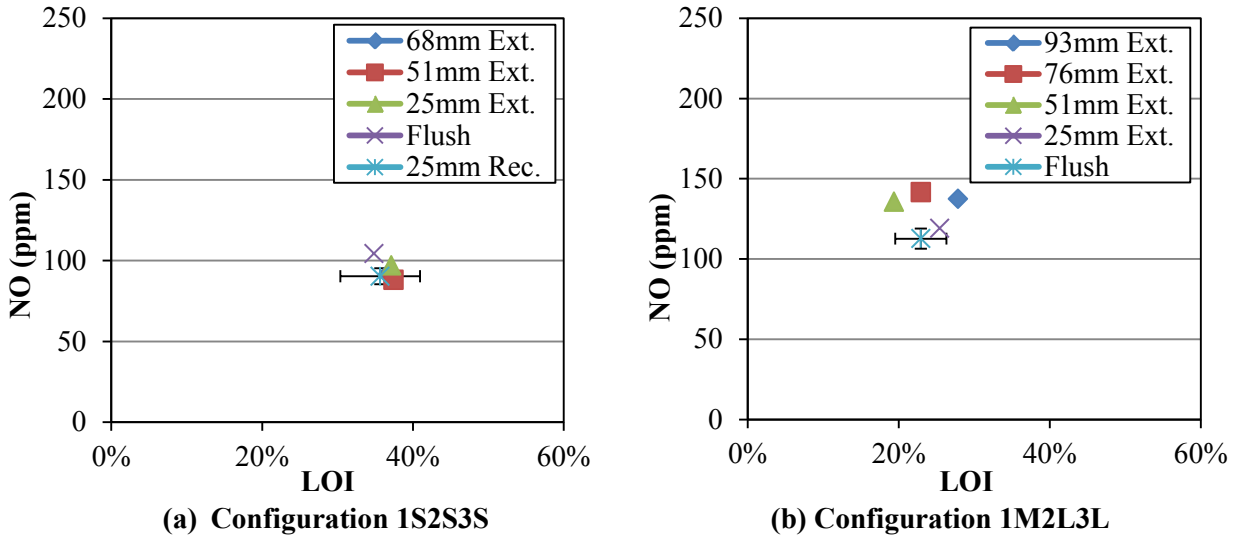

Figure 5.15: NO (ppm) vs. LOI for five heights of extension, 4 kg/hr oxygen flow rate center injection, medium hardwood, constant secondary air for (a) Configuration 1S2S3S and (b) Configuration 1M2L3L

5.3.2 Primary Air

The primary air flow was held constant for nearly all of the experiments, but was varied without oxygen being introduced to determine an appropriate flow rate. In Figure 5.16, NO versus LOI is shown for varying primary flow rates (11, 14, 17, and 20 kg/hr) and 1S2L3L configuration. The primary air entered through the annulus surrounding the center tube. In one primary air sweep the center tube was open, solid walled, and recessed 76 mm within the burner, in the other case, the center tube was flush and had six holes in the tube but no air or oxygen was flowing out of the center tube. The flow rate of 11 kg/hr was prone to clogging and was therefore the lowest flow where data could be obtained. The trend seen in Figure 5.16 is different from the normal tradeoff curve with only a slight linear increase in NO as air flow decreased while LOI decreased significantly. The flame was observed visually to shorten with lower primary air flow

rates. The decrease in primary air is likely to cause a shift from a type 1 flame toward a type 2 flame allowing more entrainment of particles.

Data with the six-hole center tube can also be seen in Figure 5.16, with a very different starting location. In this data set primary air flow rates of 11, 14, 17, 20, and 23 were attempted. Once again the trend was identical, albeit shifted, and led to the same conclusions as before, to use a low primary flow rate that successfully carries the fuel.

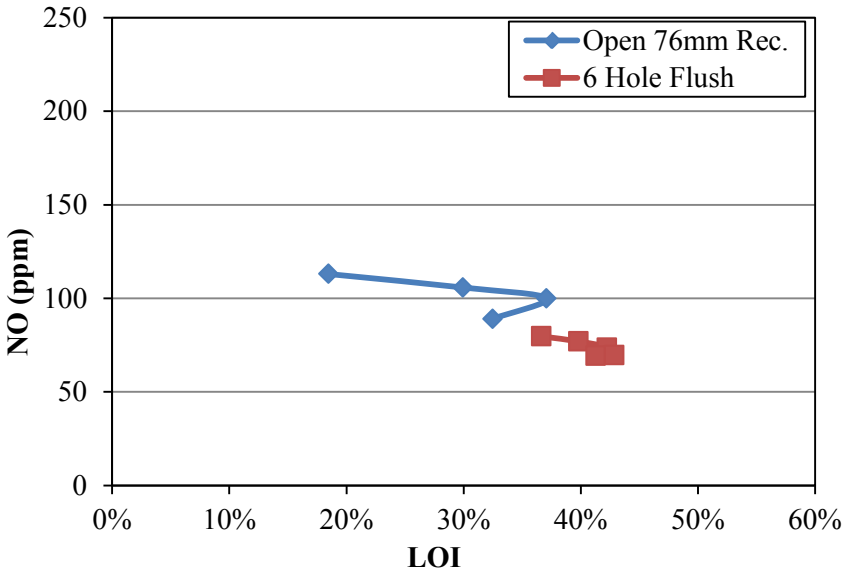

Figure 5.16: NO (ppm) vs. LOI for varying primary flow rates, no oxygen introduced, medium hardwood, configuration 1S2L3L

Data were collected at three oxygen flow rates (0, 4, and 8 kg/hr) using configuration 1S2L3L and the premix six-hole oxygen lance. This data is shown in Figure 5.17 at two primary flow rates, 11 and 14 kg/hr. In these data there is no measureable difference.

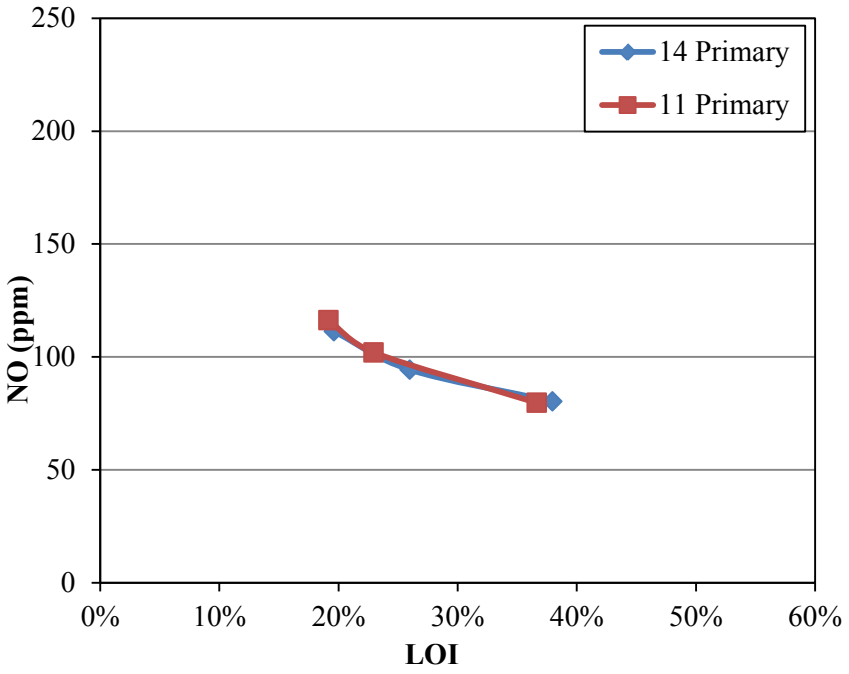

Figure 5.17: NO (ppm) vs. LOI for two primary flow rates, varying amounts of premixed oxygen (0, 4, and 8 kg/hr), medium hardwood, configuration 1S2L3L

5.3.3 Burner Configuration

Trade-off curves produced by varying the center oxygen flow rate for four different burner configurations each at their maximum swirl setting are presented in Figure 5.18. All of the points tend to fall on a combined NO-LOI trade-off curve. The starting point at zero oxygen addition is different for three of the configurations and adding O_2 allows one burner configuration to produce NO and LOI similar to another configuration without changing the geometry. The 1S2L3S configuration does produce a trade-off curve that deviates somewhat from the behavior of the other data, particularly at a high O_2 flow rate of 8 kg/hr where both NO and LOI are seen to increase.

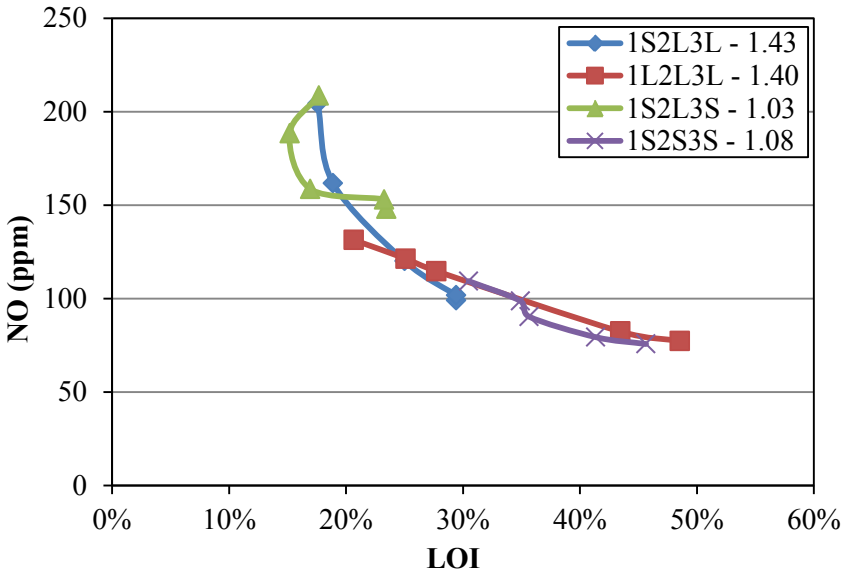

Figure 5.18: NO (ppm) vs. LOI at maximum swirl for four different configurations, varying amounts of oxygen flow rates, center injection, medium hardwood, and constant secondary air

5.3.4 Variable vs. Constant Secondary Flow Rate

For most of the data, the addition of oxygen means a greater overall flow of oxygen through the reactor and a greater exit concentration of O_2. In addition to this typical case, data were collected where the secondary air flow rate was decreased as oxygen was injected in order to keep the overall O_2 flow rate constant and the exit concentration of O_2 constant at nominally 3%. In the data in Figure 5.19, the secondary flow rate is varied such that the oxygen concentration in the exhaust is held roughly constant. The total nitrogen in the reactor is therefore effectively decreased with increasing oxygen amounts. Shown in this figure are where oxygen is injected globally, Figure 5.19a, and into the center, Figure 5.19b. Beginning with Figure 5.19a, 0 kg/hr of oxygen has the lowest LOI for each swirl value. Upon adding O_2, LOI increases with slight but varied responses of NO. The increase of LOI with additional O_2 is opposite of previous trends seen. Increasing the swirl seems to make higher NO, but with moderate improvements to LOI. For 0 kg/hr of center injection, Figure 5.19b, NO values are low.

Increasing oxygen in this case seems to increase NO with no clear trends on LOI. Increasing swirl also seems to make higher NO.

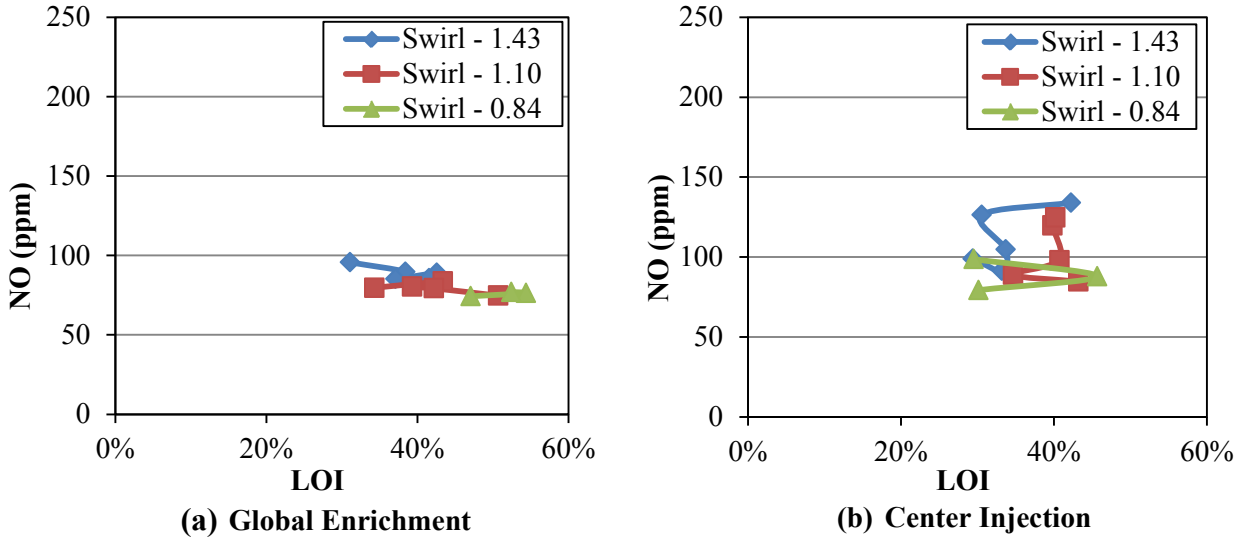

Figure 5.19: NO (ppm) vs. LOI for varied secondary air, medium hardwood, configuration 1S2L3L with (a) Global Enrichment and (b) Center Injection

5.3.5 O_2 Location

Trade-off curves for global enrichment and air addition are shown for configuration 1S2L3L in Figure 5.20. Error bars are shown for reference. Both global enrichment and air addition resulted in similar NO values. The LOI for global enrichment, however, are lower than those for air addition.

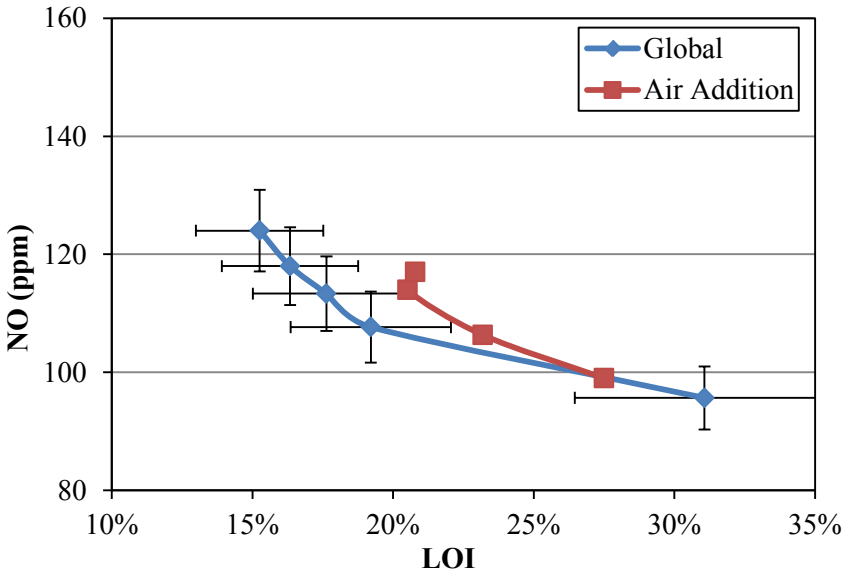

Figure 5.20: NO (ppm) vs. LOI for two oxygen addition techniques, global enrichment and air addition, configuration 1S2L3L, and medium hardwood

Trade-off curves for sweeps of O_2 for the five main oxygen injection techniques used in this work, over-fire air, premixed oxygen, center injection, global enrichment, and air addition, are shown for configuration 1S2L3L in Figure 5.21. Curves closer to the origin are considered better than those further from the origin because of the overall lower exhaust product values. Using center injection as the base case, each of the other four oxygen addition techniques resulted in an improved result. Global enrichment, air addition, and premixed oxygen resulted in very similar tradeoff curves, but global O_2 addition was able to achieve lower LOI values. Over-fire air produced a trade-off between global and center O_2 injection. Air addition matched the NO values that were obtained with global enrichment, but with worse LOI values.

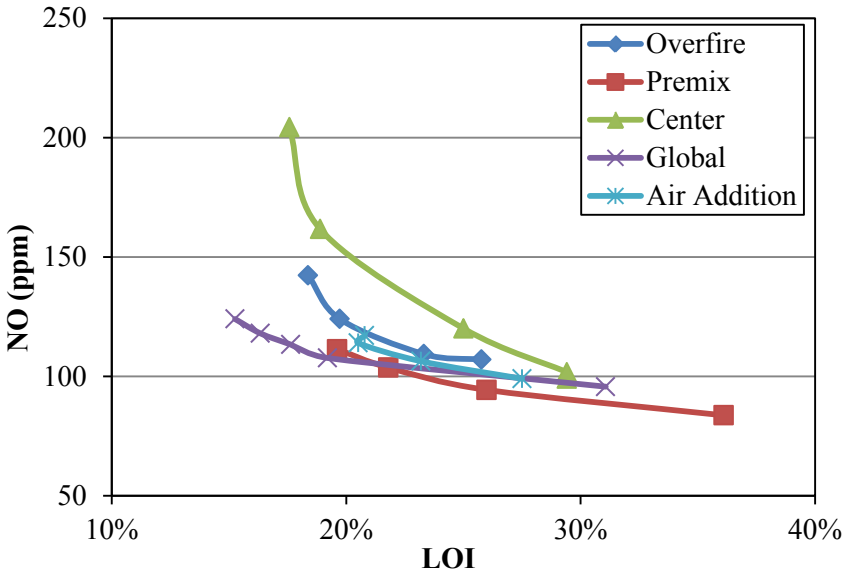

Figure 5.21: NO (ppm) vs. LOI for five oxygen addition techniques, configuration 1S2L3L, and medium hardwood

5.3.6 NO vs. LOI Summary and Discussion

A graph containing all wood particle data for NO and LOI is shown in Figure 5.22. The figure contains 244 data points and shows a strong correlation between NO and LOI that exists over various burner geometries, oxygen flow rates, swirl, and oxygen injection locations. For a swirl-stabilized flame, it appears that exhaust NO and LOI are tightly connected. This can be explained by the competing effects that oxygen has on each parameter. The addition of oxygen provides an increased concentration of oxygen surrounding burning particles and therefore increases the rate of diffusion to the surface of the particles and increases the oxidation rate. At the same time, oxygen introduced into burning volatiles can form NO by reaction with fuel derived HCN and NH_3 under oxidizing conditions or can inhibit reburning reactions where NO is reduced to N_2 under reducing conditions.

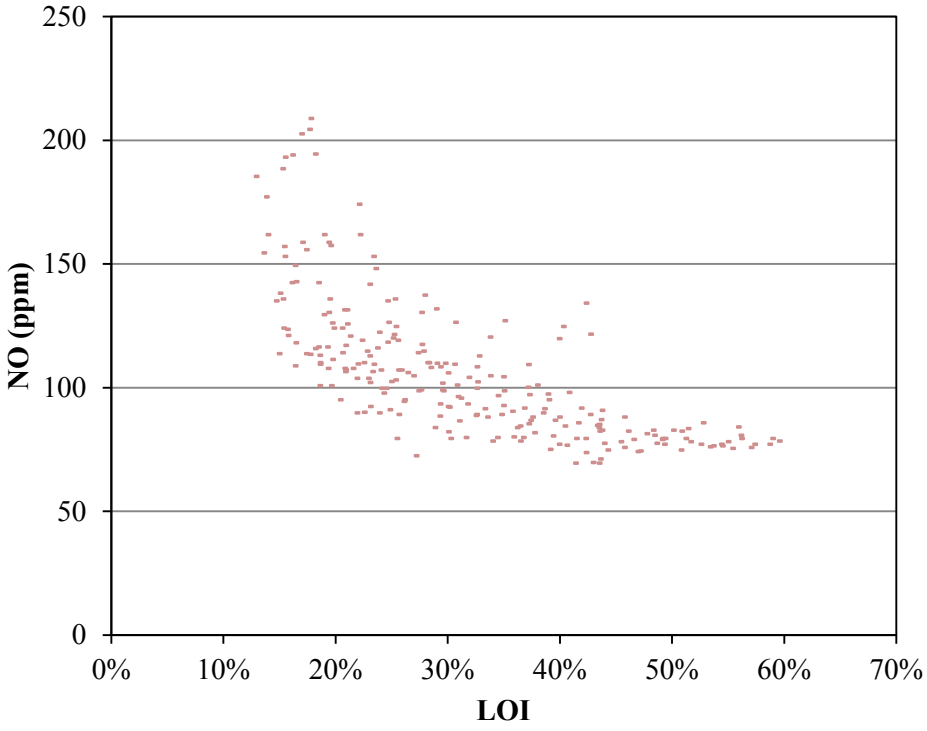

Figure 5.22: NO (ppm) vs. LOI for all wood particle data and all operating conditions

Although strongly correlated, LOI and NO reactions can be separated by the location in which they occur. Char oxidation occurs primarily after volatiles combustion and the fate of the nitrogen is determined. Therefore, it is possible to have improved LOI without increasing NO by adding oxygen to the burnout region, while maintaining the optimal stoichiometry for low NO formation and reduction near the burner in the volatiles flame. Geometries and operating conditions that will best achieve low NO and LOI are those that produce trade-off curves closer to the origin or within an acceptable exhaust products box bounded by acceptable NO and LOI.

In Figure 5.23, eight of the various operating conditions of configuration 1S2L3L are shown on the same plot with all of the available data for comparison. The larger particles, inherent in biomass combustion, burned in moderately swirled burners produce long flames with low NO and high LOI as represented by data in the lower right of the trade-off curve. Improved

burnout can be provided by increasing the swirl at the expense of increased NO as shown by the green line connecting triangular data points. Starting at the point of moderate swirl, oxygen can be added to the primary air via a premix lance to improve burnout (blue-grey line connecting plus symbols). Another strategy might be to add oxygen to the secondary air (global O_2 addition) starting at maximum swirl. Both of these oxygen addition methods produced trade-off curves on the lower left boundary and are considered optimal.

Oxygen addition in the center tube, represented by the blue line, did not produce as favorable of a trade-off as premixing or global oxygen injection. Staging the air, and adding oxygen to the center tube as shown by the orange line, also did not improve the trade-off.

Two data sets shown in the figure labeled “primary” and “secondary” produced trade-offs that were not smooth transitions or monotonically changing. This behavior was seen repeatedly for numerous data sets where the secondary air flow rate was decreased in order to hold total oxygen flow rate constant as pure oxygen was added to the center tube. One explanation for this type of data is that the change in flow rates produced a reversal or fundamental shift in flow patterns within the reacting flame region. During these transitions LOI and NO behavior trends could change direction, not just continue to increase or decrease. For example, consider a jet with zero swirl and an external recirculation zone. As swirl is introduced and increased, the jet might widen and slow, producing a continuous change in length. At some point however, the jet will transition from an external recirculation to internal recirculation and the flame length will jump or transition to a much shorter flame. These transition points would produce discontinuity in flame properties and the resulting emissions.

The Air Liquide Burner has three flows, each of a different velocity and momentum. The primary flow also has solid fuel entrained. Swirl produces a tendency to pull the core of the jets

radially outward and produce an internal recirculation zone. At some axial location the recirculation zone produces a stagnation point with incoming primary fuel and air running into recirculated products. Each of the jets also has a velocity. When the velocity of one jet that is initially higher than another jet is slowed, the shear layer between the two jets reverses. These complex flow phenomena are difficult to predict based on basic flow rates and geometries. Computational fluid dynamics (CFD) might be useful in identifying these transitions, but doing so was beyond the scope of this work.

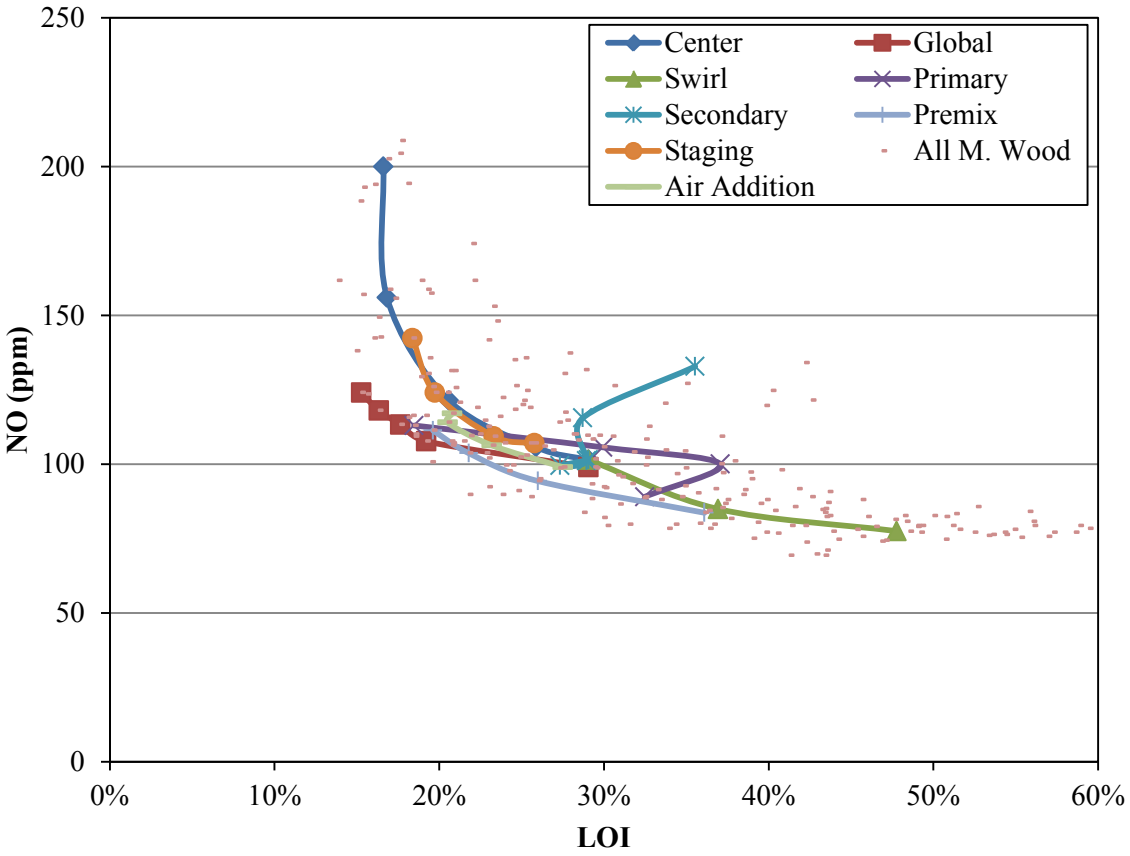

Figure 5.23: NO (ppm) vs. LOI at eight different type of operating conditions for the medium hardwood and configuration 1S2L3L

5.4 NO-LOI Data for Straw and Fine Biomass

This section presents data for several operating conditions with wheat straw and fine hardwood as the fuel. The results from these fuels are then compared to the medium hardwood data.

5.4.1 Straw NO-LOI for Variable Swirl

Results for burner configuration 1S2L3S with center oxygen injection through a 25 mm recessed tube are shown in Figure 5.24 for three swirl settings. Overall the data show a trade-off between LOI and NO but the results are not as closely correlated as most of the medium hardwood data. The maximum swirl case of 0.99 had a poor tradeoff curve and decreasing the swirl to 0.77 decreased both NO and LOI. Visual observation of the flame suggested the lower swirl setting maintained an active attached flame. At the lowest swirl, very low LOI rates were achieved with 6-8 kg/hr of oxygen but the rest of the trade-off curve at low swirl was not as favorable as medium swirl.

This trend where both NO and LOI improve as swirl was decreased was not observed in the 1S2L3S configuration with medium particles as seen in Figure 5.12 and Figure 5.18. When the medium hardwood was used in this same configuration, the flame was not as active and attached as was the wheat straw. It is not clear why the wood flame appeared to be less active but this suggests that combustion and the location of heat release which may have been significantly different because of the difference in particle size between the two fuels may have an influence on the fluid flow.

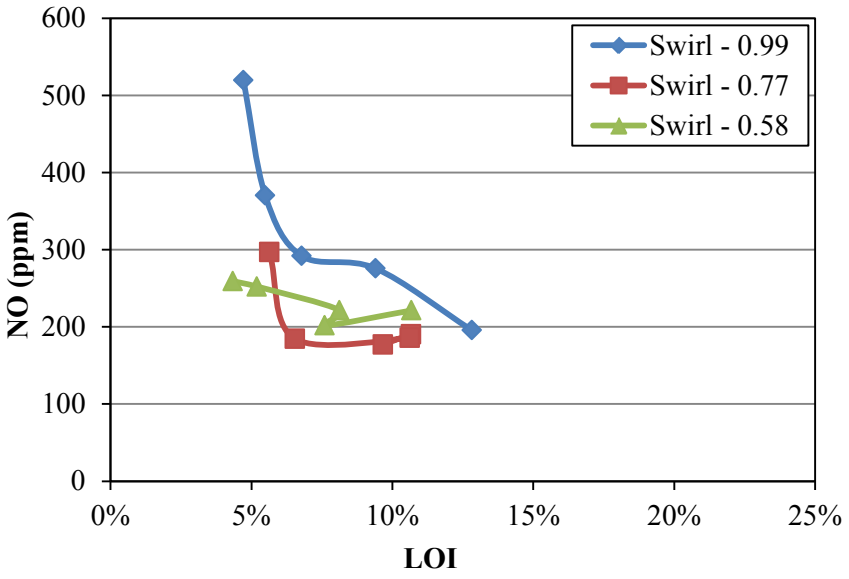

Figure 5.24: NO (ppm) vs. LOI at three different swirl values for various oxygen flow rates, center injection, configuration 1S2L3S, 25 mm recess, wheat straw biomass, and constant secondary air

5.4.2 Straw NO-LOI for Variable O_2 Location

The variables presented here include two different configurations, 1S2L3S and 1S2L3L, two oxygen injection techniques, global and center injection, as well as varied levels of extension of the center injected oxygen lance.

Two oxygen injection locations were tested. Global enrichment and center injection for 1S2L3S and 1S2L3L are shown in Figure 5.25a and Figure 5.25b respectively. In spite of a flame that appeared less attached and not as active, the NO-LOI trade-off of the 1S2L3L burner appears lower. For both configurations global enrichment provides the same, if not better LOI, with lower NO values. Both the center injection and global enrichment techniques match the same type of tradeoff curve as seen with the hardwood. Again, increases of oxygen lead to higher values of NO and lower values of LOI.

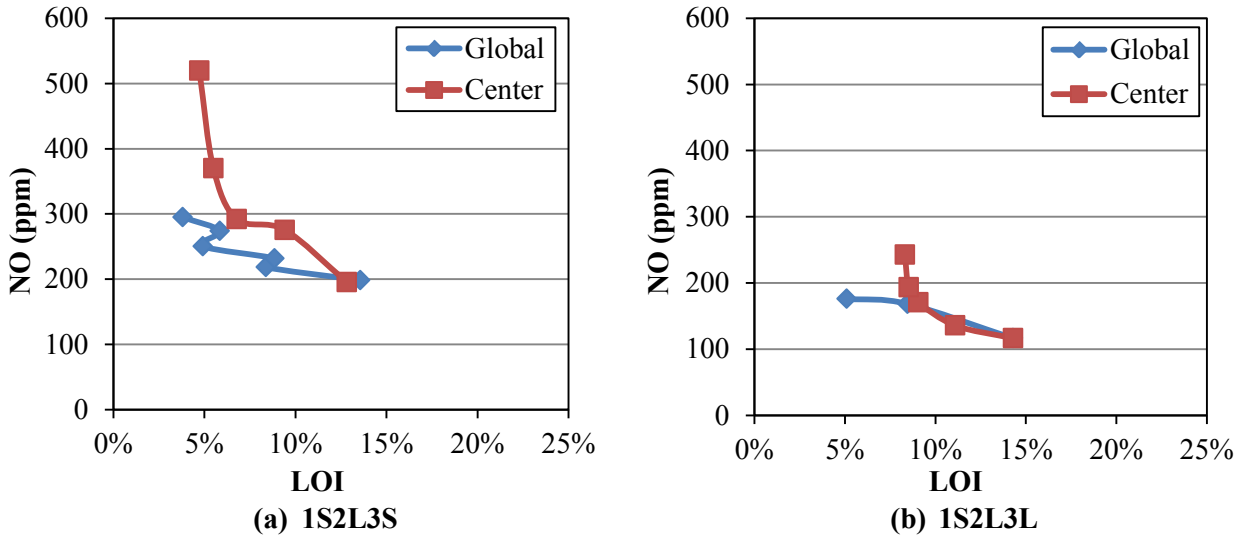

Figure 5.25: NO (ppm) vs. LOI at two oxygen injection locations (Global and Center), varying amounts of O_2 flow rate, wheat straw biomass, maximum swirl, for burner configurations (a) 1S2L3S and (b) 1S2L3L

Two configurations are shown in Figure 5.26 where the height of the center tube was varied between a recessed, flush, and extended position. These data were collected for the wheat straw at maximum swirl for three O_2 flow rates (0, 4, and 8 kg/hr) for configurations 1S2L3S, Figure 5.26a, and 1S2L3L, Figure 5.26b. The influence of the center tube position in Figure 5.26a is not clear as most of the data are within the uncertainty of each other. For the configuration 1S2L3L, the extended position has the largest range of data and the recessed position has the tightest grouping. This trend is not repeated, however, for the 1S2L3S configuration in Figure 5.26a. In this configuration, all three center tube positions yield very similar results. From this figure one could possible argue that the center tube position does not greatly affect the NO emissions or the LOI, but the 1S2L3L configuration results shown in Figure 5.26b demonstrate that for no oxygen addition, the recessed tube produced lower LOI. This is consistent with the possibility that the recessed tube provides a larger exit area and therefore a lower velocity and momentum for the primary stream. This would allow the fuel

stream to have a lower momentum and higher potential for recirculation, thus lower fuel penetration through the recirculation zone.

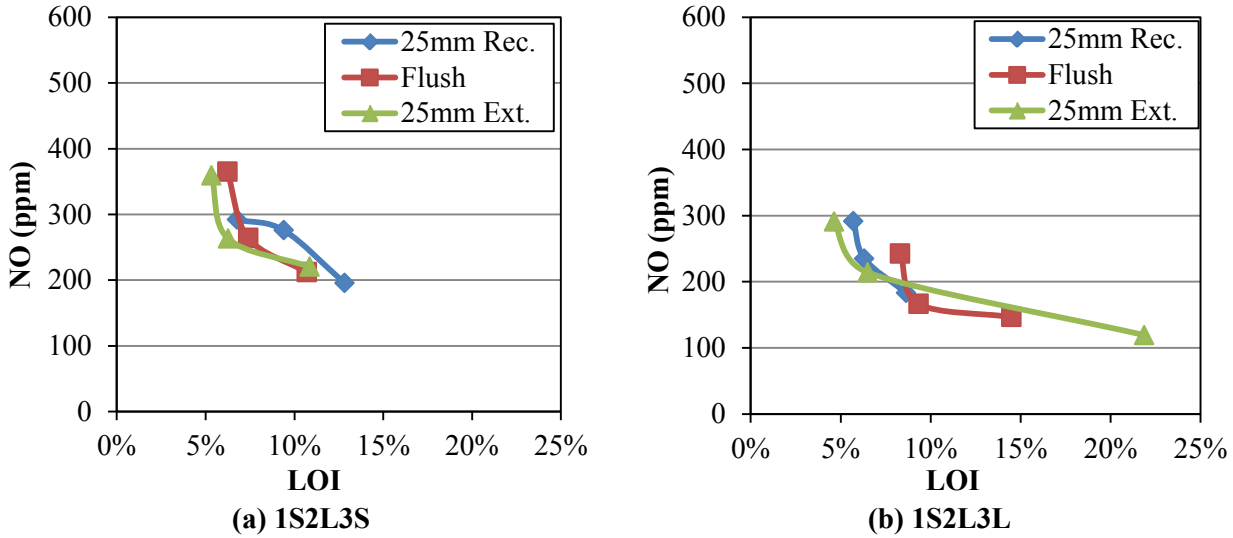

Figure 5.26: NO (ppm) vs. LOI at three different center tube extension heights, three O_2 flow rates (0, 4, and 8 kg/hr) in tube 1, wheat straw biomass, maximum swirl, for burner configurations (a) 1S2L3S and (b) 1S2L3L

5.4.3 Straw Burned in Various Burner Configurations

Results for two configurations are shown in Figure 5.27 at their respective maximum swirl value for varying levels of oxygen. Configuration 1S2L3L has lower NO values, but higher LOI. Configuration 1S2L3S, was more attached and steadier than 1S2L3L and therefore appeared to be the better flame based on visual observation.

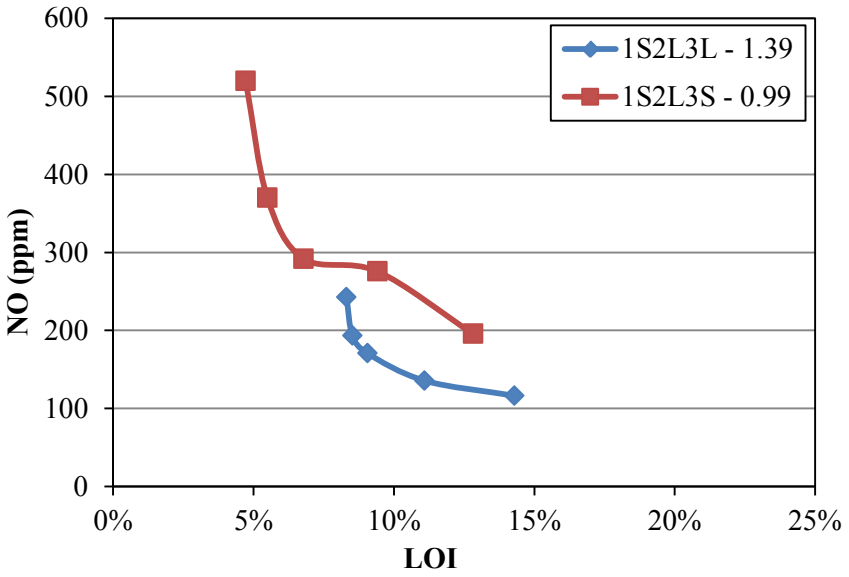

Figure 5.27: NO (ppm) vs. LOI at their respective maximum swirl value for various oxygen flow rates, center injection, wheat straw biomass, and constant secondary air

5.4.4 Fine Hardwood Results

Fine hardwood was used with configuration 1S2L3L under three swirl values and an oxygen sweep in the center tube with a flush six-hole lance. This produced premixing of the fuel and oxygen just before exiting the burner. NO versus LOI data are shown in Figure 5.28. At the highest swirl value, the flame was very short and presumably appeared to be a type 2 flame where the fuel did not penetrate through the recirculation zone but was attached to the burner and was directed along the secondary air inlet flow. At maximum swirl, LOI decreased slightly with the introduction of oxygen, but was accompanied by large increases in NO. Initially, at moderate swirl, 1.11, the LOI improved greatly with small increases in NO at a low flow rate of oxygen. As additional oxygen was added, the moderate swirl followed the highest swirl case. The lowest swirl value, 0.84, resulted in higher amounts of LOI and lower values of NO. This figure shows

that the NO versus LOI trade-off for the fine hardwood is comparable to that of the medium hardwood, simply shifted to lower values of LOI.

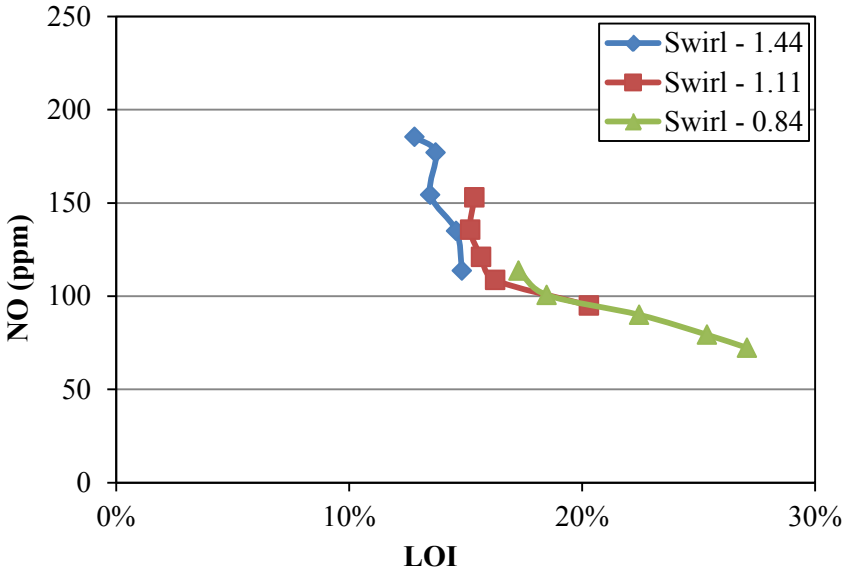

Figure 5.28: NO (ppm) vs. LOI for three swirl values at varying oxygen flow rates in six-hole lance, flush, configuration 1S2L3L, fine hardwood, and constant secondary air

5.4.5 Fuel Comparisons

Trade-off curves comparing medium hardwood and straw with global enrichment and center injection are plotted in Figure 5.29a for configuration 1S2L3L. These data confirm that both the wood and straw fuels produce trade-off curves with the straw shifted toward lower LOI and higher NO. As noted earlier, global oxygen addition produces a better trade-off curve for wood but the difference for straw is not as significant. The trade-off curves of wood with global oxygen lines up with the straw results with no oxygen added. The straw has a higher nitrogen content and smaller size which contributes to higher NO and lower burnout but it is interesting that the straw results lie on the same trade-off curve as medium wood.

When ash concentrations are small, as is the case for wood, LOI can be relatively high while burnout is almost complete. A comparison of burnout for the two fuels is shown in Figure 5.29b. The higher ash content for straw results in lower burnout. These results suggest that oxidation rate of carbon in the ash is also a function of the concentration of carbon in the ash not just the concentration of oxygen surrounding the particle.

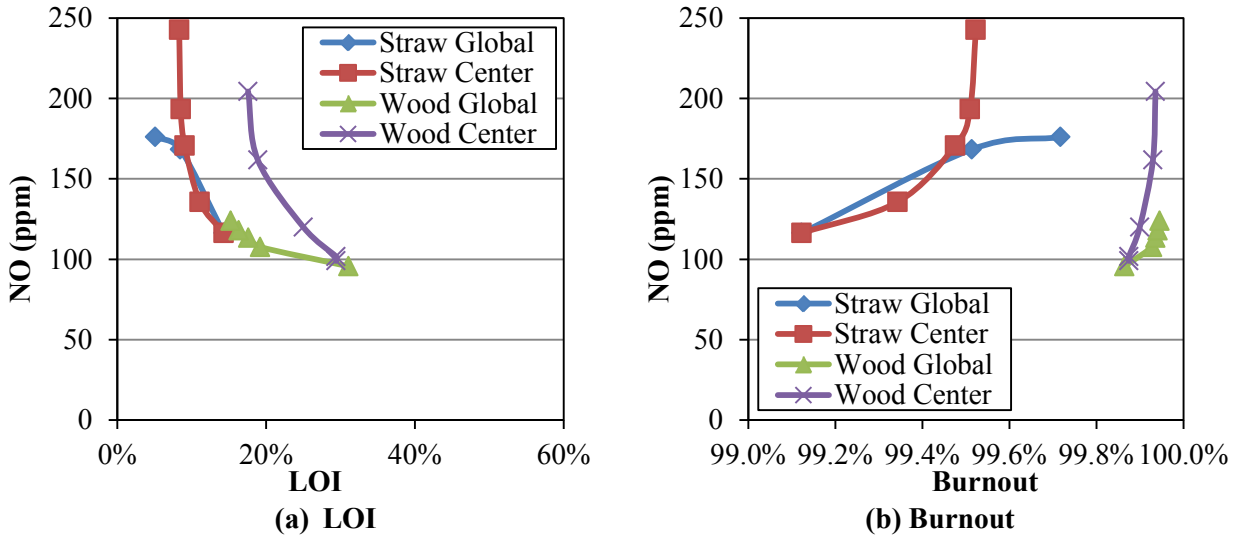

Figure 5.29: NO (ppm) vs. (a) LOI and (b) Burnout at the respective maximum swirl value for various oxygen flow rates, configuration 1S2L3L, and constant secondary air

A summary comparison of results for fine wood and medium wood is presented in Figure 5.30 for 1S2L3L for two swirl values for the fine wood and one swirl value for the medium wood using premixed oxygen injection with the six-hole oxygen lance at a flush location. A lower swirl value for this operating condition was not completed for the medium wood. As expected the fine wood had lower values of LOI for the same flow rate of oxygen. The burnout, seen in Figure 5.30b, is similar for the fine wood and medium wood, and burnout for both is excellent.

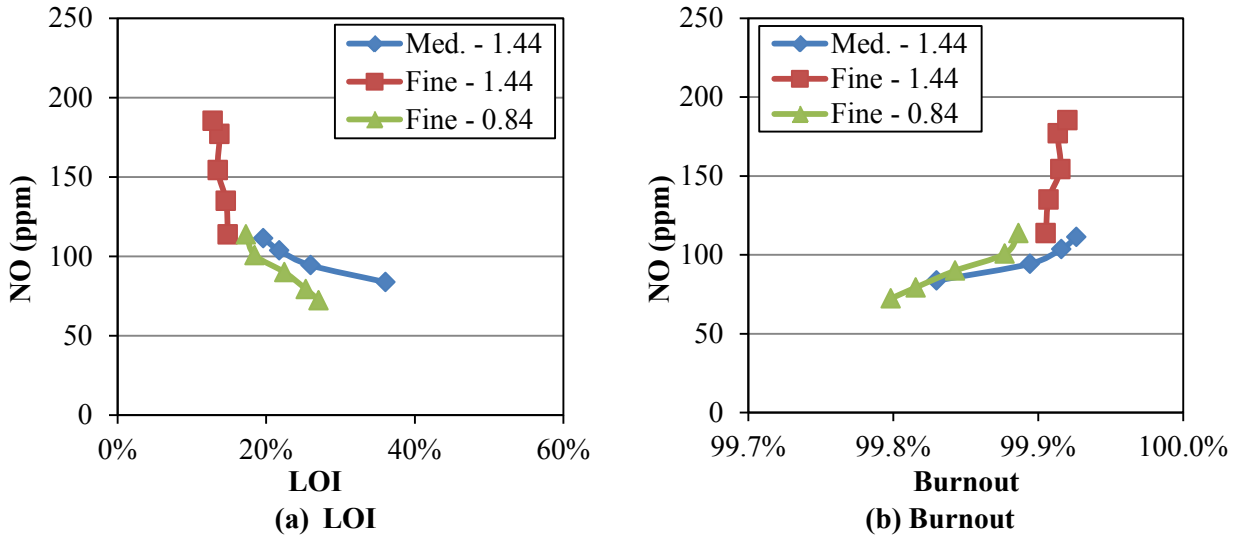

Figure 5.30: NO (ppm) vs. (a) LOI and (b) Burnout for both medium and fine hardwood at various oxygen flow rates using the six-hole oxygen lance, configuration 1S2L3L, and constant secondary air

Figure 5.31 shows NO versus LOI at three swirl values for the medium and fine hardwood. The fine wood data was collected using the six-hole lance at a flush location and the medium wood data was collected using an open tube recessed 76 mm. The zero oxygen addition cases (air only) for fine wood are all at lower LOI and similar NO to the medium wood results. Adding oxygen or changing swirl produces trade-off curves which are closer to the origin and therefore better for the fine particles. Clearly, there is an advantage to burning smaller particles. These data show that the low LOI obtained with air-fired flames and small particles can be achieved by adding oxygen but not without an increase in NO relative to the fine particles.

Seen in Figure 6.2 is all NO-LOI data for the three fuels. The straw data is at high NO and low LOI, whereas the medium wood data has lower NO and higher LOI. The fine wood has comparable NO as the medium wood, but is at lower LOI. An NO-LOI trade-off for all three fuels is evident.

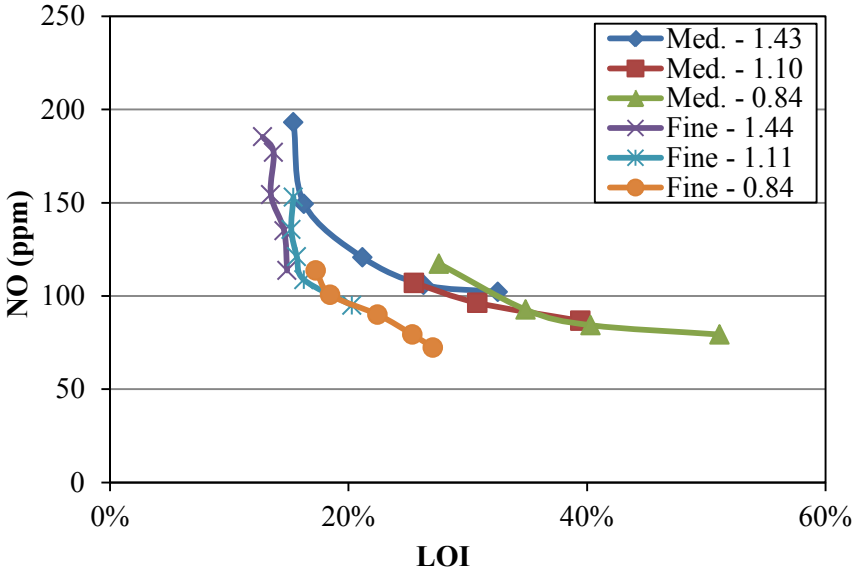

Figure 5.31: NO (ppm) vs. LOI at three swirl values for various oxygen flow rates, medium and fine hardwood, configuration 1S2L3L, and constant secondary air

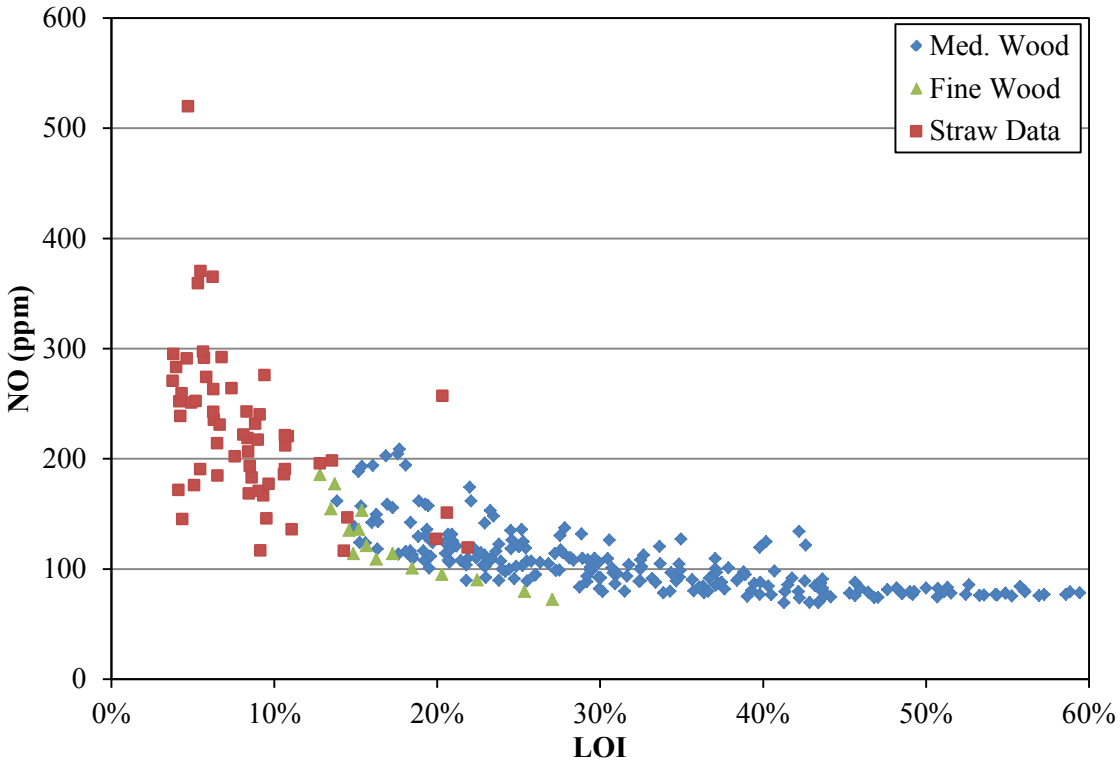

Figure 5.32: NO (ppm) vs. LOI for all data collected from each fuel

6 SCALING LAWS AND CORRELATION FOR NO AND LOI

The consistent albeit somewhat scattered correlation between LOI and NO over a broad range of operating conditions, burner configurations, oxygen addition, and fuels suggests that NO and LOI results might scale and be predicted by characteristics of the flow that are also competing. For example, the residence time of fuel particles on the fuel rich side of the flame zone and the residence time of particles in the post flame oxidation zone are two competing time scales. As the flame lengthens and residence time in the flame zone increases, the time in the particle oxidation zone decreases. While it is clear that the stoichiometry (oxidizer to fuel ratio) is important, turbulent mixing and perhaps temperature of these zones are also significant. The general trade-off of LOI and NO appears to be the first order effect with these other considerations being secondary.

This chapter explores the ability to characterize the observed flames with scaling laws and investigates the correlation of flame length obtained with these scaling laws to NO and LOI.

6.1 A Phenomenological Flame Model

A schematic diagram of a Type 1, swirl-stabilized, particle flame is shown in Figure 6.1. While the aspect ratio of the flame may change based on swirl and flow rates, some essential features of the flame are presented upon which scaling laws and correlations will be investigated. The flame consists of a jet of solid fuel particles moving down the center of the flame which enter with an initial primary fuel/air velocity, V_{prim}. This jet is surrounded by the secondary air

flow at axial velocity, V_{sec}. When center oxygen is present, a third jet exits the burner and flows down the center of the fuel jet. These three jets can mix due to shearing at their interfaces and therefore the relative velocities of these jets are important to mixing. Another mixing characteristic of the jets is created by the swirl. The swirl creates a tangential velocity (not shown) and a recirculation zone axial velocity which is shown by the vertical arrows pointing up toward the burner on the inner edge of the flame. If the fuel jet has more momentum than the recirculating flow, it will penetrate through the recirculating flow as shown and there will be no stagnation point, making this a type 1 flame. Flames with a strong recirculation zone and stagnation point are Type 2. The medium wood flames were visually observed to be Type 1.

To the left of the flame, three length and time scales are identified for the lift-off zone, the volatiles flame zone, and the particle burnout zone. The lift-off length is the distance from the burner exit to the ignition point of the flame. For this experiment, the ignition point was taken to be the location where the flame luminosity was visually observed. The further the flame is lifted from the burner, the more this point tends to move back and forth from the burner exit and can therefore be difficult to define. The volatile flame length is the point at which volatile combustion ends. In these experiments it was taken as the point at which luminous soot was no longer observed. A more rigorous definition and measurement would be beneficial as this position was also fluctuating and difficult to define. Near the end of the flame, the soot emission decreases and it is difficult to determine what emission comes from soot and what comes from solid particles. The final burnout length was not measured but was assumed to be the total reactor length minus the flame length. At the reactor exit, the cold walls were expected to end reactions relatively quickly, thus limiting the flame to the length of the reactor, 2.4 m.

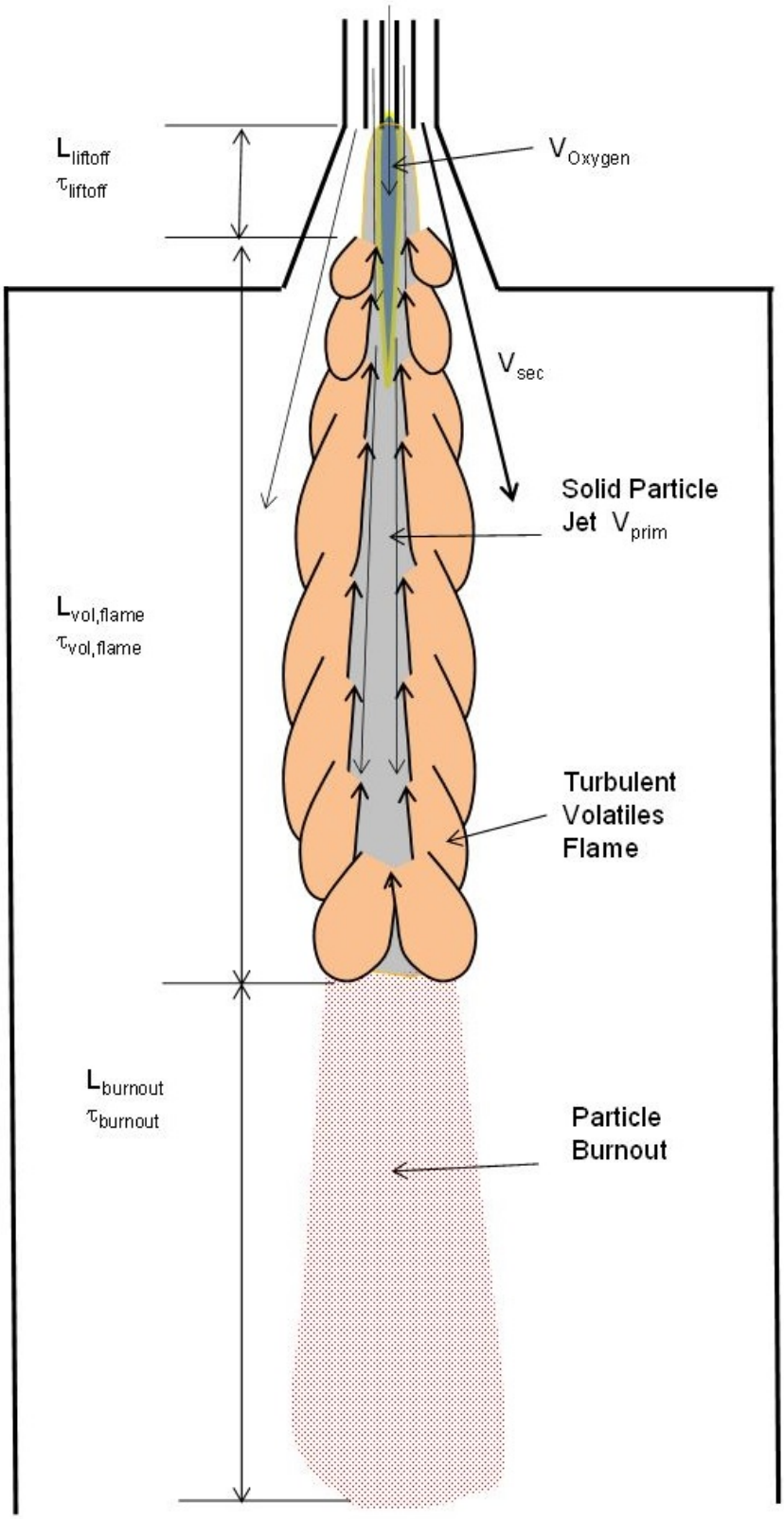

Figure 6.1: Schematic diagram of a type 1, swirl stabilized, particle flame

6.1.1 Lift-Off and Flame Length Measurements

In this section, data is shown that compares lift-off length and flame length for three burner configurations with medium wood particles. It should be noted that the data in this section are only semi-quantitative because they were gathered from visual observation of the flame from four port windows in the reactor. The data were collected visually as a first step at investigating the value of more precise measurements which would require significantly greater effort.

In Figure 6.2, lengths for three separate configurations are shown at three swirl values and varying amounts of oxygen injected in the center for the medium hardwood. These data provide some indication of flame lengths for these conditions. In Figure 6.2a, configuration 1S2L3S is shown. In this figure the lowest lift corresponds with the highest amount of oxygen. Thus with increased oxygen lift-off and volatile flame length decreases. The flame became shorter with the addition of swirl and became more attached with the addition of oxygen. In Figure 6.2b, configuration 1S2L3L, similar effects can be noted. The difference in this configuration is the amount of lift when compared to 1S2L3S. Less lift can lead to less air entrainment in the center and will decrease NO formation. When compared with 1S2L3L, 1S2L3S had similar LOI, but did have increased NO values as was seen in Figure 5.18. Lastly, Figure 6.2c shows the lift versus length data for the configuration 1L2L3L. The attachment was excellent, but the length was much longer than the other two configurations. This length of flame made decreasing the LOI very difficult as the particles had very little time to oxidize. NO values for the configuration 1L2L3L were very low due to the length of the fuel rich reducing zone. Overall, both length and lift tend to decrease with increased swirl or oxygen.

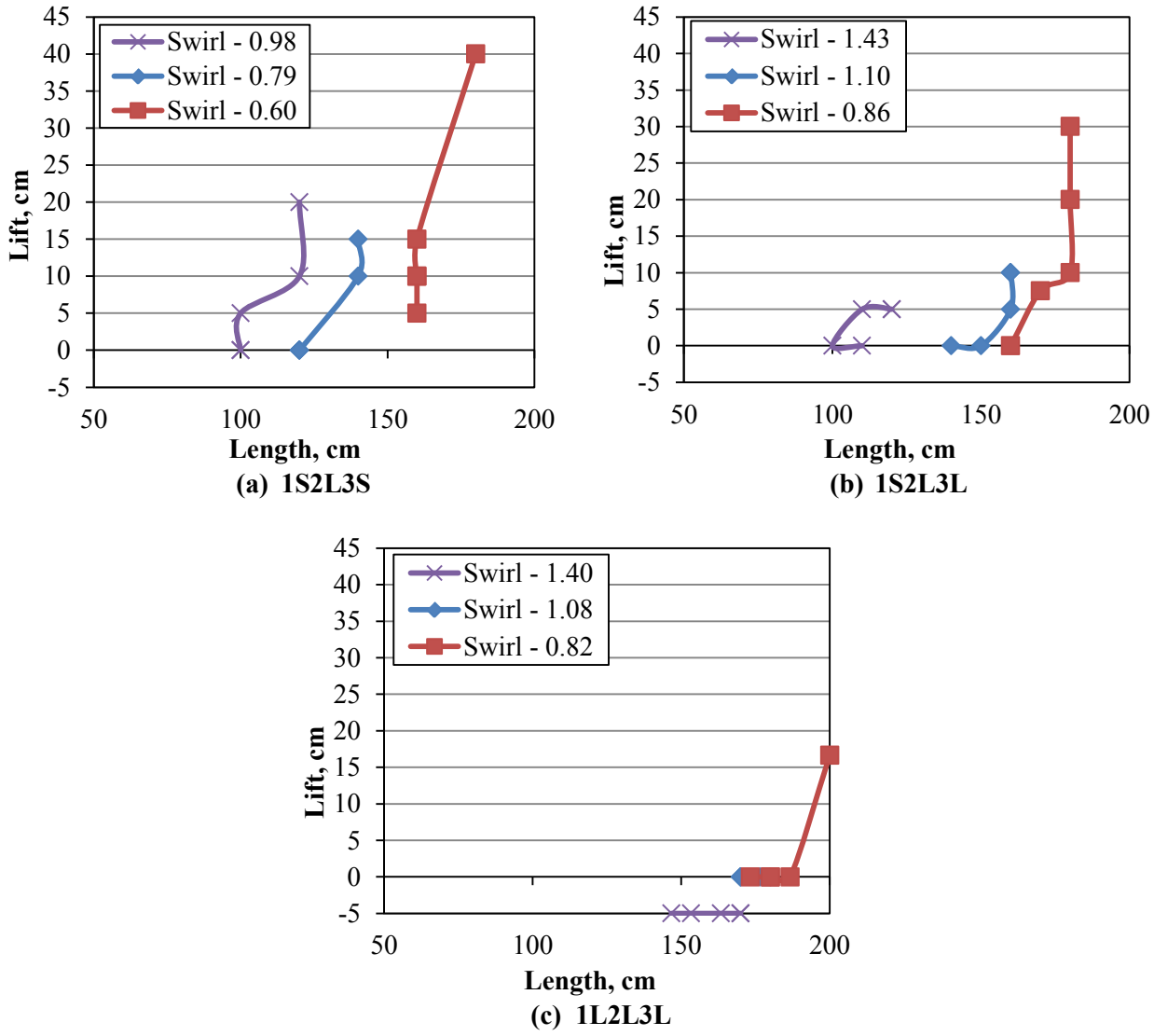

Figure 6.2: NO (ppm) vs. LOI at three different swirl settings, varying flow rates of oxygen, center injection, medium hardwood, for burner configurations (a) 1S2L3S, (b) 1S2L3L and (c) 1L2L3L

The straw flames tended to be longer with similar lift to the medium hardwood flames. The fine hardwood flames were much shorter than the medium hardwood flames and were attached for every operating condition where data were collected.

6.1.2 Flame Length Model

A flame length model was created in attempt to determine parameters that might be used to predict flame length and scaling parameters. The model will also be used to determine the correlation between predicted flame length and NO and LOI.

A common method for predicting flame length is to determine the locations where fuel and air mix to a stoichiometric composition. Using this approach, the flame length will occur at axial position. Chen and Driscoll [24] used such an approach to predict the length of a swirling gas flame. This approach was modified for a particle flame by first assuming that the volatile mass and required air fuel ratio are that of the solid fuel. This could perhaps be improved by using the volatile fraction from the proximate analysis but this was not done in this initial attempt.

The constant C_s, as shown in Equation 6.1, is the stoichiometric air to fuel ratio where $\dot{m}_{ox}$ is the mass flow rate of oxidizer and $\dot{m}_{fuel}$ is the mass flow rate of fuel.

$$c_s = \left(\frac{\dot{m}_{fuel}}{\dot{m}_{ox}}\right)_s \tag{6.1}$$

These flow rates are related to geometric and flow parameters as shown in Equation 6.2. The numerator represents the fuel flow entering through the primary annulus between the primary tube diameter d_p and the center tube diameter d_c, where ρ_{mix}, is the primary fuel air mixture density, V_P is the primary mixture velocity, and $Y_{fuel,p}$ is the fuel mixture fraction of the primary flow. The denominator consists of four terms each representing a flow of oxygen into the flame. The first term, U_{RZ}, follows the nomenclature of Chen and Driscoll [24] and represents the radial velocity along the axial circumference ($\pi b L_f$) of the flame. L_f is the flame length, b the diameter of the recirculation zone core, ρ_{sec}, is the density of the secondary air stream and

$Y_{O_2,sec}$, is the mass fraction of O_2 in the secondary stream. The magnitude of U_{RZ} was determined as a function of swirl, S, and secondary axial velocity, V_{sec}, based on a correlation of the data from Chen and Driscoll as shown in Equation 6.3. The second term in the denominator represents oxygen mixing into the fuel jet due to the axial velocity difference between the fuel jet and the secondary flow. The rate of mixing is assumed to be proportional to the absolute value of the velocity difference of V_p and V_{sec}, which has been experimentally observed for turbulent flames.

$$c_s = \frac{\rho_{mix} V_p \frac{\pi}{4}\left(d_p^2 - d_c^2\right) * Y_{fuel,p}}{Y_{O_2,sec}\left[\rho_{sec}\pi b L_f U_{RZ} c_2 + \rho_{sec}\left|V_p - V_{sec}\right| d_p L_f \pi c_1\right] + \dot{m}_{O_2,c} + \dot{m}_{O_2,p}} \tag{6.2}$$

The third term in the denominator $\dot{m}_{O_2,c}$ is the flow rate of oxygen in the center tube. The model assumes that all of the oxygen delivered from this tube is mixed into the fuel stream. This may not be the case for higher flow rates of oxygen and will be checked by a calculation discussed below. The final term in the denominator, $\dot{m}_{O_2,p}$, is the oxygen added to the primary stream by premixing oxygen with the primary fuel and air.

$$U_{RZ} = \frac{0.2 * S * V_{sec}}{0.2 + S} \tag{6.3}$$

The flame length of a swirl-stabilized flame can be re-written as shown in Equation 6.4. The constants c_1 and c_2 were found by minimizing a least squares difference between the measured and predicted flame lengths for each fuel. With the constants calculated, the flame length, L_f, for the turbulent, swirl-stabilized flame is found using Equation 6.4.

$$L_f = \frac{\frac{\dot{m}_{fuel}}{c_s} - \dot{m}_{O_2,p} - \dot{m}_{O_2,c}}{\left[\rho_{sec}\pi b U_{RZ} c_2 + \rho\left|V_p - V_{sec}\right| d_p \pi c_1\right] Y_{O_2,sec}} \tag{6.4}$$

Oxygen injected into the center tube can also form a separate flame at the stoichiometric boundary between the fuel and oxygen. The flame length of the oxygen flame can be modeled in the same way that the outer flame length is modeled as shown in Equation 6.5.

$$L_{O_2} = \frac{c_s * \dot{m}_{O_2}}{\rho_{mix} \pi d_c |V_c - V_p| c_1 \left(\frac{\dot{m}_f}{\dot{m}_{air}}\right)} \tag{6.5}$$

This oxygen flame was calculated as a check. If this flame length is longer than the outer flame length, the oxygen from the center flow will not be completely mixed into the fuel jet and the model will under predict the flame length.

6.2 Flame Length Model – Measurement Comparison

The visual flame length measurements are compared to the calculated model flame length in Figure 6.3. Given the relatively crude method of measurement and simple nature of the model, the model appears to capture first order effects on the flame length.

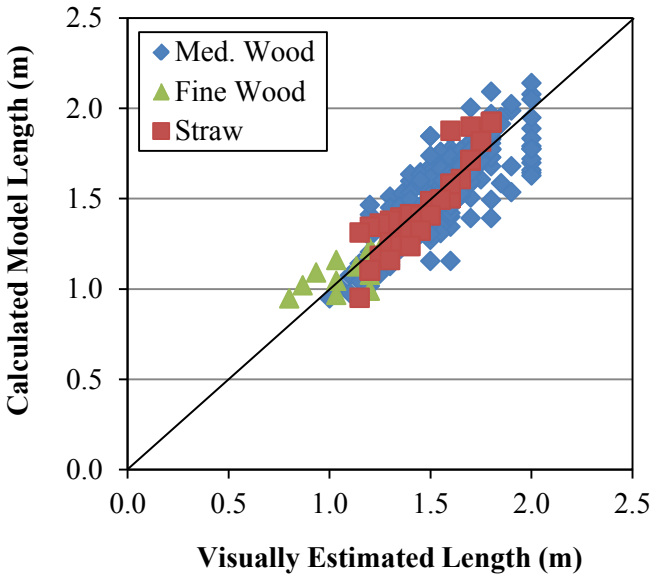

Figure 6.3: Calculated Flame Length (m) vs. Visually Estimated Length (m) for all data collected separated by fuel

The scatter in the data are on the order of 50% suggesting there are important physical processes occurring that are not captured in the model. While some attempts were made to refine the model and make it more accurate, the fidelity of the measurements does not warrant an improvement and additional details of the flow are difficult to measure without a significant effort.

Exercising the model provides some indication of how various parameters influence flame length. Figure 6.4 shows the influence of oxygen flow rate from various sources. As expected the flame length decreases in all cases when oxygen is added. When oxygen is added to the fuel rich jet directly by center injection or premixed with the primary all of the oxygen is introduced into the fuel rich region in both cases and the flame shortens a similar amount. In the case of global enrichment, only a fraction of the oxygen in the secondary is entrained and therefore the flame does not shorten as rapidly.

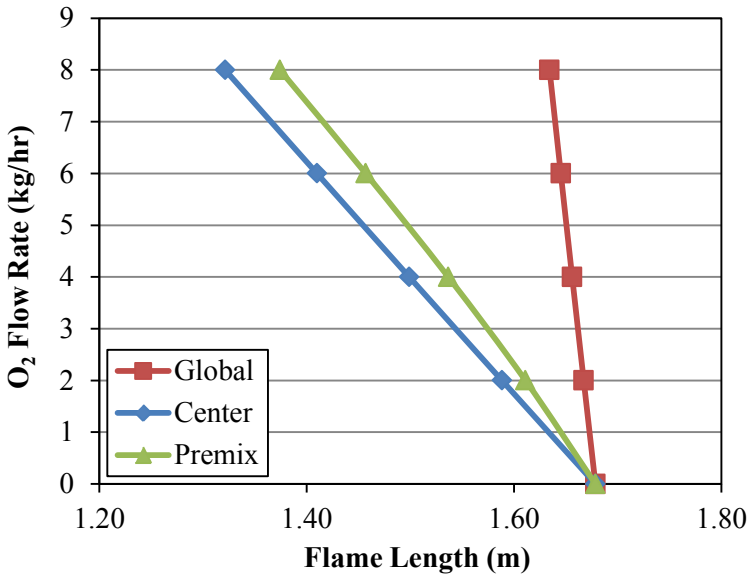

Figure 6.4: Oxygen Flow Rate (kg/hr) vs. Flame Length (m) for three oxygen addition techniques, configuration 1S2L3L, medium hardwood, and constant secondary air

If the flame length is a measure of residence time for particles in a fuel rich region, then the longer the flame, the greater the tendency to convert fuel nitrogen to N_2 instead of NO. At the same time, the longer flame reduces the length of the particle flame or particle burnout zone. A comparison of measured NO concentration and measured LOI versus the predicted flame length for the 1S2L3L configuration for five different oxygen injection strategies is shown in Figure 6.5. The data show a linear correlation with flame length and NO for each injection strategy and similar result for each injection strategy. To a first order approximation, the exhaust NO is correlated to flame length. A similar result with the opposite trend is seen for LOI. LOI is seen to increase with increasing flame length.

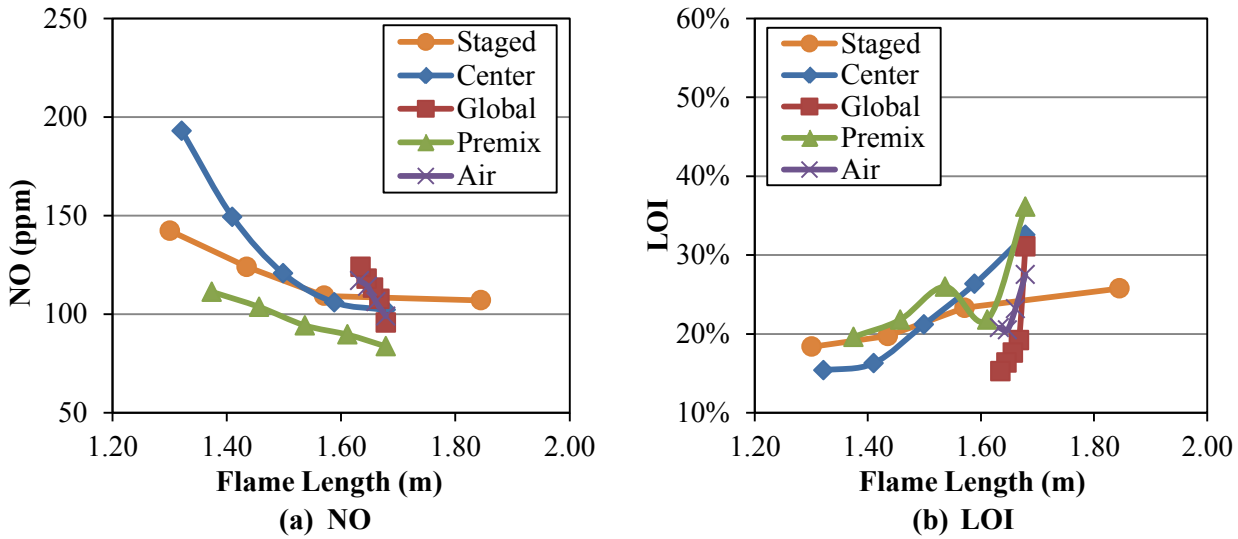

Figure 6.5: (a) NO (ppm) and (b) LOI vs. Flame Length (m) for five oxygen addition techniques, medium hardwood, and configuration 1S2L3L

Figure 6.6a shows NO versus calculated flame length (m) for all of the medium wood data. In this figure five burner configurations are represented as well as four oxygen addition strategies and variable amounts of oxygen. The data show a scattered but identifiable correlation between NO and flame length. Long flames all tend to produce an NO minimum in the range of 75-80 ppm. NO concentration increases as flame length decreases. Figure 6.6b shows LOI versus

calculated flame length (m) for all of the medium wood data and each of the configurations. The decrease in LOI with decreasing length is apparent among each of the configurations.

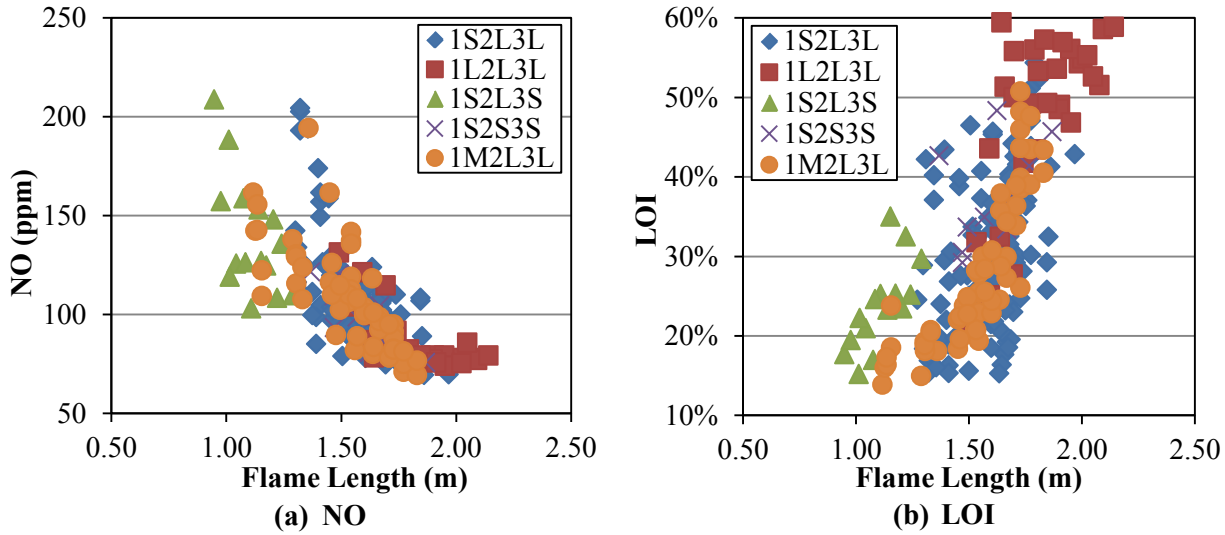

(a) NO (b) LOI

Figure 6.6: (a) NO (ppm) and (b) LOI vs. Flame Length (m) for all medium hardwood data collected separated by configuration

Figure 6.7a and Figure 6.7b show measured NO and LOI versus calculated flame length for three burner configurations with straw. The correlation for NO may be better for straw than for wood. The decrease in LOI with decreasing length is also apparent.

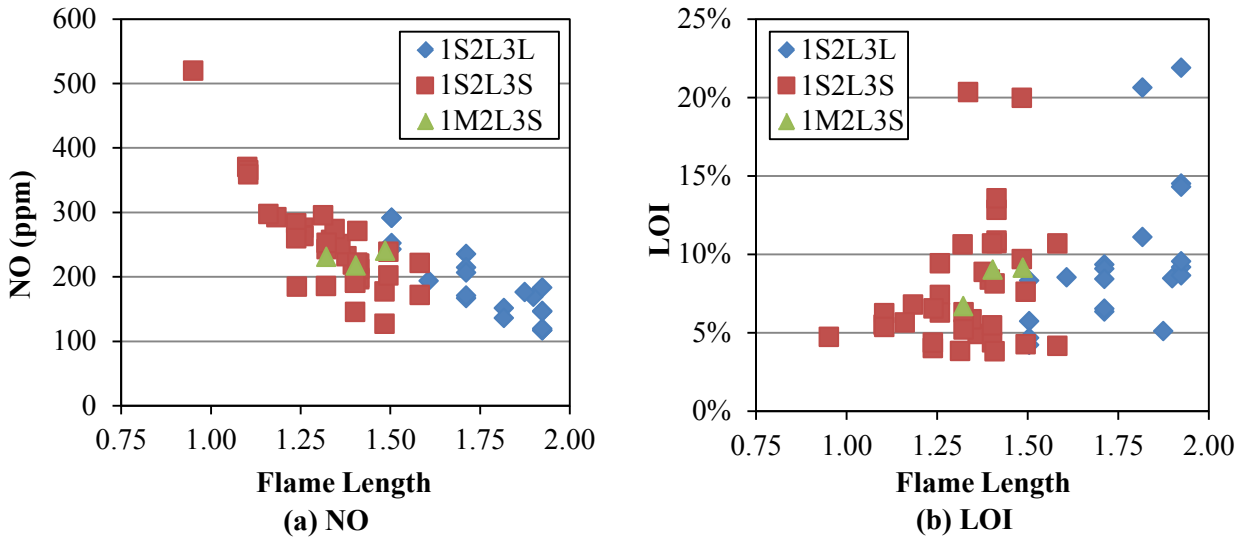

(a) NO (b) LOI

Figure 6.7: (a) NO (ppm) and (b) LOI vs. Flame Length (m) for all wheat straw data collected separated by configuration

Finally, all data are shown in Figure 6.8a for NO and Figure 6.8b for LOI. The basic trends of decreasing NO and increasing LOI with increasing flame length can be seen but the correlation is weak and scattered when all data are concerned. The mismatch with NO and LOI points out a weakness of the direct correlation of NO and flame length. It is well known that the NO depends on the local mixture fraction, turbulent mixing, and temperature which are not all considered by simply predicting flame length.

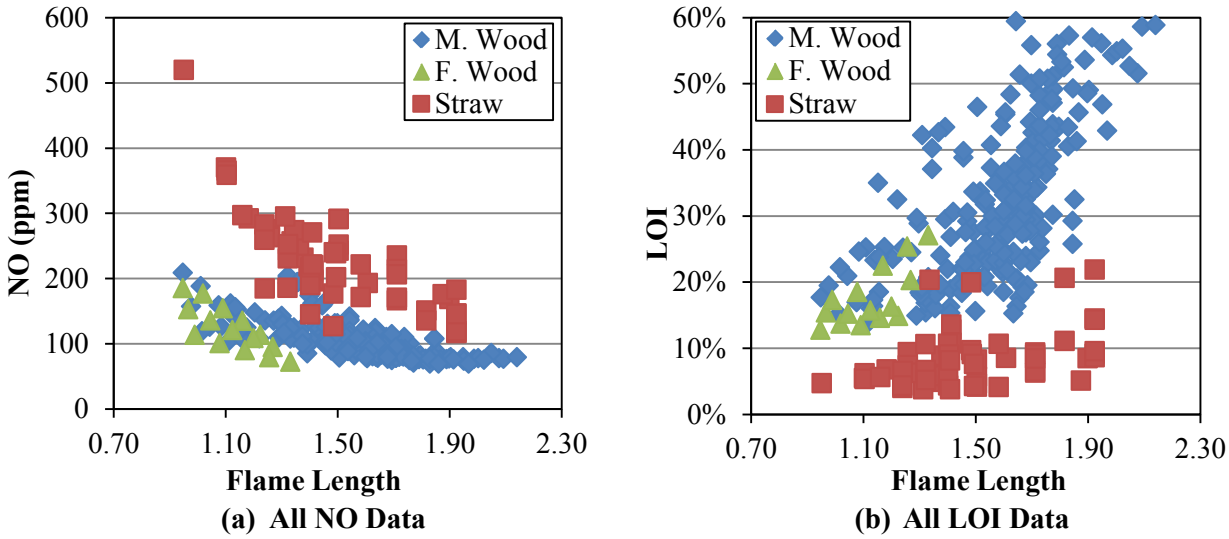

Figure 6.8: (a) NO (ppm) and (b) LOI vs. Flame Length (m) for all data collected

7 SUMMARY AND CONCLUSIONS

An Air Liquide designed pipe-in-pipe burner was used in conjunction with three biomass fuels, wheat straw, medium hardwood, and fine hardwood, to explore the impact of oxygen enrichment. Exhaust gas species, O_2, CO_2, CO, and NO, were collected along with exhaust ash samples and visual flame characteristics. NO emissions and LOI data were reported. Six configurations and numerous operating conditions were used to determine relationships and trends.

NO emissions and LOI were dependent on numerous variables including swirl, oxygen flow rate, oxygen injection location, primary air flow rate, and burner configuration. The change in LOI and NO were so frequently in opposite directions that it was advantageous and important to consider them both at the same time rather than individually. For this reason, NO-LOI trade-off curves were developed. The trade-off curves for hardwood appeared to asymptote to a minimum of 70 ppm NO at high LOI and 15% LOI and high NO. A trade-off curve that was shifted closer to the origin was deemed to be better than those further from the origin.

Changing swirl or oxygen flow rate typically produced NO-LOI trade off curves where increasing swirl or adding oxygen produced higher NO and lower LOI. The more favorable trade-off curves were produced when oxygen was introduced into the secondary air or into the primary air-fuel mixture. Adding oxygen in the center tube in small amounts (2 kg/hr) moved the trade-off favorably but higher flow rates of O_2 in the center tube tended to increase NO at a higher rate without as much benefit in LOI as when oxygen was added to the secondary or

primary. Adding O_2 radially or from a lance extended beyond the burner outlet also had a tendency to produce a less favorable trade-off curve as oxygen was added. Decreasing the amount of primary air or the primary air momentum produced a very favorable trade-off curve where reductions in LOI were seen without a large increase in NO. The reduction of primary flow was limited to the amount required to transport the fuel without plugging up the flow lines.

Oxygen injection was found to be an effective tool for LOI reduction, extending the capacity of increased swirl. This was particularly true for larger fuel particles where LOI was initially high and NO low when burned in air. The addition of oxygen was less useful for the fine wood particles because LOI was already low and NO was high. Reducing swirl and adding oxygen had a slightly better trade-off than swirl alone. Also, the addition of oxygen in the center tube accompanied by reduced secondary flow designed to keep overall O_2 concentration in the exhaust constant had a negative effect on the trade-off curve where conditions existed in which both NO and LOI increased.

It is believed the addition of oxygen generally had the effect of reducing the local equivalence ratio, residence time, and size of fuel rich regions that reduce NO to N_2 and inhibit NO formation. Thus adding O_2 was generally detrimental to NO. At the same time, it was beneficial to LOI by providing a higher oxygen concentration in the burnout zone.

The actual volatile region equivalence ratio and change caused by O_2 addition, swirl, or burner configuration is difficult to predict as it is complicated by the existence of three jets (center fuel, primary, and secondary) and swirl that interact and mix with each other. Swirl was also assumed to cause increased O_2 concentration or a leaner volatiles region. The reason that center O_2 injection produced an inferior trade-off curve to the other oxygen injection locations is not clear. One potential explanation is that the center O_2 jet was able in certain circumstances to

penetrate through the fuel rich recirculation zone. Because of the high temperature of pure O_2 flames, thermal NO may become important. If not thermal NO, the NO formed between volatiles and this O_2 jet would have less opportunity for reburning if formed outside of the fuel rich jet region.

The NO and LOI data appeared to correlate with observed flame lengths. As such a relatively simple model was developed to predict flame length. The model requires two constants to be selected based on a fit to at least two flame length data points. The model was moderately successful in predicting the measured flame lengths and these flame lengths were found to correlate the general trend of increasing NO with shorter flame length.

The burner configuration had a large impact on flame structure and characteristics. Different configurations led to various primary and secondary velocities, which led to a wide range of flame lengths and appearances. Configuration 1S2L3L was used primarily for hardwood and produced a reasonably well attached Type 1 flame with the fuel jet penetrating through the recirculation zone and producing a relatively high aspect ratio (long) flame. A change in variable such as swirl or O_2 flow rate that maintained the basic structure of this flame produced smoothly changing, monotonic trade-off curves. Geometries that changed flow patterns caused NO-LOI behavior that was erratic and less predictable. Configuration 1S2S3S along with 1L2L3L, associated with high primary velocities, had long flames with LOI values that were difficult to improve. Configuration 1S2S3S was skinny and elongated, whereas 1L2L3L was lazy, long, and wide. It was found that configuration 1S2L3S led to better flame characteristics for the wheat straw fuel. Recessing the center tube generally reduced flame length and acted as if the primary momentum was slowed due to the wider pipe diameter opening to the primary flow just below

the center tube. Extending the center tube typically led to decreased mixing, lower NO and higher LOI.

The straw fuel was compared to the medium hardwood with configurations 1S2L3L and 1S2L3S. Overall, the straw had a shifted NO versus LOI tradeoff curve toward higher values of NO and lower values of LOI. This shifted curve is attributed to the ash and nitrogen content in the fuel as well as the size distribution differences.

The fine hardwood fuel had comparable results to the medium hardwood, but with an NO versus LOI tradeoff curve that had lower values of LOI. NO values were comparable to those obtained with the medium wood. With the addition of oxygen or swirl LOI decreased at the cost of increasing NO.

REFERENCES

[1] "Carbon Dioxide Emissions," 14 June 2012. [Online]. Available: http://www.epa.gov/climatechange/ghgemissions/gases/co2.html. [Accessed 5 April 2013].

[2] L. Baxter, "Biomass-Coal Co-Combustion: Opportunity for Affordable Renewable Energy," Fuel, vol. 84, pp. 1295-1302, 2005.

[3] R. Guerreo-Lemus and J. M. Martinez-Duart, Renewable Energies and CO2, London: Springer-Verlag, 2013.

[4] L. Baxter, "Solid Biofuels for Energy," in Solid Biofuels for Energy, Springer London, 2011, pp. 43-73.

[5] L. Baxter, "Co-Firing Overview," in Second World Conference and Exhibition on Biomass for Energy, Industry and Climate Protection, Rome, Italy, May 10-14, 2004.

[6] J. Koppejan, "Introduction and Overview of Technologies Applied Worldwide," in Second World Conference and Exhibition on Biomass for Energy, Industry and Climate Protection, Rome, Italy, May 10-14, 2004.

[7] "Nitrogen Dioxide," 15 August 2014. [Online]. Available: http://www.epa.gov/airquality/nitrogenoxides. [Accessed 24 February 2015].

[8] "Sulfer Dioxide," 15 August 2014. [Online]. Available: http://www.epa.gov/air/sulferdioxide. [Accessed 24 February 2015].

[9] S. Y. Luo, B. Xiao, Z. Q. Hu, S. M. Liu and Y. W. Guan, "Experimental Study on Oxygen-Enriched Combustion of Biomass Micro Fuel," Energy, vol. 34, pp. 1880-1884, 2009.

[10] M. Fang, D. Shen, Y. Li, C. Yu, Z. Yuo and K. Cen, "Kinetic Study on Pyrolysis and Combustion of Wood Under Different Oxygen Concentrations by Using TG-FTIR Analysis," Journal of Analytical and Applied Pyrolysis, vol. 77, no. 1, pp. 22-27, 2006.

[11] L. Bool, H. Kobayashi, K. Wu, D. Thompson, E. Eddings, O. Okerlund, J. Wendt, M. Cremer and D. Wang, "Oxygen for NOx Control - A Step Change Technology," in

Proceedings of the Nineteenth Annual International Pittsburg Coal Conference, Pittsburg, PA, 2002.

[12] L. E. Bool and S. Laux, "Oxygen Enhanced Combustion - A Demonstrated Option for NOx Control," in Proceedings of the 37th International Technical Conference on Clean Coal & Fuel Systems, Clearwater, FL, 2012.

[13] S. R. Turns, "Oxides of Nitrogen Formation," in An Introduction to Combustion Concepts and Applications, New York, The McGraw-Hill Companies, Inc., 2011, pp. 170-174.

[14] J. D. Thornock, "Burnout, NO, Flame Temperature, and Radiant Intensity from Oxygen-Enriched Combustion of a Hardwood Biomass," Brigham Young University, Provo, UT, 2013.

[15] P. Glarborg, A. D. Jensen and J. E. Johnsson, "Fuel Nitrogen Conversion in Solid Fuel Fired Systems," Progress in Energy and Combustion Science, vol. 29, no. 2, pp. 89-113, 2003.

[16] J. Wendt, "Mechanisms Governing the Formation and Destruction of NOx and Other Nitrogenous Species in Low NOx Coal Combustion Systems," Combustion Science and Technology, vol. 108, no. 4-6, pp. 323-344, 1995.

[17] W. P. Linak, J. A. McSorley, R. E. Hall, J. V. Ryan, R. K. Srivastava, J. Wendt and J. B. Mereb, "N2O Emissions From Fossil Fuel Combustion," in Proceedings of the 82nd Annual Meeting of the Air and Waste Management Association, Anaheim, CA, 1989.

[18] A. J. MacKrory and D. R. Tree, "Measurement of Nitrogen Evolution in a Staged Oxy-combustion Coal Flame," Fuel, no. 93, pp. 298-304, 2012.

[19] S. R. Turns, "Burning of Carbon," in An Introduction to Combustion Concepts and Applications, New York, The McGraw-Hill Companies, Inc., 2011, pp. 530-551.

[20] N. Dong, "Reducing Carbon-in-Ash," IEA Clean Coal Centre, London, 2010.

[21] J. Beer and N. Chigier, Combustion Aerodynamics, Essex: Applied Science Publishers LTD, 1972, pp. 109-114.

[22] M. Hupa, "International Flame Research Foundation," 24 January 2006. [Online]. Available: www.ffrc.fi/Liekkipaiva_2006/Liekkipaiva2006_IFRF_Today_HUPA.pdf. [Accessed 11 March 2015].

[23] A. Garg, "Trimming NOx from Furnaces," Chemical Engineering, vol. 99, no. 11, pp. 122-124, 1992.

[24] R.-H. Chen and J. F. Driscoll, "The Role of the Recirculation Vortex in Improving Fuel-Air Mixing within Swirling Flames," in The Combustion Institute, Pittsburgh, PA, 1988.

[25] T. Draper, D. Zeltner, D. R. Tree, Y. Xue, C. Periasamy, T. Kang and R. Tsiava, "Characterization of a Primary-Swirled, High Oxygen Participation Coal Flame: Flame Temperature, Emissivity, NO, and Burnout Measurements," Proceedings of the Combustion Institute, vol. 34, pp. 2779-2786, 2013.

[26] H. Kruczek, P. Raczka and A. Tatarek, "The Effect of Biomass on Pollutant Emission and Burnout in Co-Combustion," Combustion Science and Technology, vol. 178, no. 8, pp. 1511-1539, 2006.

[27] D. M. Boylan, "Southern Company Tests of Wood/Coal Cofiring in Pulverized Coal Units," Biomass and Bioenergy, vol. 10, no. 2-3, pp. 139-147, 1996.

[28] M. Pronobis, "Evaluation of the Influence of Biomass Co-Combustion on Boiler Furnace Slagging by Means of Fusibility Correlations," Biomass Bioenergy, vol. 28, pp. 375-283, 2005.

[29] S. Munir, W. Nimmo and B. M. Gibbs, "The Effect of Air Staged, Co-Combustion of Pulverised Coal and Biomass Blends on NOx Emissions and Combustion Efficiency," Fuel, vol. 90, pp. 126-135, 2011.

[30] H. Pawlak-Kruczek, M. Ostrycharczyk, M. Baranowski, M. Czerep and J. Zgora, "Co-Firing of Biomass with Pulverized Coal in Oxygen Enriched Atmosphere," Chemical and Process Engineering, vol. 34, no. 2, pp. 215-226, 2013.

[31] C. Yin, L. Rosendahl and S. K. Kaer, "Towards a Better Understanding of Biomass Suspension Co-Firing Impacts Via Investigating a Coal Flame and a Biomass Flame in a Swirl-Stabilized Burner Flow Reactor Under Same Conditions," Fuel Processing Technology, vol. 98, pp. 65-73, 2012.

[32] C. E. Baukal, Oxygen-Enhanced Combustion, Boca Raton, FL: CRC Press, 2013.

[33] M. B. Toftegaard, J. Brix, P. A. Jensen, P. Glarborg and A. D. Jensen, "Oxy-Fuel Combustion of Solid Fuels," Progress in Energy and Combustion Science, vol. 36, pp. 581-625, 2010.

[34] B. J. P. Buhre, L. K. Elliot, C. D. Sheng, R. P. Gupta and T. F. Wall, "Oxy-Fuel Combustion Technology for Coal Fired Power Generation," Progress in Energy and Combustion Science, vol. 31, pp. 283-307, 2005.

[35] T. Wall, Y. Liu, C. Spero, L. Elliott, S. Khare, R. Rathnam, F. Zeenathal, B. Moghtaderi, B. Buhre, C. Sheng, R. Gupta, T. Yamada, K. Makino and J. Yu, "An Overview of Oxy-Fuel Coal Combustion - State of the Art Research and Technology

Development," Chemical Engineering Research and Design, vol. 87, pp. 1003-1016, 2009.

[36] J. P. Smart and G. S. Riley, "Use of Oxygen Enriched Air Combustion to Enhance Combined Effectiveness of Oxyfuel Combustion and Post-Combustion Flue Gas Cleanup," Journal of the Energy Institute, vol. 85, no. 3, pp. 123-130, 2012.

[37] S. S. Daood, W. Nimmo, P. Edge and B. M. Gibbs, "Deep-Staged, Oxygen Enriched Combustion of Coal," Fuel, vol. 101, pp. 187-196, 2012.

[38] Y.-C. Chang, K.-K. Wu, C.-H. Chen and Y.-D. Chen, "Influences of Oxygen-Enriched Air on Combustion Characteristics of Industrial Furnaces," in 22nd International Symposium of Transport Phenomena, Delft, The Netherlands, 2011.

[39] W. Nimmo, S. S. Daood and B. M. Gibbs, "The Effect of O2 Enrichment on NOx Formation in Biomass Co-Fired Pulverised Coal Combustion," Fuel, vol. 89, pp. 2945-2952, 2010.

[40] J. Bai, C. Yu, L. Li, P. Wu, Z. Luo and M. Ni, "Experimental Study on the NO and N2O Formation Characteristics During Biomass Combustion," Energy and Fuels, no. 27, pp. 515-522, 2013.

[41] J. Riaza, M. V. Gil, L. Alvarez, C. Pevida, J. J. Pis and F. Rubiera, "Oxy-Fuel Combustion of Coal and Biomass Blends," Energy, vol. 41, no. 1, pp. 429-435, May 2012.

[42] O. Marin, F. Chatel-Pelage, M. U. Ghani, N. Perrin, R. Carty, G. R. Philo, H. Farzan and S. J. Vecci, "Low-Oxygen Enrichment in Coal-Fired Utility Boilers," in The 28th International Technical Conference on Coal Utilization & Fuel Systems, Clearwater, FL, 2003.

[43] D. Zeltner, "NO, Burnout, Flame Temperature, Emissivity, and Radiation Intensity from Oxycombustion Flames," Brigham Young University, Provo, UT, 2012.

[44] B. Damstedt, J. M. Pederson, D. Hansen, T. Knighton, J. Jones, C. Christensen, L. Baxter and D. Tree, "Biomass Cofiring Impacts on Flame Structure and Emissions," Proceedings of the Combustion Institute, vol. 31, pp. 2813-2820, 2007.

[45] T. A. Reeder, "Corrosion-related Gas Measurements and Analysis for a Suite of Coals in Staged Pulverized Coal Combustion," Brigham Young University, Provo, UT, 2010.

[46] S. C. Chamberlain, "Measurement and Analysis of Gas Composition in a Staged and Unstaged Oxy-Fired Pulverized Coal Reactor with Warm Flue Gas Recycle," Brigham Young University, Provo, UT, 2012.

APPENDIX A: AIR LIQUIDE BURNER SWIRL

A.1 Swirl Calculations

Swirl, S, has been studied by Beer and Chigier [21] and is defined in Equation A.1, where G_φ, is axial flux of angular momentum in Equation A.2 (shown is for a three concentric pipe in pipe burner), G_z is the axial flux of axial momentum in Equation A.3, and R is the burner radius, for this case R_5.

$$S = \frac{G_\varphi}{G_z R} \tag{A.1}$$

$$G_\varphi = \int_0^{r_1} (r\rho uw)2\pi r dr + \int_{r_2}^{r_3} (r\rho uw)2\pi r dr + \int_{r_4}^{r_5} (r\rho uw)2\pi r dr \tag{A.2}$$

$$G_z = \int_0^{r_1} \rho u^2 2\pi r dr + \int_{r_2}^{r_3} \rho u^2 2\pi r dr + \int_{r_4}^{r_5} \rho u^2 2\pi r dr + \int p dA \tag{A.3}$$

In these equations, u and w are the axial and tangential velocities respectively, A is the flow area, p is the static pressure, r is the radius, and ρ is the flow density. G_φ can be approximated, Equation A.4, as can G_z, Equation A.5, assuming a uniform velocity profile and constant static pressure across the flow area.

$$G_\varphi = \left[\frac{2}{3}\pi\rho uw(r_{i+1}^3 - r_i^3)\right] \tag{A.4}$$

$$G_z = [\rho u^2 \pi(r_{i+1}^2 - r_i^2)] \tag{A.5}$$

Total swirl was calculated in a similar fashion where the sum of all tangential momentum was divided by the product of the radius of the secondary flow and the sum of all axial

momentum flows. Beer and Chigier [21] estimated swirl for the variable block burners. These equations have been discussed by Reeder [45] and Thornock [14]. The equations for swirl, S, and angular momentum flux, σ, are shown in Equations A.6 and A.7.

$$S = \frac{\sigma R}{zB}\left[1 - \left(\frac{R_h}{R}\right)^2\right] \tag{A.6}$$

$$\sigma = \frac{2\pi}{z\xi_m}\sin(\alpha)\frac{\cos(\alpha)\,[1 + \tan(\alpha)\tan(\xi/2)](\xi/\xi_m)}{\{1 - [1 - \cos(\alpha)\,(1 + \tan(\alpha)\tan(\xi/2))]\xi/\xi_m\}^2} \tag{A.7}$$

Selected dimensions of the Air Liquide burner used in this work are seen in Table A.1. The angle of the swirl plate, ξ, versus the number of rotations of the threaded rod for the moveable block on the Air Liquide burner is shown in Figure A.1. The number of rotations, or turns, of the threaded rod and the corresponding theoretical secondary swirl number for the four possible configurations is shown in Table A.2.

Table A.1: Selected dimensions of Air Liquide burner

Variable	Value
α	45.00°
ξ_m	26°
B	1.00 in.
R	2.63 in.
R_h	1.19 in.
z	8

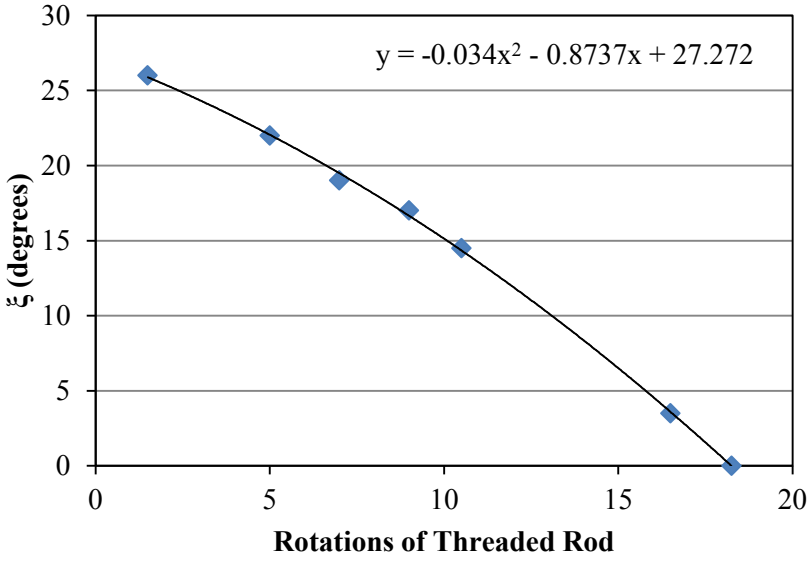

Figure A.1: Angle ξ (degrees) vs. Rotations of Threaded Rod for Air Liquide burner

Table A.2: Multiple rod rotations matched with corresponding theoretical secondary swirl numbers for the four possible configurations

Turns	2L3L	2S3L	2L3S	2S3S
0-1.5	1.473	1.610	1.031	1.200
2	1.441	1.574	1.008	1.173
3	1.372	1.499	0.960	1.117
4	1.298	1.418	0.909	1.057
5	1.219	1.332	0.853	0.993
6	1.135	1.240	0.795	0.925
7	1.047	1.144	0.733	0.853
8	0.955	1.044	0.669	0.778
9	0.861	0.940	0.602	0.701
10	0.763	0.834	0.534	0.622
11	0.664	0.726	0.465	0.541
12	0.565	0.617	0.396	0.460
13	0.466	0.509	0.326	0.380
14	0.369	0.403	0.258	0.301
15	0.275	0.300	0.192	0.224
16	0.184	0.201	0.129	0.150
17	0.099	0.108	0.069	0.080
18	0.019	0.021	0.013	0.015

A.2 Axial Profile Data

A hot wire anemometer was used to collect velocity data at the burner plane exit. This was collected radially for 2 burner configurations, 2L3S and 2L3L, and for 2 flow rates, 158 and 170 kg/hr. Figure A.2 shows axial and tangential velocity measurements for secondary flow rates of 158 and 170 kg/hr for configuration 2L3S. Axial velocity measurements were taken with the wire in a horizontal position and tangential velocity measurements were taken with the wire in a vertical position. Axial velocity measurements reveal a fairly uniform profile in the radial direction. Maximum swirl had the highest axial velocity and decreasing the swirl also decreased the axial velocity. For the tangential direction, maximum swirl saw higher velocities in the center, whereas lower swirl values had more of a uniform velocity profile. These trends were consistent for both flow rates.

Figure A.3 shows axial and tangential velocity measurements for secondary flow rates of 158 and 170 kg/hr for configuration 2L3L. This configuration is dramatically different from 2L3S. In this configuration at maximum swirl the axial velocity increased with an increase in radial distance away from the center. The slope of this line decreased with a decrease in swirl until it became level at no swirl. The tangential velocity for both flow rates showed identical trends, with the higher swirl values achieving the highest velocity measurements in the center and becoming slower at the tube walls.

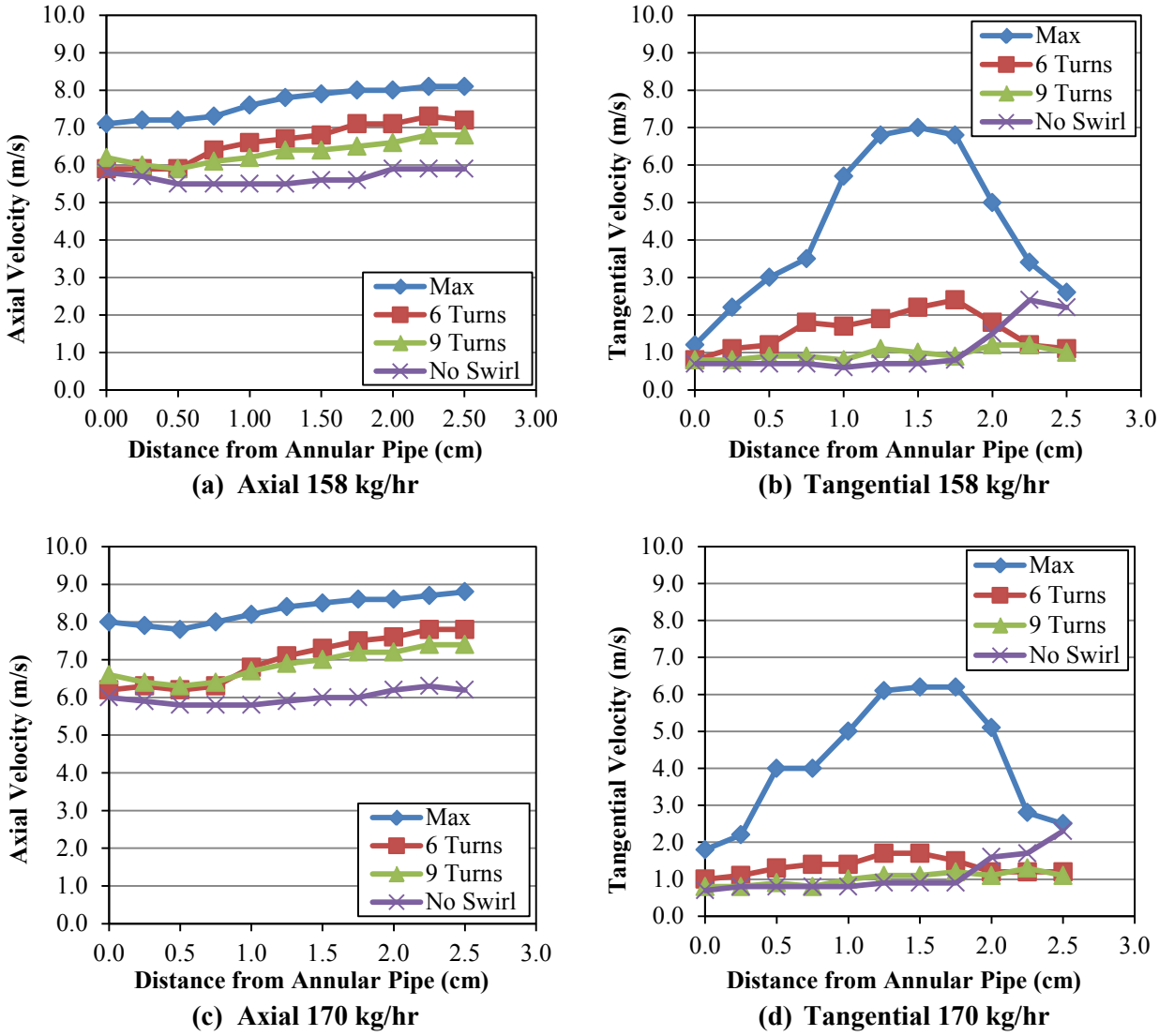

Figure A.2: Velocity (m/s) vs. Distance from Annular Pipe (cm) for configuration 2L3S and the following conditions: (a) Axial 158 kg/hr, (b) Tangential 158 kg/hr, (c) Axial 170 kg/hr, and (d) Tangential 170 kg/hr

Due to the way the anemometer works, the axial velocity shown is not very accurate. The anemometer is not able to differentiate between the directions of the flow as it allows air from numerous angles to flow pass the bead. The shape of the curve found in the axial velocity plots is assumed to be correct. Figure A.4 shows a corrected velocity versus radial distance from the annular pipe for the configuration 2L3S. In this correction the velocities were integrated to calculate a mass flow rate. The ratio of the calculated to the actual mass flow rate was used as a

correction factor to normalize the velocities. The mass flow rate could be calculated upon integration of the values shown in the figure.

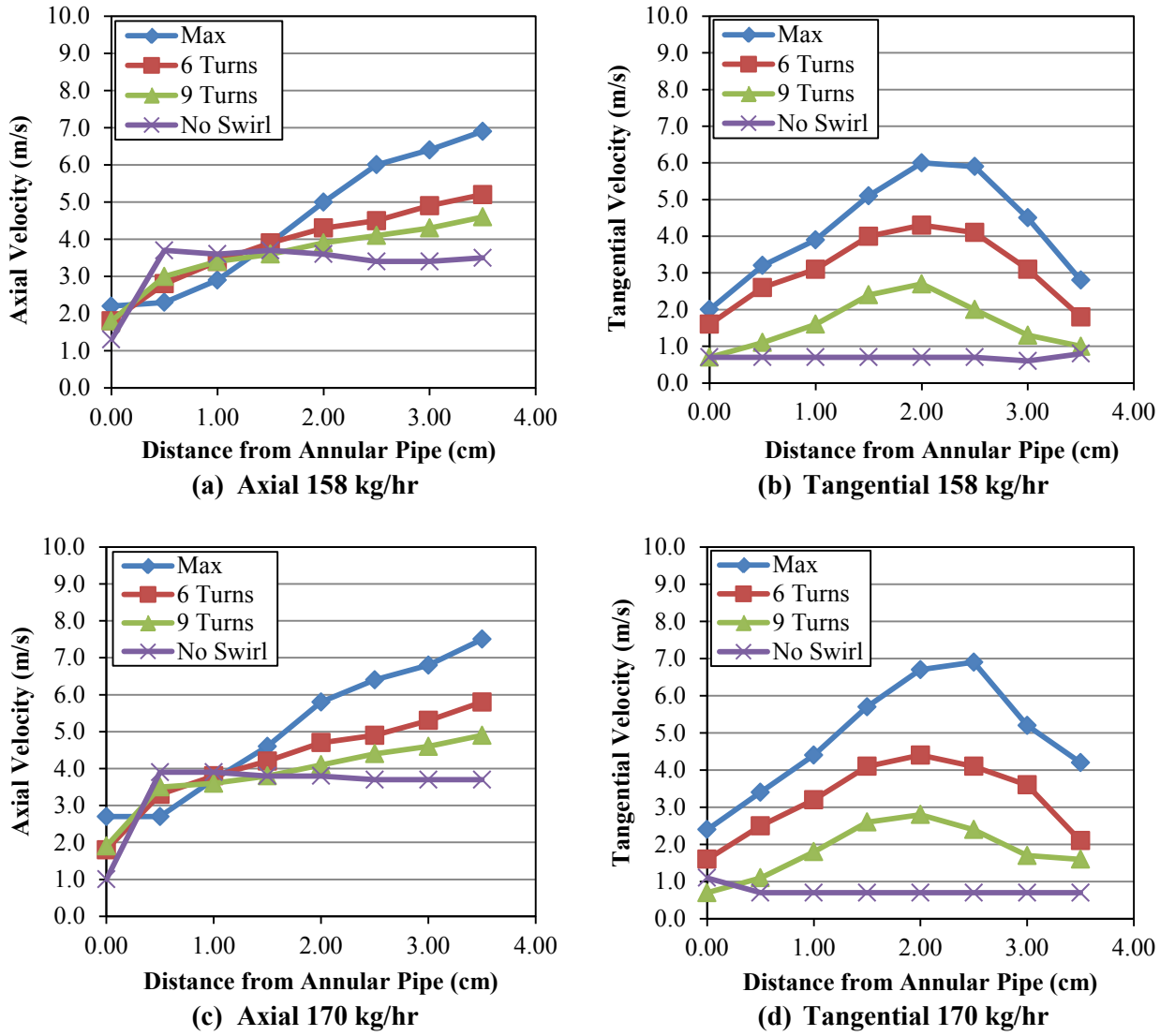

Figure A.3: Velocity (m/s) vs. Distance from Annular Pipe (cm) for configuration 2L3L and the following conditions: (a) Axial 158 kg/hr, (b) Tangential 158 kg/hr, (c) Axial 170 kg/hr, and (d) Tangential 170 kg/hr

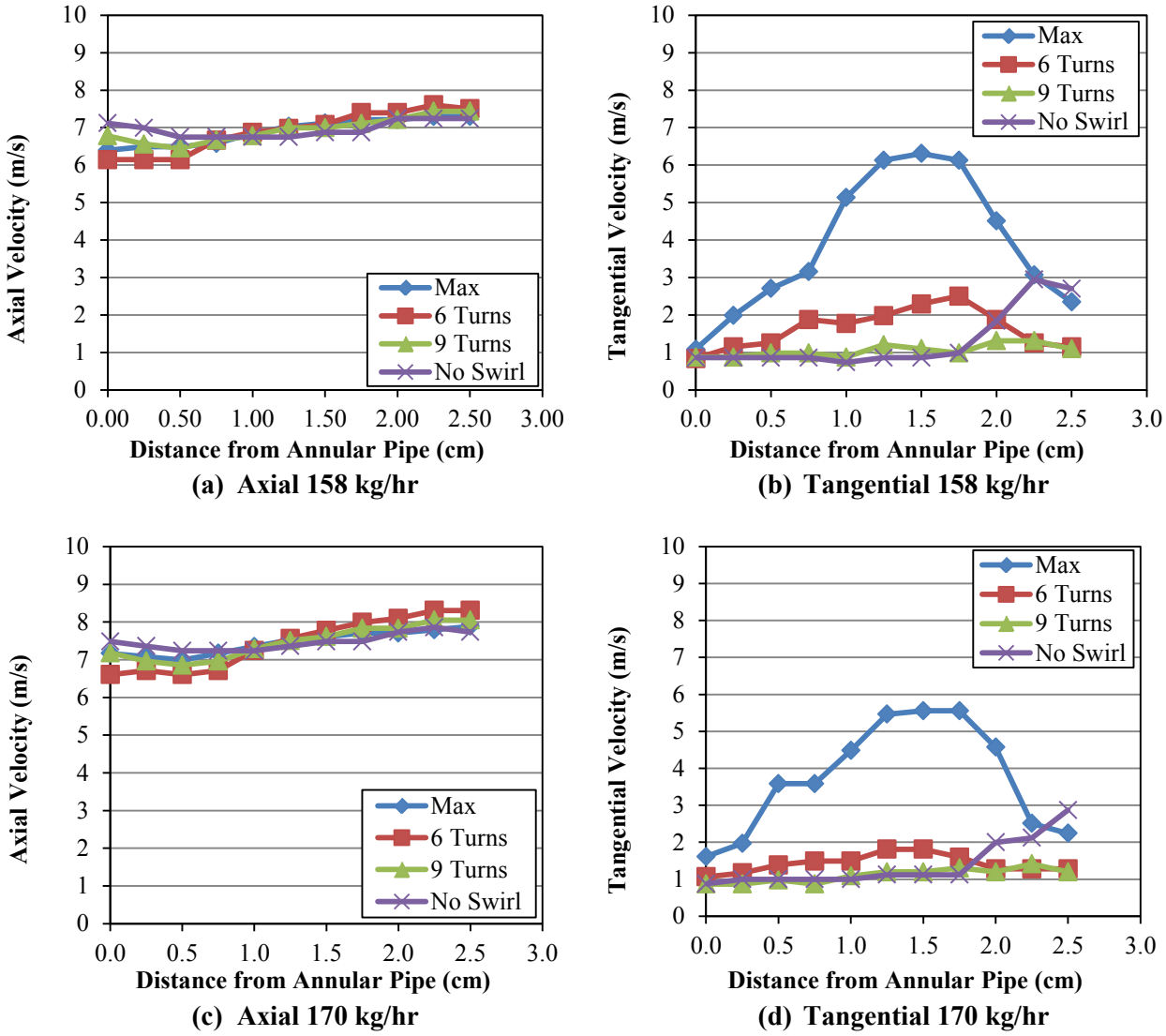

Figure A.4: Corrected Velocity (m/s) vs. Distance from Annular Pipe (cm) for configuration 2L3S and the following conditions: (a) Axial 158 kg/hr, (b) Tangential 158 kg/hr, (c) Axial 170 kg/hr, and (d) Tangential 170 kg/hr

This correction factor was calculated using only the axial velocity data, but was then applied to both the axial and tangential velocity plots. Shown in Figure A.5 is the corrected velocity versus radial distance from the annular pipe for the configuration 2L3L.

It should be noted however, that the collected values and the corrected values do not account for the temperature. All radial velocity profile tests were completed at room temperature. However, collection of combustion data took place with the secondary air temperature heated to

260°C. It is assumed that the profile for a higher temperature would not change, but rather scale the velocity due to the difference in density. The radial profile plots in this section are meant to give an idea of the accuracy of the swirl calculation, which assumes a constant velocity profile. Data was not taken for the other configurations, 2S3L and 2S3S.

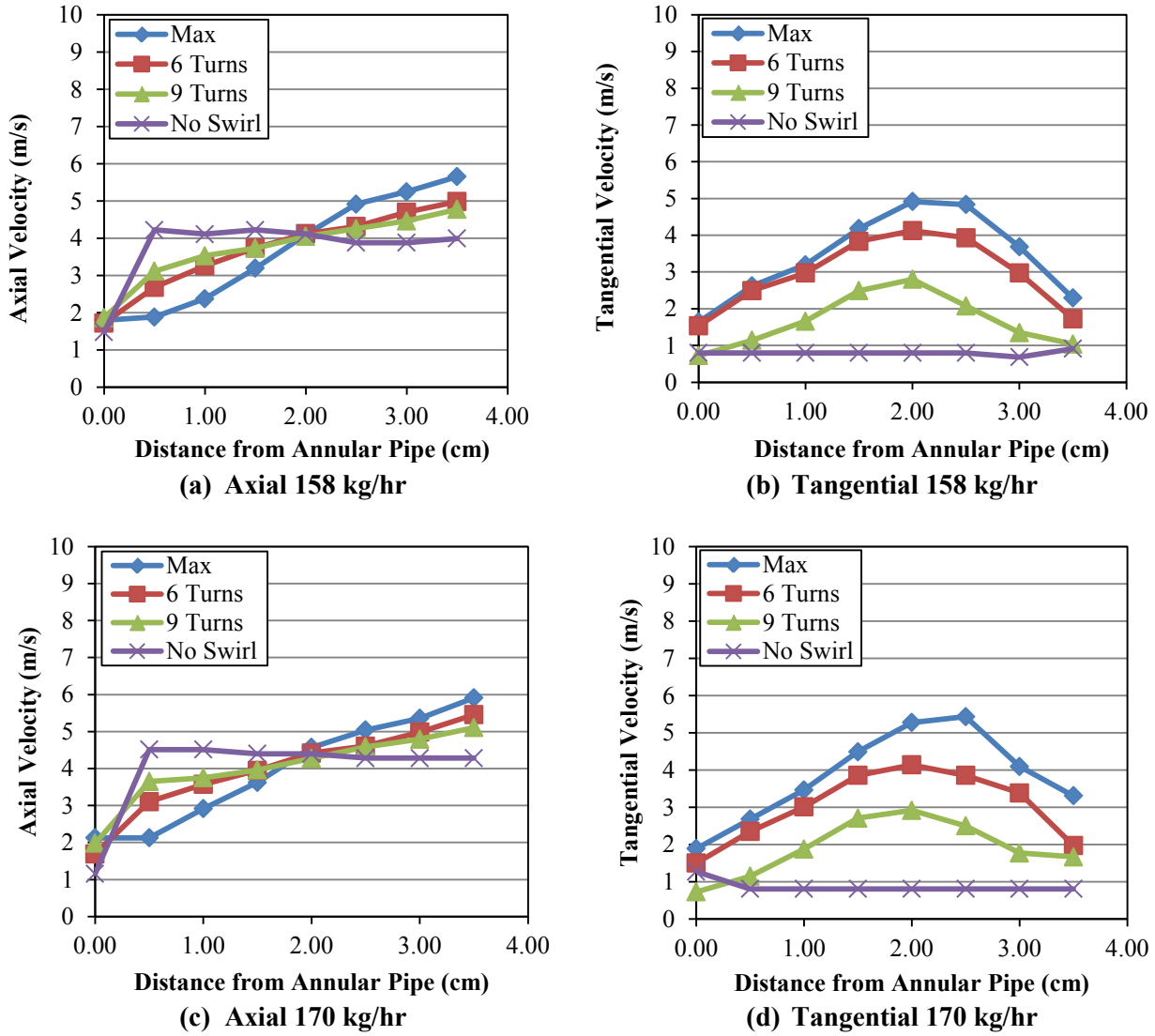

Figure A.5: Corrected Velocity (m/s) vs. Distance from Annular Pipe (cm) for configuration 2L3L and the following conditions: (a) Axial 158 kg/hr, (b) Tangential 158 kg/hr, (c) Axial 170 kg/hr, and (d) Tangential 170 kg/hr

APPENDIX B: DATA FROM REACTOR

NO_x can be converted from ppm to lb/MMBtu. For the reader's information, using the reactor in this work with medium hardwood and accounting for an energy conversion efficiency of 33%, 125 ppm is calculated to be roughly 0.385 lb NO/MMBtu. For the fine hardwood and wheat straw, 125 ppm is calculated to be about 0.412 and 0.383 lb NO/MMBtu respectively.

B.1 Uncertainty Analysis

There are a variety of sources for error in data, including precision error, bias error, and operating variability. Precision error refers to error associated with a range of values, or the closeness of agreement, wherein the data lies. Bias error refers to error that is an offset from true values or the trueness of data. Daily calibration of instruments was done to ensure that bias error was kept as low as possible. Unquantified bias error includes changes in the flow rate and pressure of the sample line and the unsteady flow of ash from the cyclone. Operating variability refers to error in repeatability of data due to the method or procedure of experiments and fluctuations due to the nature of the system setup.

In the operation of the BFR and in working with combustion, repeatability of the experiments becomes a major factor in error. Much effort is done ensuring the method of operation is consistent, instrumentation is properly calibrated, and that flow rates are constant. Upon repeated conditions, questions are raised as to why or why not data is in agreement with previous data. The temperature of the walls and pressure within the reactor, the consistency of

the fuel being used, the flow rate of the exhaust sample lines, the ash build up in the cyclone, and visual characteristics of the flame are a few of the aspects of the system that were explored when data did not seem to be repeatable.

Previous experience in working with the BFR has shown that day-to-day operation is usually not as consistent as same day experiments. Due to the nature of the error associated with the BFR a total error was estimated from repeated experiments and a relative error was determined for operating conditions that were the exact same, for all controllable variables. 12 such operating conditions were performed at various times with most of them being repeated just once. The average NO and LOI values were calculated as well as the standard deviation for each. A 95% relative confidence level was calculated for each of the operating conditions, the standard deviation multiplied by two and divided by the average value. The average 95% confidence level of all the operating conditions was estimated to be the total error for the NO and LOI measurements. Included in the operating conditions are various day-to-day operations and same day experiments. Most of the operating conditions that were repeated had 0 kg/hr oxygen being introduced, however two operating conditions had flow rates of 4 and 8 kg/hr, listed as operating condition 12 and 10 respectively. The summary of the uncertainty analysis is summarized in Table B.1. The estimated total error for NO was found to be 5.58%, thus for a nominal value of 125 ppm NO there would be a 95% confidence that the true value is 125 ± 6.97 ppm. The estimated total error for LOI was found to be 14.83%, and therefore a nominal value of 30% LOI would yield a 95% confidence that the true value is 30 ± 4.45%.

The total relative error estimated seems reasonable and brings confidence in and a better understanding of the trends shown. It should be noted that relative error for LOI are for data that are repeated conditions and not for a given ash sample. The LOI of a given ash sample was

averaged from three measurements from the same operating condition. There is greater confidence for a given ash sample than 14.83%. The 95% relative confidence level for a given ash sample is estimated to be 3.04% (e.g. 30 ± 0.91%), taken from the calculated average of 93 different ash samples.

Table B.1: Summary of uncertainty in the measurements taken

Operating Condition	# of Samples	Avg NO	σ NO	2σ/Avg NO	Avg LOI	σ LOI	2σ/Avg LOI
1	2	104	2.57	4.94%	31.24%	1.85%	11.87%
2	2	99	0.00	0.00%	28.46%	1.35%	9.49%
3	2	89	3.77	8.44%	34.76%	6.65%	38.29%
4	2	81	1.41	3.51%	35.98%	2.35%	13.09%
5	2	79	0.23	0.59%	50.07%	1.50%	5.99%
6	2	76	2.12	5.59%	45.47%	2.27%	9.98%
7	2	82	0.00	0.00%	48.37%	3.37%	13.95%
8	2	85	3.77	8.83%	41.75%	2.69%	12.87%
9	3	88	4.82	10.93%	43.46%	4.86%	22.36%
10	2	101	11.33	22.38%	29.84%	0.91%	6.07%
11	2	108	0.94	1.75%	27.51%	2.46%	17.89%
12	2	88	0.00	0.00%	35.44%	2.86%	16.12%
				5.58%			**14.83%**

B.2 Extra Plots

Figure B.1 shows NO versus LOI for all of the wood data collected. Shown also, are the various configurations highlighted to allow a comparison of each. Configurations 1S2L3L and 1M2L3L have the most data and also seem to have the most potential for NO versus LOI improvement.

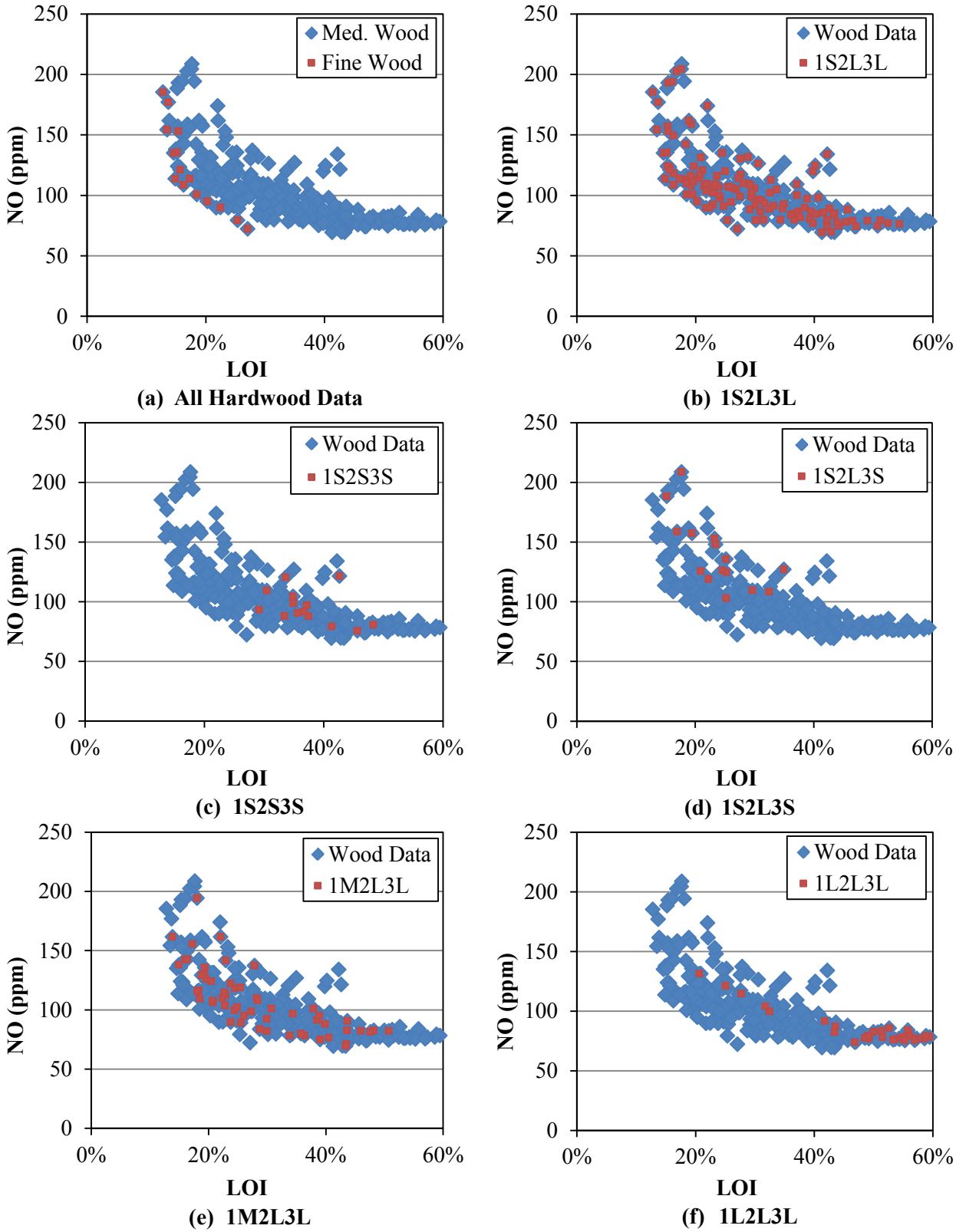

Figure B.1: NO (ppm) vs. LOI showing (a) All Hardwood Data and configurations (b) 1S2L3L, (c) 1S2S3S, (d) 1S2L3S, (e) 1M2L3L, and (f) 1L2L3L

Figure B.2 shows NO versus LOI for all of the straw data collected. The individual configurations are highlighted against all the data to make a comparison. Configuration 1S2L3S seems to have a better potential for low LOI and still maintain a relatively low NO value. However, both 1S2L3S and 1S2L3L have overlapping data, so both may be successful with determining an optimum operating condition.

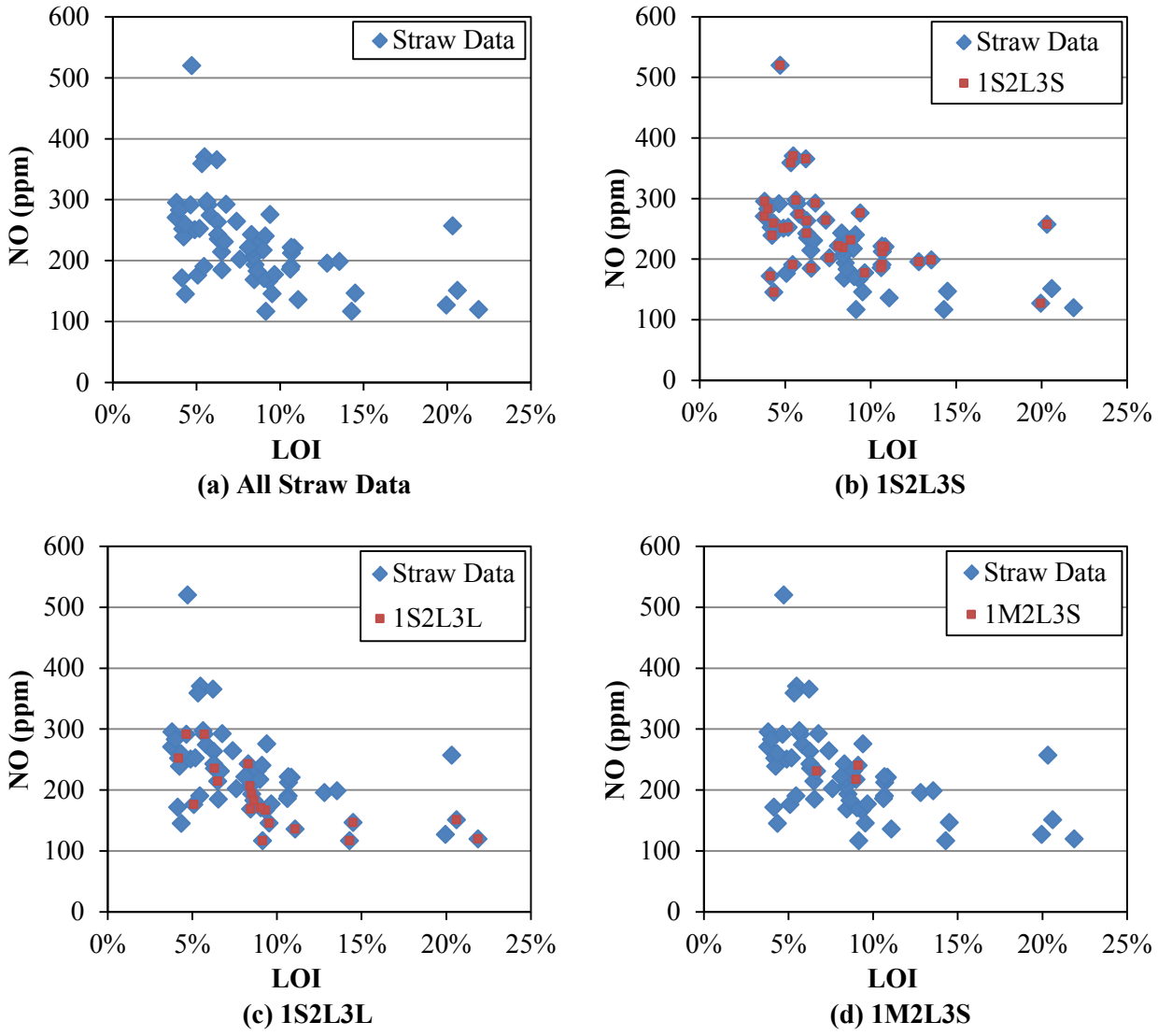

Figure B.2: NO (ppm) vs. LOI showing (a) All Straw Data and configurations (b) 1S2L3S, (c) 1S2L3L, and (d) 1M2L3S

B.3 All Data

The following tables, Table B.2 through Table B.18, list all the data collected from the BFR during this research.

Table B.2: Medium hardwood data with oxygen in the center tube, recessed 76 mm, using configuration 1S2L3L

Data	Date	Turns	O2	Prim	Sec	Fuel	NOx	LOI
1	12/10/13	0	0	20	164	29	89	32.5%
2	12/10/13	0	0	17	167	29	100	37.1%
3	12/10/13	0	0	11	173	29	113	18.5%
4	12/10/13	0	0	14	170	29	106	29.9%
5	12/10/13	0	2	14	162	29	108	21.5%
6	12/10/13	0	4	14	153	29	98	24.2%
7	12/10/13	0	6	14	144	29	105	26.8%
8	12/10/13	0	8	14	135	29	132	28.9%
9	12/11/13	6	0	14	170	29	92	30.1%
10	12/11/13	6	2	14	162	29	87	30.9%
11	12/11/13	6	4	14	153	29	87	37.3%
12	12/11/13	6	6	14	144	29	97	38.8%
13	12/11/13	6	8	14	135	29	109	37.1%
14	12/11/13	9	0	14	170	29	79	49.0%
15	12/11/13	9	2	14	162	29	75	44.2%
16	12/11/13	9	4	14	153	29	78	45.3%
17	12/11/13	9	6	14	144	29	79	46.5%
18	12/11/13	9	8	14	135	29	85	43.4%

Table B.3: Medium hardwood data with oxygen in the annulus, fuel in the center tube, recessed 76 mm, using configuration 1L2L3L

Data	Date	Turns	O2	Prim	Sec	Fuel	NOx	LOI
19	12/12/13	0	0	14	170	29	78	51.5%
20	12/12/13	0	2	14	162	29	77	54.3%
21	12/12/13	0	4	14	153	29	76	53.6%
22	12/12/13	0	6	14	144	29	77	49.2%
23	12/12/13	0	8	14	135	29	78	59.5%
24	12/12/13	3	0	14	170	29	77	58.6%
25	12/12/13	3	2	14	162	29	78	54.9%
26	12/12/13	3	4	14	153	29	79	49.0%
27	12/12/13	3	6	14	144	29	81	56.0%
28	12/12/13	3	8	14	135	29	83	51.3%
29	12/12/13	6	0	14	170	29	79	58.9%
30	12/12/13	6	2	14	162	29	86	52.7%
31	12/12/13	6	4	14	153	29	79	56.1%
32	12/12/13	6	6	14	144	29	77	57.3%
33	12/12/13	6	8	14	135	29	84	55.8%

Table B.4: Medium hardwood data with oxygen in the center, using configuration 1S2L3L

Data	Date	Ext. (mm)	Turns	O2	Prim	Sec	Fuel	NOx	LOI
34	3/11/14	-76	0	0	14	170	29	102	32.6%
35	3/11/14	-76	0	2	14	170	29	106	26.3%
36	3/11/14	-76	0	4	14	170	29	121	21.2%
37	3/11/14	-76	0	6	14	170	29	149	16.3%
38	3/11/14	-76	0	8	14	170	29	193	15.4%
39	3/11/14	-76	6	0	14	170	29	87	39.5%
40	3/11/14	-76	6	2	14	170	29	96	30.8%
41	3/11/14	-76	6	4	14	170	29	107	25.5%
42	3/11/14	-76	9	0	14	170	29	79	51.1%
43	3/11/14	-76	9	2	14	170	29	84	40.3%
44	3/11/14	-76	9	4	14	170	29	93	34.9%
45	3/11/14	-76	9	6	14	170	29	117	27.6%
46	3/27/14	-10	0	0	14	170	29	107	23.9%
47	3/27/14	-10	0	2	14	170	29	110	21.9%
48	3/27/14	-10	0	4	14	170	29	124	15.6%
49	3/27/14	-10	0	6	14	170	29	157	15.3%
50	3/27/14	-10	0	8	14	170	29	203	16.9%

Table B.5: Medium hardwood data with oxygen added to the secondary, center tube recessed 10 mm, using configuration 1S2L3L

Data	Date	Turns	O2	Prim	Sec	Fuel	NOx	LOI
51	5/5/14	0	2	14	162	29	90	38.4%
52	5/5/14	0	4	14	153	29	85	37.1%
53	5/5/14	0	6	14	144	29	89	42.6%
54	5/5/14	0	8	14	135	29	86	41.5%
55	5/5/14	0	0	14	170	29	96	31.1%
56	5/5/14	0	2	14	170	29	108	19.2%
57	5/5/14	0	4	14	170	29	113	17.6%
58	5/5/14	0	6	14	170	29	118	16.3%
59	5/5/14	0	8	14	170	29	124	15.3%
60	5/5/14	6	0	14	170	29	80	34.3%
61	5/5/14	6	2	14	162	29	84	43.4%
62	5/5/14	6	4	14	153	29	80	39.3%
63	5/5/14	6	6	14	144	29	79	42.2%
64	5/5/14	6	8	14	135	29	75	50.7%
65	5/6/14	6	0	14	170	29	82	37.6%
66	5/6/14	6	2	14	170	29	88	29.2%
67	5/6/14	6	4	14	170	29	92	23.0%
68	5/6/14	6	6	14	170	29	101	19.5%
69	5/6/14	6	8	14	170	29	110	18.5%
70	5/6/14	9	0	14	170	29	77	43.9%
71	5/6/14	9	4	14	170	29	84	36.3%
72	5/6/14	9	8	14	170	29	91	24.7%
73	5/6/14	9	0	14	170	29	74	47.1%
74	5/6/14	9	4	14	153	29	76	54.4%
75	5/6/14	9	8	14	135	29	77	52.5%

Table B.6: Medium hardwood data with oxygen in the center using configuration 1S2L3L

Data	Date	Ext. (mm)	Turns	O2	Prim	Sec	Fuel	NOx	LOI
76	5/6/14	70	9	0	14	170	29	79	30.2%
77	5/6/14	70	9	4	14	170	29	110	28.9%
78	5/6/14	70	9	8	14	170	29	174	22.0%
79	5/6/14	70	9	4	14	153	29	88	45.7%
80	5/6/14	70	9	8	14	135	29	99	29.5%
81	5/6/14	70	6	0	14	170	29	85	43.2%
82	5/6/14	70	6	2	14	170	29	93	31.7%
83	5/6/14	70	6	4	14	170	29	116	23.6%
84	5/6/14	70	6	6	14	170	29	159	19.3%
85	5/6/14	70	6	8	14	170	29	194	16.1%
86	5/6/14	70	6	2	14	162	29	89	34.7%
87	5/6/14	70	6	4	14	153	29	98	40.7%
88	5/6/14	70	6	6	14	144	29	120	39.8%
89	5/6/14	70	6	8	14	135	29	125	40.2%
90	5/7/14	70	0	0	14	170	29	99	29.4%
91	5/7/14	70	0	2	14	170	29	102	29.4%
92	5/7/14	70	0	4	14	170	29	120	25.0%
93	5/7/14	70	0	6	14	170	29	162	18.9%
94	5/7/14	70	0	8	14	170	29	204	17.6%
95	5/7/14	70	0	0	14	170	29	99	27.5%
96	5/7/14	70	0	0	14	179	29	106	23.2%
97	5/7/14	70	0	0	14	187	29	114	20.5%
98	5/7/14	70	0	0	14	196	29	117	20.8%
99	5/7/14	70	0	2	14	162	29	91	33.2%
100	5/7/14	70	0	4	14	153	29	105	33.7%
101	5/7/14	70	0	6	14	144	29	126	30.6%
102	5/7/14	70	0	8	14	135	29	134	42.2%
103	5/7/14	44	0	4	14	170	29	131	20.9%
104	5/7/14	44	0	4	14	153	29	113	32.7%

Table B.7: Medium hardwood data with oxygen in the center using configuration 1M2L3L with bluff-body

Data	Date	Ext. (mm)	Turns	O2	Prim	Sec	Fuel	NOx	LOI
105	5/7/14	93	0	0	14	170	29	95	26.1%
106	5/7/14	93	0	2	14	170	29	118	24.5%
107	5/7/14	93	0	4	14	170	29	137	27.9%
108	5/7/14	93	0	6	14	170	29	162	22.1%
109	5/7/14	93	0	8	14	170	29	194	18.1%
110	5/7/14	76	0	4	14	170	29	142	22.9%
111	5/7/14	51	0	4	14	170	29	136	19.4%
112	5/7/14	25	0	4	14	170	29	119	25.4%
113	5/7/14	0	0	4	14	170	29	113	22.9%

Table B.8: Medium hardwood data with oxygen in the center using configuration 1S2S3S

Data	Date	Ext. (mm)	Turns	O2	Prim	Sec	Fuel	NOx	LOI
114	5/8/14	-25	0	0	24	160	29	76	45.7%
115	5/8/14	-25	0	8	24	160	29	93	29.2%
116	5/8/14	-25	0	8	24	125	29	81	48.3%
117	5/8/14	-25	0	2	24	160	29	79	41.4%
118	5/8/14	-25	0	4	24	160	29	90	35.7%
119	5/8/14	-25	0	6	24	160	29	99	34.9%
120	5/8/14	-25	0	8	24	160	29	109	30.5%
121	5/8/14	0	0	4	24	160	29	104	34.9%
122	5/8/14	25	0	4	24	160	29	97	37.2%
123	5/8/14	51	0	4	24	160	29	88	33.4%
124	5/8/14	51	0	4	24	160	29	88	37.5%
125	5/8/14	68	0	4	24	160	29	92	36.7%
126	5/8/14	68	0	8	24	211	45	122	42.6%
127	5/8/14	68	0	4	24	217	40	120	33.7%

Table B.9: Wheat straw data with oxygen in the center using configuration 1S2L3L

Data	Date	Ext. (mm)	Turns	O2	Prim	Sec	Fuel	NOx	LOI
128	5/20/14	0	0	0	20	158	29	147	14.5%
129	5/20/14	0	0	2	20	158	29	151	20.6%
130	5/20/14	0	0	4	20	158	29	167	9.3%
131	5/20/14	0	0	6	20	158	29	193	8.5%
132	5/20/14	0	0	8	20	158	29	243	8.3%
133	5/20/14	0	0	0	20	158	29	117	9.2%
134*	5/20/14	0	0	4	20	158	29	168	8.5%
135*	5/20/14	0	0	8	20	158	29	176	5.1%
136	5/20/14	0	0	0	20	158	29	116	14.3%
137	5/20/14	0	0	2	20	158	29	136	11.1%
138	5/20/14	0	0	4	20	158	29	171	9.1%
139	5/20/14	-25	0	0	20	158	29	183	8.6%
140	5/20/14	-25	0	4	20	158	29	235	6.3%
141	5/20/14	-25	0	8	20	158	29	291	5.7%
142	5/20/14	25	0	0	20	158	29	119	21.9%
143	5/20/14	25	0	4	20	158	29	214	6.5%
144	5/20/14	25	0	8	20	158	29	291	4.7%
145	5/20/14	68	0	0	20	158	29	146	9.5%
146	5/20/14	68	0	4	20	158	29	206	8.4%
147	5/20/14	68	0	8	20	158	29	252	4.2%

* These data have oxygen in the secondary, rather than in the center

Table B.10: Wheat straw data with oxygen in the center using configuration 1S2L3S

Data	Date	Ext. (mm)	Turns	O2	Prim	Sec	Fuel	NOx	LOI
148	5/21/14	-25	0	0	20	158	29	196	12.8%
149	5/21/14	-25	0	2	20	158	29	257	20.3%
150	5/21/14	-25	0	4	20	158	29	276	9.4%
151	5/21/14	-25	0	8	20	158	29	370	5.5%
152	5/21/14	-25	0	6	20	158	29	292	6.8%
153	5/21/14	-25	0	12	20	158	29	520	4.7%
154	5/21/14	-25	0	0	20	158	29	198	13.6%
155*	5/21/14	-25	0	2	20	158	29	219	8.4%
156*	5/21/14	-25	0	4	20	158	29	232	8.9%
157*	5/21/14	-25	0	6	20	158	29	251	4.9%
158*	5/21/14	-25	0	8	20	158	29	274	5.8%
159*	5/21/14	-25	0	12	20	158	29	295	3.8%
160	5/21/14	0	0	0	20	158	29	212	10.7%
161	5/21/14	0	0	4	20	158	29	264	7.4%
162	5/21/14	0	0	8	20	158	29	365	6.2%
163	5/21/14	25	0	0	20	158	29	220	10.9%
164	5/21/14	25	0	4	20	158	29	263	6.3%
165	5/21/14	25	0	8	20	158	29	359	5.3%
166	5/22/14	-25	6	0	20	158	29	127	20.0%
167	5/22/14	-25	6	2	20	158	29	145	4.4%
168	5/22/14	-25	6	0	20	158	29	177	9.7%
169	5/22/14	-25	6	2	20	158	29	190	5.5%
170	5/22/14	-25	6	2	20	158	29	190	10.7%
171	5/22/14	-25	6	4	20	158	29	186	10.6%
172	5/22/14	-25	6	6	20	158	29	185	6.5%
173	5/22/14	-25	6	8	20	158	29	297	5.6%
174	5/22/14	-25	9	0	20	158	29	172	4.1%
175	5/22/14	-25	9	2	20	158	29	239	4.3%
176	5/22/14	-25	9	4	20	158	29	271	3.8%
177	5/22/14	-25	9	6	20	158	29	243	6.3%
178	5/22/14	-25	9	8	20	158	29	283	4.0%

* These data have oxygen in the secondary, rather than in the center

Table B.11: Wheat straw data with oxygen in the center, tube recessed 25 mm, using configuration 1S2L3S

Data	Date	Turns	O2	Prim	Sec	Fuel	NOx	LOI
179*	5/23/14	6	0	20	158	29	240	9.1%
180*	5/23/14	6	2	20	158	29	217	9.0%
181*	5/23/14	6	4	20	158	29	231	6.7%
182	5/23/14	9	0	20	158	29	221	10.7%
183	5/23/14	9	2	20	158	29	202	7.6%
184	5/23/14	9	4	20	158	29	222	8.1%
185	5/23/14	9	6	20	158	29	252	5.2%
186	5/23/14	9	8	20	158	29	259	4.3%

* These data were taken using configuration 1M2L3S with the bluff-body

Table B.12: Medium hardwood data with oxygen in the center, tube recessed 25 mm, using configuration 1S2L3S

Data	Date	Turns	O2	Prim	Sec	Fuel	NOx	LOI
187	7/16/14	0	0	24	160	29	148	23.5%
188	7/16/14	0	2	24	160	29	153	23.3%
189	7/16/14	0	4	24	160	29	159	16.9%
190	7/16/14	0	6	24	160	29	188	15.2%
191	7/16/14	0	8	24	160	29	209	17.7%
192	7/16/14	6	0	24	160	29	136	25.2%
193	7/16/14	6	2	24	160	29	125	25.3%
194	7/16/14	6	4	24	160	29	103	25.2%
195	7/16/14	6	6	24	160	29	126	20.9%
196	7/16/14	6	8	24	160	29	157	19.5%
197	7/16/14	9	0	24	160	29	110	29.7%
198	7/16/14	9	2	24	160	29	108	32.5%
199	7/16/14	9	4	24	160	29	127	35.0%
200	7/16/14	9	6	24	160	29	126	24.6%
201	7/16/14	9	8	24	160	29	119	22.2%

Table B.13: Hardwood data under over-fire air conditions, 52 kg/hr tertiary air, oxygen in the center, center tube flush, using configuration 1S2L3L

Data	Date	Turns	O2	Prim	Sec	Fuel	NOx	LOI
202	10/29/14	0	0	14	118	29	107	25.8%
203	10/29/14	0	4	14	118	29	109	23.3%
204	10/29/14	0	6	14	118	29	124	19.7%
205	10/29/14	0	8	14	118	29	142	18.4%
206	10/29/14	0	0	14	118	29	108	29.3%
207	10/29/14	0	2	14	110	29	110	28.1%
208	10/29/14	0	4	14	101	29	114	27.2%
209	10/29/14	0	6	14	92	29	130	27.6%
210	10/29/14	0	8	14	83	29	135	24.5%

Table B.14: Medium hardwood data with oxygen in the center, center tube flush, using configuration 1L2L3L

Data	Date	Turns	O2	Prim	Sec	Fuel	NOx	LOI
211	11/20/14	0	0	14	170	29	77	48.5%
212	11/20/14	0	2	14	170	29	82	43.5%
213	11/20/14	0	4	14	170	29	115	27.7%
214	11/20/14	0	6	14	170	29	121	25.1%
215	11/20/14	0	8	14	170	29	131	20.7%
216	11/20/14	6	0	14	170	29	74	46.8%
217	11/20/14	6	2	14	170	29	79	49.3%
218	11/20/14	6	4	14	170	29	92	41.8%
219	11/20/14	6	6	14	170	29	100	32.5%
220	11/20/14	6	8	14	170	29	104	31.8%
221	11/20/14	9	0	14	170	29	75	55.3%
222	11/20/14	9	2	14	170	29	76	57.0%
223	11/20/14	9	4	14	170	29	76	53.3%
224	11/20/14	9	6	14	170	29	83	50.0%
225	11/20/14	9	8	14	170	29	87	43.6%

Table B.15: Medium hardwood data with oxygen in four-hole lance, center tube flush, using configuration 1M2L3L

Data	Date	Turns	O2	Prim	Sec	Fuel	NOx	LOI
226	12/9/14	0	0	14	170	29	83	48.2%
227	12/9/14	0	0	14	170	28	91	43.7%
228	12/9/14	0	0	14	170	28	91	38.5%
229	12/9/14	0	2	14	170	28	99	27.3%
230	12/9/14	0	4	14	170	28	104	22.8%
231	12/9/14	0	6	14	170	28	107	20.8%
232	12/9/14	0	8	14	170	28	116	18.4%
233	12/9/14	0	12	14	170	28	138	14.9%
234	12/9/14	0	16	14	170	28	162	13.9%
235	12/9/14	6	0	14	170	28	71	43.5%
236	12/9/14	6	2	14	170	28	78	36.4%
237	12/9/14	6	4	14	170	28	80	35.8%
238	12/9/14	6	6	14	170	28	82	30.0%
239	12/9/14	6	8	14	170	28	90	23.8%
240	12/9/14	6	12	14	170	28	116	18.1%
241	12/9/14	6	16	14	170	28	142	16.0%
242	12/9/14	9	0	14	170	28	69	43.4%

Table B.16: Medium hardwood data with oxygen in the center tube being premixed using eight-hole lance, using configuration 1M2L3L

Data	Date	Ext. (mm)	Turns	O2	Prim	Sec	Fuel	NOx	LOI
243	12/10/14	0	0	0	14	170	28	88	39.9%
244	12/10/14	0	0	0	14	170	28	83	43.7%
245	12/10/14	0	0	2	14	170	28	92	29.9%
246	12/10/14	0	0	4	14	170	28	100	24.4%
247	12/10/14	0	0	6	14	170	28	106	20.8%
248	12/10/14	0	0	8	14	170	28	126	19.6%
249	12/10/14	0	0	12	14	170	28	130	19.3%
250	12/10/14	0	0	16	14	170	28	143	16.4%
251	12/10/14	0	6	0	14	170	28	75	39.0%
252	12/10/14	0	6	2	14	170	28	78	33.9%
253	12/10/14	0	6	4	14	170	28	84	28.7%
254	12/10/14	0	6	6	14	170	28	89	25.5%
255	12/10/14	0	6	8	14	170	28	102	24.9%
256	12/10/14	0	6	12	14	170	28	108	20.7%
257	12/10/14	0	6	16	14	170	28	109	18.5%
258	12/10/14	0	9	0	14	170	28	77	40.5%
259	12/11/14	-51	0	0	14	170	28	82	46.0%
260	12/11/14	-51	0	0	14	170	28	82	50.8%
261	12/11/14	-51	0	2	14	170	28	97	34.4%
262	12/11/14	-51	0	4	14	170	28	101	30.7%
263	12/11/14	-51	0	6	14	170	28	110	28.2%
264	12/11/14	-51	0	8	14	170	28	110	22.4%
265	12/11/14	-51	0	12	14	170	28	129	18.8%
266	12/11/14	-51	0	16	14	170	28	156	17.3%
267	12/11/14	-51	6	0	14	170	28	81	47.6%
268	12/11/14	-51	6	2	14	170	28	95	38.9%
269	12/11/14	-51	6	4	14	170	28	101	37.9%
270	12/11/14	-51	6	6	14	170	28	108	28.4%
271	12/11/14	-51	6	8	14	170	28	115	22.7%
272	12/11/14	-51	6	12	14	170	28	124	20.5%
273	12/11/14	-51	6	16	14	170	28	122	23.8%

Table B.17: Medium hardwood data with oxygen in the center tube being premixed using six-hole lance, using configuration 1S2L3L

Data	Date	Ext. (mm)	Turns	O2	Prim	Sec	Fuel	NOx	LOI
274	2/19/15	0	0	0	14	170	28	84	36.1%
275	2/19/15	0	0	2	14	170	28	90	21.8%
276	2/19/15	0	0	4	14	170	28	94	26.0%
277	2/19/15	0	0	6	14	170	28	104	21.8%
278	2/19/15	0	0	8	14	170	28	111	19.6%
279	2/19/15	0	0	0	11	173	28	80	36.6%
280	2/19/15	0	0	0	14	170	28	77	39.8%
281	2/19/15	0	0	0	17	167	28	74	42.2%
282	2/19/15	0	0	0	20	164	28	69	41.3%
283	2/19/15	0	0	0	23	161	28	70	42.9%
284	2/19/15	0	0	4	11	173	28	102	23.0%
285	2/19/15	0	0	8	11	173	28	116	19.2%
286	2/19/15	38	0	0	14	170	28	80	31.5%
287	2/19/15	38	0	4	14	170	28	89	32.4%
288	2/19/15	38	0	8	14	170	28	100	24.0%

Table B.18: Fine hardwood data with oxygen in the center tube being premixed using six-hole lance, using configuration 1S2L3L

Data	Date	Ext. (mm)	Turns	O2	Prim	Sec	Fuel	NOx	LOI
289	3/24/15	0	0	0	14	180	28	114	14.9%
290	3/24/15	0	0	2	14	180	28	135	14.6%
291	3/24/15	0	0	4	14	180	28	154	13.5%
292	3/24/15	0	0	6	14	180	28	177	13.7%
293	3/24/15	0	0	8	14	180	28	185	12.8%
294	3/24/15	0	6	0	14	180	28	95	20.3%
295	3/24/15	0	6	2	14	180	28	109	16.3%
296	3/24/15	0	6	4	14	180	28	121	15.7%
297	3/24/15	0	6	6	14	180	28	136	15.2%
298	3/24/15	0	6	8	14	180	28	153	15.4%
299	3/24/15	0	9	0	14	180	28	72	27.1%
300	3/24/15	0	9	2	14	180	28	79	25.4%
301	3/24/15	0	9	4	14	180	28	90	22.5%
302	3/24/15	0	9	6	14	180	28	101	18.5%
303	3/24/15	0	9	8	14	180	28	114	17.3%

APPENDIX C: FOURIER TRANSFORM INFRARED SPECTROMETER

A Fourier Transform Infrared Spectrometer (FT-IR) is a tool that is used in a variety of applications, including that of improved gas species mapping within a reactor. The FT-IR can be used to collect infrared light from an internal source and determine infrared light absorbed by gases extracted from a reactor. Various gas species have specific bands of light over which they absorb, which can be detected by the FT-IR. Gases such as NO and CO have small, yet specific bands where they are known to absorb infrared light. CO_2 and H_2O, on the other hand, both absorb over a larger bands. The amount of light absorbed by a gas is dependent on a number of variables. Gas concentration, gas flow rate, temperature and pressure all play a role in the amount of light the detector senses. The gas flow rate, temperature, and pressure are held constant to eliminate variables and to yield gas species concentrations.

Due to the various bands over which different gases absorb, it can be extremely difficult to differentiate between the various gas species and their concentration. For example, H_2O absorbs over the same wavenumber as NO. Since the baseline has neither of these gas species it becomes a difficult mathematical challenge. Adding to the difficulty is that NO is in much smaller quantities and does not absorb light to the level, by an order of magnitude, as does H_2O. A classical least squares (CLS) method can be used to compare various spectra in order to create a calibration. Once the calibration is made, the FTIR can then display gas species concentration over a very short time frame. For more theory and general information, see previous work by Reeder [45] and Chamberlain [46].

FT-IR technology has been developed greatly since its first use and it has enormous potential as a non-intrusive means of analyzing samples. The FT-IR can be an excellent tool in mapping gas species concentrations within the reactor. The FT-IR connects to a computer to allow data acquisition through a program named OMNIC. Another program, TQ Analyst, can be used to create methods for the determination of gas species concentrations and compared with another software package, MKS, with its own libraries of data. A method acts like a library and is a collection of spectra. A method allows a comparison of spectra from an unknown gas to the known gases and calculates the unknown gas based on specified infrared light bands.

A heated pump pulls gas through heated lines from the reactor to a gas cell allowing infrared absorption levels to be measured using the FT-IR. The absorption levels then allow a gas concentration within the cell to be calculated using a method created by multiple spectra. A standard operating procedure for using the gas cell with the FT-IR is shown.

Standard Operating Procedure to use FT-IR with Gas Cell

1. Make sure FT-IR and gas cell heater are hooked up properly
    a. Plug in power cord and white cord from FT-IR to computer
    b. Plug in thermocouple and power cord into the temperature controller
    c. Purge FT-IR with N_2 to reduce background noise
2. Get Liquid Nitrogen from Central Stockroom (C100 BNSN)
    a. Approximately 1 liter needed to cool MCT detector
    b. Use funnel and slowly add liquid nitrogen
    c. Be careful not to overfill
    d. It takes about 60 minutes to cool detector
3. Turn on gas cell heater
    a. Set gas cell heater to run.
    b. Ensure it is set at 302°F (150°C)
    c. It will take about 30 minutes to heat up
4. Ensure Pressure Transducer is working properly
5. The gas cell needs to be at 101.325 kPa (1 atm or 760 torr) total pressure when collecting samples
    a. Do not overpressure gas cell!
    b. The maximum pressure it can withstand is 15 psi gauge.
    c. The gas cell must be at correct total pressure or reading will be inaccurate
6. Collect background with N_2 in gas cell
    a. Make sure N_2 is hooked up with the inlet valve to gas cell closed
    b. Slowly open inlet valve and adjust the inlet valve and flow meter so that the gas cell is appropriately pressurized
    c. Flow meter should be about 30 cc/min
    d. Wait about 3 minutes for other gases to leave gas cell
    e. Collect background using an appropriate experiment set-up in OMNIC
        i. (Suggested settings: Mid IR, N_2 Det, 6 Scans, .5cm-1, 5000-500cm-1)
    f. If there appears to be unusual absorptions in background wait additional time to ensure N_2 is the only gas present in the gas cell and re-collect background
    g. Once background has been collected turn the three way valve before inlet to collect sample gases
7. Collect Series with gases you want to sample
    a. Open the flow meter valve all the way
    b. Open the inlet valve to the gas cell
    c. Turn on the pump and watch the cell pressure
    d. Adjust valves appropriately to ensure correct cell pressure
    e. Wait enough time for N_2 to leave cell
    f. Choose “Collect Series…” from the “Collect” drop down menu to begin data acquisition, be sure to save any desired data
    g. If needed, repeat step 6 for new background
8. Shut down equipment
    a. Purge the gas cell with N_2 and close valves to prevent corrosion and condensation in the gas cell
    b. Turn off all assisting equipment